Published as Chapter 5 in "*Handbook of Surface and Colloid Chemistry*"
Second Expanded and Updated Edition; K. S. Birdi, Ed.; CRC Press, New York, 2002.

5. CHEMICAL PHYSICS OF COLLOID SYSTEMS AND INTERFACES

Authors: Peter A. Kralchevsky, Krassimir D. Danov, and Nikolai D. Denkov

Laboratory of Chemical Physics and Engineering, Faculty of Chemistry, University of Sofia, Sofia 1164, Bulgaria

CONTENTS

5.1 INTRODUCTION

A *colloidal system* represents a multiphase (heterogeneous) system, in which at least one of the phases exists in the form of very small particles: typically smaller than 1 μm but still much larger than the molecules. Such particles are related to phenomena like Brownian motion, diffusion and osmosis. The terms "microheterogeneous system" and "disperse system" (dispersion) are more general because they include also bicontinuous systems (in which none of the phases is split into separate particles) and systems containing larger, non-Brownian, particles. The term dispersion is often used as a synonym of colloidal system.

A classification of the colloids with respect to the state of aggregation of the *disperse* and the *continuous* phases is shown in Table 1. Some examples are following.

1. Examples for *gas-in-liquid* dispersions are the foams or the boiling liquids. *Gas-in-solid* dispersions are the various porous media like filtration membranes, sorbents, catalysts, isolation materials, etc.

2. Examples for *liquid-in-gas* dispersions are the mist, the clouds and other aerosols. *Liquid-in-liquid* dispersions are the emulsions. At room temperature there are only four types of mutually immiscible liquids: water, hydrocarbon oils, fluorocarbon oils and liquid metals (Hg and Ga). Many raw materials and products in food and petroleum industries exist in the form of oil-in-water or water-in-oil emulsions. The soil and some biological tissues can be considered as *liquid-in-solid* dispersions.

3. Smoke, dust and some other aerosols are examples for *solid-in-gas* dispersions. The *solid-in-liquid* dispersions are termed *suspensions* or *sols*. The pastes and some glues are highly concentrated suspensions. The *gels* represent *bicontinuous* structures of solid and liquid. The pastes and some glues are highly concentrated suspensions. *Solid-in-solid* dispersions are some metal alloys, many kinds of rocks, some colored glasses, etc.

Table 1: Types of Disperse Systems

continuous phase / disperse phase	GAS	LIQUID	SOLID
GAS	-	G in L	G in S
LIQUID	L in G	L_1 in L_2	L in S
SOLID	S in G	S in L	S_1 in S_2

Below we will consider mostly liquid dispersions, i.e., dispersions with liquid continuous phase, like foams, emulsions and suspensions. Sometimes these are called "complex fluids".

In general, the area of the interface between the disperse and continuous phases is rather large. For instance, 1 cm^3 of dispersion with particles of radius 100 nm and volume fraction 30% contains interface of area about 10 m^2. This is the reason why the interfacial properties are of crucial importance for the properties and stability of colloids.

The *stabilizing* factors for dispersions are the repulsive surface forces, the particle thermal motion, the hydrodynamic resistance of the medium, the high surface elasticity of fluid particles and films.

On the opposite, the factors *destabilizing* dispersions are the attractive surface forces, the factors suppressing the repulsive surface forces, the low surface elasticity, gravity and other external forces tending to separate the phases.

Below, in Sections 5.2 and 5.3 we consider effects related to the surface tension of surfactant solution and capillarity. In Section 5.4 we present a review on the surface forces due to the intermolecular interactions. In Section 5.5 we describe the hydrodynamic interparticle forces originating from the effects of bulk and surface viscosity and related to surfactant diffusion. Section 5.6 is devoted to the kinetics of coagulation in dispersions. Section 5.7 regards foams containing oil drops and solid particulates in relation to the antifoaming mechanisms and the exhaustion of antifoams. Finally, Sections 5.8 and 5.9 address the electrokinetic and optical properties of dispersions.

5.2 SURFACE TENSION OF SURFACTANT SOLUTIONS

5.2.1 STATIC SURFACE TENSION

As a rule the fluid dispersions (emulsions, foams) are stabilized by adsorption layers of amphiphile molecules. These can be ionic[1,2] and nonionic[3] surfactants, lipids, proteins, etc., see Chapter 4 of this Handbook. All of them have the property to lower the value of the surface (or interfacial) tension, σ, in accordance with the *Gibbs adsorption equation*,[4-6]

$$d\sigma = -\sum_i \Gamma_i d\mu_i \tag{1}$$

where Γ_i is the surface concentration (adsorption) of the i-th component and μ_i is its chemical potential. The summation in Equation 1 is carried out over all components. Usually an equimolecular dividing surface with respect to the solvent is introduced for which the adsorption of the solvent is set zero by definition.[4,5] Then the summation is carried out over all other components. Note that Γ_i is an excess surface concentration with respect to the bulk; Γ_i is positive for surfactants, which decrease σ in accordance with Equation 1. On the contrary, Γ_i is negative for aqueous solutions of electrolytes, whose ions are repelled from the surface by the electrostatic image forces;[5] consequently, the addition of electrolytes increases the surface tension of water.[6] For surfactant concentrations above the CMC (critical micellization concentration) μ_i =const. and, consequently, σ = const., see Equation 1 and Chapter 8 of this Handbook.

5.2.1.1 Nonionic Surfactants

5.2.1.1.1 Types of adsorption isotherms

Consider the boundary between an aqueous solution of a nonionic surfactant and a hydrophobic phase, air or oil. The dividing surface is usually chosen to be the equimolecular surface with respect to water, that is $\Gamma_w = 0$. Then Equation 1 reduces to $d\sigma = -\Gamma_1 d\mu_1$, where the subscript "1" denotes the surfactant. Since the bulk surfactant concentration is usually not too high, one can use the expression for the chemical potential of a solute in an ideal solution: $\mu_1 = \mu_1^{(0)} + kT \ln c_1$, where k is the Boltzmann constant, T is the absolute temperature, c_1 is

the concentration of nonionic surfactant, and $\mu_1^{(0)}$ is its standard chemical potential, which is independent of c_1. Thus the Gibbs adsorption equation acquires the form

$$d\sigma = -kT\,\Gamma_1\, d\ln c_1 \tag{2}$$

The surfactant adsorption isotherms, expressing the connection between Γ_1 and c_1, are usually obtained by means of some molecular model of adsorption. Table 2 contains the 6 most popular surfactant adsorption isotherms, those of Henry, Freundlich,[7] Langmuir,[8] Volmer,[9] Frumkin[10] and van der Waals.[11] For $c_1 \to 0$ all isotherms (except that of Freundlich) reduce to the Henry isotherm: $\Gamma_1/\Gamma_\infty = Kc_1$. The physical difference between the Langmuir and Volmer isotherms is that the former corresponds to a physical model of *localized* adsorption, whereas the latter – to *non-localized* adsorption. The Frumkin and van der Walls isotherms generalize, respectively, the Langmuir and Volmer isotherms for case, in which the is interaction between neighboring adsorbed molecules is not negligible. (If the interaction parameter β is set zero, the Frumkin and van der Walls isotherms reduce to the Langmuir and Volmer isotherms, correspondingly.) The comparison between theory and experiment shows that for air-water interfaces $\beta > 0$, whereas for oil-water interfaces one can set $\beta = 0$.[12,13] The latter facts lead to the conclusion that for air-water interfaces β takes into account the van der Waals attraction between the hydrocarbon tails of the adsorbed surfactant molecules across air; such attraction is missing when the hydrophobic phase is oil. (Note that in the case of ionic surfactants it is possible to have $\beta < 0$, see the next section.) The adsorption parameter K in Table 2 characterizes the surface activity of the surfactant: the greater K, the higher the surface activity. K is related to the standard free energy of adsorption, $\Delta f = \mu_1^{(0)} - \mu_{1s}^{(0)}$, which is the energy gain for bringing a molecule from the bulk of the aqueous phase to a diluted adsorption layer:[14,15]

$$K = \frac{\delta_1}{\Gamma_\infty}\exp\left(\frac{\mu_1^{(0)} - \mu_{1s}^{(0)}}{kT}\right) \tag{3}$$

The parameter δ_1 characterizes the thickness of the adsorption layer; δ_1 can be set (approximately) equal to the length of the amphiphilic molecule. Γ_∞ represents the maximum possible value of the adsorption. In the case of localized adsorption (Langmuir and Frumkin isotherms) $1/\Gamma_\infty$ is the area per adsorption site. In the case of non-localized adsorption (Volmer and van der Waals isotherms) $1/\Gamma_\infty$ is the excluded area per molecule.

TABLE 2. Types of Adsorption and Surface-Tension Isotherms

Type of isotherm	• **Surfactant adsorption isotherms** (for nonionic surfactants: $a_{1s} \equiv c_1$)
Henry	$Ka_{1s} = \dfrac{\Gamma_1}{\Gamma_\infty}$
Freundlich	$Ka_{1s} = \left(\dfrac{\Gamma_1}{\Gamma_\infty}\right)^{1/m}$
Langmuir	$Ka_{1s} = \dfrac{\Gamma_1}{\Gamma_\infty - \Gamma_1}$
Volmer	$Ka_{1s} = \dfrac{\Gamma_1}{\Gamma_\infty - \Gamma_1}\exp\left(\dfrac{\Gamma_1}{\Gamma_\infty - \Gamma_1}\right)$
Frumkin	$Ka_{1s} = \dfrac{\Gamma_1}{\Gamma_\infty - \Gamma_1}\exp\left(-\dfrac{2\beta\Gamma_1}{kT}\right)$
van der Waals	$Ka_{1s} = \dfrac{\Gamma_1}{\Gamma_\infty - \Gamma_1}\exp\left(\dfrac{\Gamma_1}{\Gamma_\infty - \Gamma_1} - \dfrac{2\beta\Gamma_1}{kT}\right)$
	• **Surface tension isotherm** $\sigma = \sigma_0 - kTJ + \sigma_d$ (for nonionic surfactants: $\sigma_d \equiv 0$)
Henry	$J = \Gamma_1$
Freundlich	$J = \dfrac{\Gamma_1}{m}$
Langmuir	$J = -\Gamma_\infty \ln\left(1 - \dfrac{\Gamma_1}{\Gamma_\infty}\right)$
Volmer	$J = \dfrac{\Gamma_\infty\Gamma_1}{\Gamma_\infty - \Gamma_1}$
Frumkin	$J = -\Gamma_\infty \ln\left(1 - \dfrac{\Gamma_1}{\Gamma_\infty}\right) - \dfrac{\beta\Gamma_1^2}{kT}$
van der Waals	$J = \dfrac{\Gamma_\infty\Gamma_1}{\Gamma_\infty - \Gamma_1} - \dfrac{\beta\Gamma_1^2}{kT}$

Note: The surfactant adsorption isotherm and the surface tension isotherm, which are combined to fit experimental data, obligatorily must be of the same type.

As already mentioned, the Freundlich adsorption isotherm, unlike the other ones in Table 2, does not become linear at low concentrations, but remains convex to the concentration axis. Moreover, it does not show a saturation or limiting value. Hence, for the Freundlich adsorption isotherm in Table 2 Γ_∞ is a parameter scaling the adsorption (rather than saturation adsorption). This isotherm can be derived assuming that the surface (as a rule solid) is heterogeneous.[16,17] Consequently, if the data fit the Freundlich equation, this is an indication, but not a proof, that the surface is heterogeneous.[6]

The *adsorption* isotherms in Table 2 can be applied to both fluid and solid interfaces. The *surface tension* isotherms in Table 2, which relate σ and Γ_1, are usually applied to fluid interfaces, although they could be used also for solid-liquid interfaces if σ is identified with the Gibbs[4] *superficial* tension. (The latter is defined as the force per unit length which opposes every increase of the wet area without any deformation of the solid.)

The surface tension isotherms in Table 2 are deduced from the respective adsorption isotherms in the following way. The integration of Equation 2 yields

$$\sigma = \sigma_0 - kTJ\,, \tag{4}$$

where σ_0 is the interfacial tension of the pure solvent and

$$J \equiv \int_0^{c_1} \Gamma_1 \frac{dc_1}{c_1} = \int_0^{\Gamma_1} \Gamma_1 \frac{d\ln c_1}{d\Gamma_1} d\Gamma_1 \tag{5}$$

The derivative $d\ln c_1/d\Gamma_1$ is calculated for each adsorption isotherm, and then the integration in Equation 5 is carried out analytically. The obtained expressions for J are listed in Table 2. Each surface tension isotherm, $\sigma(\Gamma_1)$, has the meaning of a *two-dimensional equation of state* of the adsorption monolayer, which can be applied to both *soluble* and *insoluble* surfactants.[6,18]

An important thermodynamic property of a surfactant adsorption monolayer is its Gibbs (surface) elasticity

$$E_G \equiv -\Gamma_1 \left(\frac{\partial \sigma}{\partial \Gamma_1} \right)_T \tag{6}$$

Expressions for E_G, corresponding to various adsorption isotherms, are shown in Table 3. The Gibbs elasticity characterizes the lateral fluidity of the surfactant adsorption monolayer. At high values of the Gibbs elasticity the adsorption monolayer behaves as tangentially immobile. In such case, if two emulsion droplets approach each other, the hydrodynamic flow

pattern, and the hydrodynamic interaction as well, is almost the same as if the droplets were solid. For lower values of the surfactant adsorption the so called "Marangoni effect" appears, which is equivalent to appearance of gradients of surface tension due to gradients of surfactant adsorption: $\nabla_s\sigma = -(E_G/\Gamma_1)\nabla_s\Gamma_1$ (here ∇_s denotes surface gradient operator). The Marangoni effect can considerably affect the hydrodynamic interactions of fluid particles (drops, bubbles), see section 5.5 below.

Table 3. Elasticity of Adsorption Monolayers at a Fluid Interface

Type of isotherm (cf. Table 2)	Gibbs elasticity E_G
Henry	$E_G = kT\Gamma_1$
Freundlich	$E_G = kT\dfrac{\Gamma_1}{m}$
Langmuir	$E_G = kT\Gamma_1 \dfrac{\Gamma_\infty}{\Gamma_\infty - \Gamma_1}$
Volmer	$E_G = kT\Gamma_1 \dfrac{\Gamma_\infty^2}{(\Gamma_\infty - \Gamma_1)^2}$
Frumkin	$E_G = kT\Gamma_1\left(\dfrac{\Gamma_\infty}{\Gamma_\infty - \Gamma_1} - \dfrac{2\beta\Gamma_1}{kT}\right)$
van der Waals	$E_G = kT\Gamma_1\left[\dfrac{\Gamma_\infty^2}{(\Gamma_\infty - \Gamma_1)^2} - \dfrac{2\beta\Gamma_1}{kT}\right]$

Note: The above expressions are valid for both nonionic and ionic surfactants.

5.2.1.1.2 Derivation from first principles

Each surfactant adsorption isotherm (that of Langmuir, Volmer, Frumkin, etc.), and the related expressions for the surface tension and surface chemical potential, can be derived from an expression for the surface free energy, F_s, which corresponds to a given physical model. This derivation helps one to obtain (or identify) the selfconsistent system of equations, referring to a given model, which is to be applied to interpret a set of experimental data.

Combination of equations corresponding to different models (say Langmuir adsorption isotherm with Frumkin surface tension isotherm) is incorrect and must be avoided.

The general scheme for derivation of the adsorption isotherms is the following:

(i) With the help of statistical mechanics an expression is obtained, say, for the canonical ensemble partition function, Q, from which the surface free energy F_s is determined:[11]

$$F_s(T, A, N_1) = -kT \ln Q(T, A, N_1) \tag{7}$$

where A is the interfacial area and N_1 is the number of adsorbed surfactant molecules; see Table 4.

(ii) Differentiating the expression for F_s one derives expressions for the *surface pressure*, π_s, and the *surface chemical potential* of the adsorbed surfactant molecules, μ_{1s}:[11]

$$\pi_s \equiv \sigma_0 - \sigma = -\left(\frac{\partial F_s}{\partial A}\right)_{T,N_1}, \qquad \mu_{1s} = \left(\frac{\partial F_s}{\partial N_1}\right)_{T,A} \tag{8}$$

Combining the obtained expressions for π_s and μ_{1s}, one can deduce the respective form of the Butler equation,[19] see Equation 16 below.

(iii) The surfactant adsorption isotherm (Table 2) can be derived by setting the obtained expression for the surface chemical potential μ_{1s} equal to the bulk chemical potential of the surfactant molecules in the subsurface layer (that is, equilibrium between surface and subsurface is assumed):[11]

$$\mu_{1s} = \mu_1^{(0)} + kT \ln(a_{1s}\delta_1/\Gamma_\infty) \tag{9}$$

Here a_{1s} is the activity of the surfactant molecule in the subsurface layer; a_{1s} is scaled with the volume per molecule in a dense (saturated) adsorption layer, $v_1 = \delta_1/\Gamma_\infty$, where δ_1 is interpreted as the thickness of the adsorption layer, or the length of an adsorbed molecule. In terms of the subsurface activity, a_{1s}, Equation 9 can be applied to ionic surfactants and to dynamic processes. In the simplest case of nonionic surfactants and equilibrium processes we have $a_{1s} \approx c_1$, where c_1 is the bulk surfactant concentration.

Table 4. Free Energy and Chemical Potential for Surfactant Adsorption Layers

Type of isotherm	• **Surface Free Energy $F_s(T, A, N_1)$** ($M = \Gamma_\infty A$)
Henry	$F_s = N_1 \mu_{1s}^{(0)} + kT[N_1 \ln(N_1/M) - N_1]$
Freundlich	$F_s = N_1 \mu_{1s}^{(0)} + \frac{kT}{m}[N_1 \ln(N_1/M) - N_1]$
Langmuir	$F_s = N_1 \mu_{1s}^{(0)} + kT[N_1 \ln N_1 + (M - N_1)\ln(M - N_1) - M \ln M]$
Volmer	$F_s = N_1 \mu_{1s}^{(0)} + kT[N_1 \ln N_1 - N_1 - N_1 \ln(M - N_1)]$
Frumkin	$F_s = N_1 \mu_{1s}^{(0)} + kT[N_1 \ln N_1 + (M - N_1)\ln(M - N_1) - M \ln M] + \frac{\beta \Gamma_\infty N_1^2}{2M}$
van der Waals	$F_s = N_1 \mu_{1s}^{(0)} + kT[N_1 \ln N_1 - N_1 - N_1 \ln(M - N_1)] + \frac{\beta \Gamma_\infty N_1^2}{2M}$
	• **Surface Chemical Potential μ_{1s}** ($\theta \equiv \Gamma_1/\Gamma_\infty$)
Henry	$\mu_{1s} = \mu_{1s}^{(0)} + kT \ln\theta$
Freundlich	$\mu_{1s} = \mu_{1s}^{(0)} + \frac{kT}{m} \ln\theta$
Langmuir	$\mu_{1s} = \mu_{1s}^{(0)} + kT \ln\frac{\theta}{1-\theta}$
Volmer	$\mu_{1s} = \mu_{1s}^{(0)} + kT\left(\frac{\theta}{1-\theta} + \ln\frac{\theta}{1-\theta}\right)$
Frumkin	$\mu_{1s} = \mu_{1s}^{(0)} + kT \ln\frac{\theta}{1-\theta} - 2\beta\Gamma_1$
van der Waals	$\mu_{1s} = \mu_{1s}^{(0)} + kT\left(\frac{\theta}{1-\theta} + \ln\frac{\theta}{1-\theta}\right) - 2\beta\Gamma_1$

First, let us apply the above general scheme to derive the *Frumkin isotherm*, which corresponds to *localized* adsorption of *interacting* molecules. (Expressions corresponding to the Langmuir isotherm can be obtained by setting $\beta = 0$ in the respective expressions for the Frumkin isotherm.) Let us consider the interface as a two-dimensional lattice having M adsorption sites. The corresponding partition function is[11]

$$Q(T, M, N_1) = \frac{M!}{N_1!\,(M - N_1)!}\,[q(T)]^{N_1} \exp\left(-\frac{n_c w N_1^2}{2kTM}\right) \tag{10}$$

The first multiplier in the right-hand side of Equation 10 expresses the number of ways N_1 indistinguishable molecules can be distributed among M labeled sites; the partition function for a single adsorbed molecule is $q = q_x\, q_y\, q_z$, where q_x, q_y and q_z are one-dimensional harmonic-oscillator partition functions. The exponent in Equation 10 accounts for the interaction between adsorbed molecules in the framework of the Bragg-Williams approximation.[11] w is the nearest-neighbor interaction energy of two molecules and n_c is the number of nearest-neighbor sites to a given site (for example $n_c = 4$ for a square lattice). Next, we substitute Equation 10 into Equation 7 and using the known Stirling approximation, $\ln M! = M \ln M - M$, we get the expression for the surface free energy corresponding to the Frumkin model:

$$F_s = kT[N_1 \ln N_1 + (M - N_1)\ln(M - N_1) - M \ln M - N_1 \ln q(T)] + \frac{n_c w N_1^2}{2M} \tag{11}$$

Note that

$$M = \Gamma_\infty A, \qquad N_1 = \Gamma_1 A \tag{12}$$

where Γ_∞^{-1} is the area per one adsorption site in the lattice. Differentiating Equation 11 in accordance with Equation 8 one deduces expressions for the surface pressure and chemical potential:[11]

$$\pi_s = -\Gamma_\infty kT \ln(1 - \theta) - \beta \Gamma_1^2 \tag{13}$$

$$\mu_{1s} = \mu_{1s}^{(0)} + kT \ln\frac{\theta}{1-\theta} - 2\beta\Gamma_1 \tag{14}$$

where we have introduced the notation

$$\theta = \frac{\Gamma_1}{\Gamma_\infty}, \qquad \beta = -\frac{n_c w}{2\Gamma_\infty}, \qquad \mu_{1s}^{(0)} = -kT \ln q(T) \tag{15}$$

One can check that Equation 13 is equivalent to the Frumkin's surface tension isotherm in Table 2 for a nonionic surfactant. Furthermore, eliminating $\ln(1-\theta)$ between Equations 13 and 14 one obtains the Butler's[19] equation in the form

$$\mu_{1s} = \mu_{1s}^{(0)} + \Gamma_\infty^{-1}\pi_s + kT\ln(\gamma_{1s}\theta) \qquad \text{(Butler equation)} \tag{16}$$

where we have introduced the surface activity coefficient

$$\gamma_{1s} = \exp\left[-\frac{\beta\Gamma_\infty\theta(2-\theta)}{kT}\right] \qquad \text{(for Frumkin isotherm)} \tag{17}$$

(In the special case of Langmuir isotherm we have $\beta = 0$, and then $\gamma_{1s} = 1$.) The Butler equation is used by many authors[12,20-22] as a starting point for development of thermodynamic adsorption models. It should be kept in mind that the specific form of the expressions for π_s and γ_{1s}, which are to be substituted in Equation 16, is not arbitrary, but must correspond to the *same* thermodynamic model (to the same expression for F_s – in our case Equation 11). At last, substituting Equation 16 into Equation 9 one derives the Frumkin adsorption isotherm in Table 2, where K is defined by Equation 3.

Now, let us apply the same general scheme, but this time to the derivation of the *van der Waals isotherm*, which corresponds to *non-localized* adsorption of *interacting* molecules. (Expressions corresponding to the Volmer isotherm can be obtained by setting $\beta = 0$ in the respective expressions for the van der Waals isotherm.) Now the adsorbed N_1 molecules are considered as a two-dimensional gas. The corresponding expression for the canonical ensemble partition function is

$$Q(T, M, N_1) = \frac{1}{N_1!}\, q^{N_1} \exp\left(-\frac{n_c w N_1^2}{2kTM}\right) \tag{18}$$

where the exponent accounts for the interaction between adsorbed molecules, again in the framework of the Bragg-Williams approximation. The partition function for a single adsorbed molecule is $q = q_{xy}\, q_z$, where q_z is one-dimensional (normal to the interface) harmonic-oscillator partition function. On the other hand, the adsorbed molecules have free translational motion in the xy-plane (the interface); therefore we have[11]

$$q_{xy} = \frac{2\pi\tilde{m}kT}{h_{\mathrm{p}}^2}\hat{A} \tag{19}$$

where $\tilde{m}$ is the molecular mass, h_p is the Planck constant and $\hat{A} = A - N_1\Gamma_\infty^{-1}$ is the area accessible to the moving molecules; the parameter Γ_∞^{-1} is the excluded area per molecule, which accounts for the molecular size. Having in mind that $M \equiv \Gamma_\infty A$, we can bring Equation 18 into the form

$$Q(T,M,N_1) = \frac{1}{N_1!}\, q_0^{N_1} (M - N_1)^{N_1} \exp\left(-\frac{n_c w N_1^2}{2kTM}\right) \tag{20}$$

where

$$q_0(T) \equiv \frac{2\pi\tilde{m}kT}{h_p^2\Gamma_\infty} q_z(T) \tag{21}$$

Further, we substitute Equation 20 into Equation 7 and, using the Stirling approximation, we determine the surface free energy corresponding to the van der Waals model:[11,18,23]

$$F_s = kT[N_1 \ln N_1 - N_1 - N_1 \ln q_0(T) - N_1 \ln(M - N_1)] + \frac{n_c w N_1^2}{2M} \tag{22}$$

Again, having in mind that $M \equiv \Gamma_\infty A$, we differentiate Equation 22 in accordance with Equation 8 to deduces expressions for the surface pressure and chemical potential:

$$\pi_s = \Gamma_\infty kT \frac{\theta}{1-\theta} - \beta\Gamma_1^2 \tag{23}$$

$$\mu_{1s} = \mu_{1s}^{(0)} + kT\left(\frac{\theta}{1-\theta} + \ln\frac{\theta}{1-\theta}\right) - 2\beta\Gamma_1 \tag{24}$$

where $\mu_{1s}^{(0)} = -kT \ln q_0(T)$ and β is defined by Equation 15. One can check that Equation 23 is equivalent to the van der Waals surface tension isotherm in Table 2 for a nonionic surfactant. Furthermore, combining Equations 23 and 24 one obtains the Butler's equation 16, but this time with another expression for the surface activity coefficient

$$\gamma_{1s} = \frac{1}{1-\theta}\exp\left[-\frac{\beta\Gamma_\infty\theta(2-\theta)}{kT}\right] \qquad \text{(for van der Waals isotherm)} \tag{25}$$

[In the special case of Volmer isotherm we have $\beta = 0$, and then $\gamma_{1s} = 1/(1 - \theta)$.] Finally, substituting Equation 24 into Equation 9 one derives the van der Waals adsorption isotherm in Table 2, with K defined by Equation 3.

In Table 4 we summarize the expressions for the surface free energy, F_s, and chemical potential μ_{1s}, for several thermodynamic models of adsorption. We recall that the parameter Γ_∞ is defined in different ways for the different models. On the other hand, the parameter K is defined in the same way for all models, viz. by Equation 3. The expressions in Tables 2–4 can be generalized for multicomponent adsorption layers.[18,27]

At the end of this section, let us consider n general expression, which allows one to obtain the surface activity coefficient γ_{1s} directly from the surface pressure isotherm $\pi_s(\theta)$. From the Gibbs adsorption isotherm, $d\pi_s = \Gamma_1 d\mu_{1s}$, it follows

$$\left(\frac{\partial \mu_{1s}}{\partial \Gamma_1}\right)_T = \frac{1}{\Gamma_1}\left(\frac{\partial \pi_s}{\partial \Gamma_1}\right)_T \tag{26}$$

By substituting μ_{1s} from the Butler's equation 16 into Equation 26, and integrating one can derive the sought for expression:

$$\ln\gamma_{1s} = \int_0^\theta \left(\frac{(1-\theta)}{\Gamma_\infty kT}\frac{\partial \pi_s}{\partial \theta} - 1\right)\frac{d\theta}{\theta} \tag{27}$$

One can check that a substitution of π_s from Equations 13 and 23 into Equation 27 yields, respectively, the Frumkin and van der Waals expressions for γ_{1s}, viz. Equations 17 and 25.

5.2.1.2 Ionic Surfactants

5.2.1.2.1 The Gouy equation

The thermodynamics of adsorption of *ionic* surfactants[13,24-28] is more complicated (in comparison with that of nonionics) because of the presence of long-range electrostatic interactions and, in particular, of electric double layer (EDL) in the system, see Figure 1. The electro-chemical potential of the ionic species can be expressed in the form[29]

$$\mu_i = \mu_i^{(0)} + kT\ln a_i + Z_i e\psi \tag{28}$$

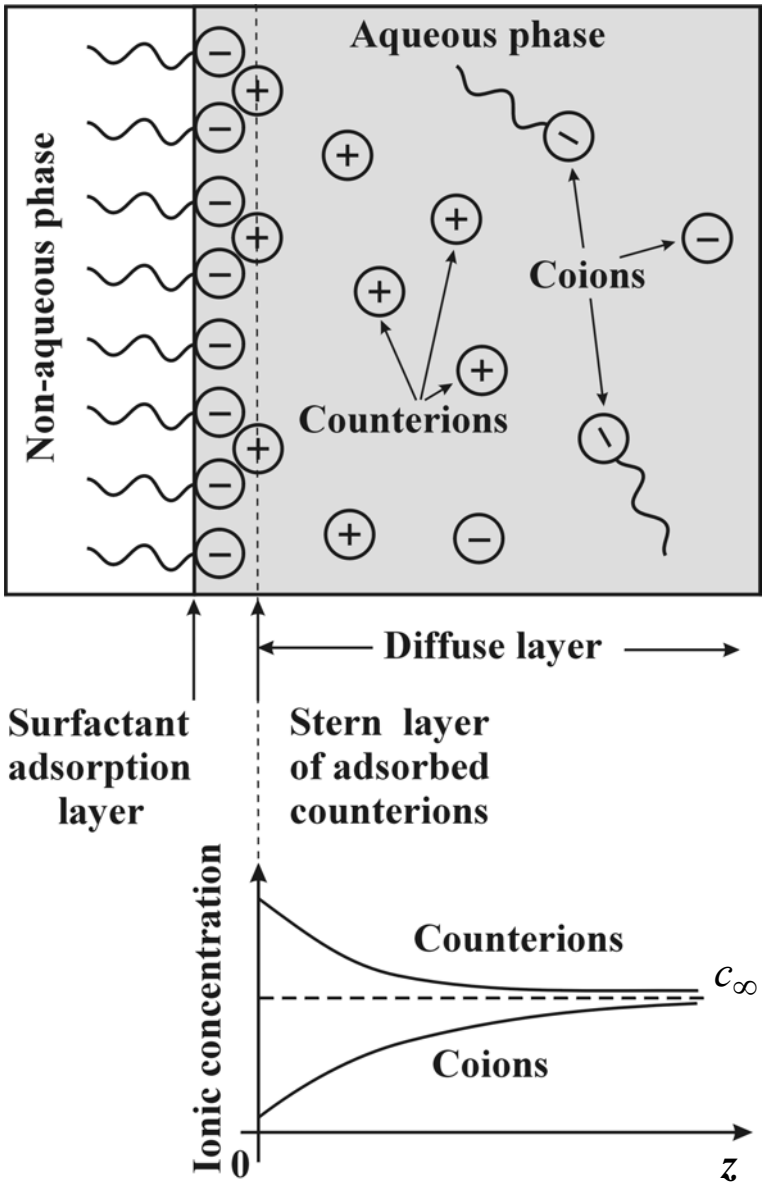

FIGURE 1 Electric double layer in the vicinity of an adsorption layer of ionic surfactant. (a) The diffuse layer contains free ions involved in Brownian motion, while the Stern layer consists of adsorbed (bound) counterions. (b) Near the charged surface there is an accumulation of counterions and a depletion of coions.

where e is the elementary electric charge, ψ is the electric potential, Z_i is the valency of the ionic component *"i"*, and a_i is its activity. In the electric double layer (Figure 1) the electric potential and the activities of the ions are dependent on the distance z from the phase boundary: $\psi = \psi(z)$, $a_i = a_i(z)$. At equilibrium the electrochemical potential, μ_i, is uniform throughout the whole solution, including the electric double layer (otherwise diffusion fluxes would appear).[29] In the bulk of solution ($z \to \infty$) the electric potential tends to a constant

value, which is usually set equal to zero, that is $\psi \to 0$ and $\partial\psi/\partial z \to 0$ for $z \to \infty$. If the expression for μ_i at $z \to \infty$ and that for μ_i at some finite z are set equal, from Equation 28 one obtains a Boltzmann-type distribution for the activity across the EDL:[29]

$$a_i(z) = a_{i\infty} \exp\left[-\frac{Z_i e \psi(z)}{kT}\right] \tag{29}$$

where $a_{i\infty}$ denotes the value of the activity of ion *"i"* in the bulk of solution. If the activity in the bulk, $a_{i\infty}$, is known, then Equation 29 determines the activity $a_i(z)$ in each point of the EDL. A good agreement between theory and experiment can be achieved[12,13,27] using the following expression for $a_{i\infty}$:

$$a_{i\infty} = \gamma_{\pm}\, c_{i\infty} \tag{30}$$

where $c_{i\infty}$ is the bulk concentration of the respective ion, and the activity coefficient $\gamma_{\pm}$ is calculated from the known formula[30]

$$\log \gamma_{\pm} = -\frac{A|Z_+ Z_-|\sqrt{I}}{1 + B\, d_i \sqrt{I}} + bI \tag{31}$$

which originates from the Debye-Hückel theory; I denotes the ionic strength of the solution:

$$I \equiv \tfrac{1}{2} \sum_i Z_i^2 c_{i\infty} \tag{32}$$

where the summation is carried out over all ionic species in the solution. When the solution contains a mixture of several electrolytes, then Equation 31 defines $\gamma_{\pm}$ for each separate electrolyte, with Z_+ and Z_- being the valences of the cations and anions of *this* electrolyte, but with I being the *total* ionic strength of the solution, accounting for all dissolved electrolytes.[30] The log in Equation 31 is decimal, d_i is the ionic diameter, A, B, and b are parameters, whose values can be found in the book by Robinson and Stokes.[30] For example, if I is given in moles per liter (M), the parameters values are $A = 0.5115$ $M^{-1/2}$, $Bd_i = 1.316$ $M^{-1/2}$ and $b = 0.055$ M^{-1} for solutions of NaCl at 25°C.

The theory of EDL provides a connection between surface charge and surface potential (known as the Gouy equation[31,32] of Graham equation[33,34]), which can be presented in the form[27,35]

$$\sum_{i=1}^{N} z_i \Gamma_i = \frac{2}{\kappa_c}\left\{\sum_{i=1}^{N} a_{i\infty}\left[\exp(-z_i \Phi_s) - 1\right]\right\}^{1/2} \qquad \text{(Gouy equation)} \tag{33}$$

where Γ_i (i = 1,...,N) are the adsorptions of the ionic species, $z_i = Z_i/Z_1$, and the index $i = 1$ corresponds to the surfactant ions,

$$\kappa_c^2 \equiv \frac{2Z_1^2 e^2}{\varepsilon_0 \varepsilon kT}, \qquad \Phi_s \equiv \frac{Z_1 e \psi_s}{kT} \tag{34}$$

ε is the dielectric permittivity of the medium (water), $\psi_s = \psi(z=0)$ is the surface potential. Note that the Debye parameter is $\kappa^2 = \kappa_c^2 I$.

For example, let us consider a solution of an ionic surfactant, which is a symmetric 1:1 electrolyte, in the presence of a symmetric, 1:1, inorganic electrolyte (salt). We assume that the counterions due to the surfactant and salt are identical. For example, this can be a solution of sodium dodecyl sulfate (SDS) in the presence of NaCl. We denote by $c_{1\infty}$, $c_{2\infty}$ and $c_{3\infty}$ the bulk concentrations of the surface active ions, counterions, and coions, respectively (Figure 1). For the special system of SDS with NaCl $c_{1\infty}$, $c_{2\infty}$ and $c_{3\infty}$ are the bulk concentration of the DS^-, Na^+ and Cl^- ions, respectively. The requirement for the bulk solution to be electroneutral implies $c_{2\infty} = c_{1\infty} + c_{3\infty}$. The multiplication of the last equation by $\gamma_\pm$ yields

$$a_{2\infty} = a_{1\infty} + a_{3\infty} \tag{35}$$

The adsorption of the coions of the non-amphiphilic salt is expected to be equal to zero, $\Gamma_3 = 0$, because they are repelled by the similarly charged interface.[27,36-38] However, the adsorption of surfactant at the interface, Γ_1, and the binding of counterions in the Stern layer, Γ_2, are different from zero (Figure 1). For this system the Gouy equation 33 acquires the form

$$\Gamma_1 - \Gamma_2 = \frac{4}{\kappa_c}\sqrt{a_{2\infty}}\sinh\left(\frac{\Phi_s}{2}\right) \qquad (Z_1{:}Z_1 \text{ electrolyte}) \tag{36}$$

5.2.1.2.2 Contributions from the adsorption and diffuse layers

In general, the *total* adsorption $\widetilde{\Gamma}_i$ of an ionic species include contributions from *both* the adsorption layer (surfactant adsorption layer + adsorbed counterions in the Stern layer), Γ_i, and the diffuse layer, Λ_i:[13,24,26,27]

$$\widetilde{\Gamma}_i = \Gamma_i + \Lambda_i, \qquad \text{where} \qquad \Lambda_i \equiv \int_0^\infty [a_i(z) - a_{i\infty}]\, dz \tag{37}$$

$\widetilde{\Gamma}_i$ represents a surface excess of component *"i"* with respect to the *uniform* bulk solution. Since the solution is electroneutral, one has $\sum_{i=1}^{N} z_i \widetilde{\Gamma}_i = 0$. Note, however, that $\sum_{i=1}^{N} z_i \Gamma_i \neq 0$, see the Gouy equation 33. Expressions for Λ_i can be obtained by using the theory of EDL. For example, because of the electroneutrality of the solution, the right-hand side of Equation 36 is equal to $\Lambda_2 - \Lambda_1 - \Lambda_3$, where

$$\Lambda_2 = 2a_{2\infty}\kappa^{-1}[\exp(\Phi_s/2) - 1]; \qquad \Lambda_j = 2a_{j\infty}\kappa^{-1}[\exp(-\Phi_s/2) - 1], \qquad j = 1,3. \tag{38}$$

($\kappa^2 = \kappa_c^2 I$; Z_1:Z_1 electrolyte). In analogy with Equation 37, the interfacial tension of the solution, σ, can be expressed as a sum of contributions from the adsorption and diffuse layers:[24,27,32]

$$\sigma = \sigma_a + \sigma_d \tag{39}$$

where

$$\sigma_a = \sigma_0 - kTJ \qquad \text{and} \qquad \sigma_d = -\varepsilon_0 \varepsilon \int_0^\infty \left(\frac{d\psi}{dz}\right)^2 dz \tag{40}$$

Expressions for J are given in Table 2 for various types of isotherms. Note that Equations 39 and 40 are valid under both equilibrium and dynamic conditions. In the special case of SDS + NaCl solution (see above), *at equilibrium*, one can use the theory of EDL to express $d\psi/dz$; then from equation 40 one derives[24,27,32]

$$\sigma_d = -\frac{8kT}{\kappa_c}\sqrt{a_{2\infty}}\left[\cosh\left(\frac{\Phi_s}{2}\right) - 1\right] \qquad (Z_1{:}Z_1 \text{ electrolyte, at equilibrium}) \tag{41}$$

Analytical expressions for σ_d for the cases of 2:1, 1:2 and 2:2 electrolytes can be found in References 27 and 35.

In the case of ionic surfactant Equation 1 can be presented in two alternative, but equivalent forms[27,35]

$$d\sigma = -kT\sum_{i=1}^{N}\widetilde{\Gamma}_i\, d\ln a_{i\infty} \qquad (T = \text{const.}) \tag{42}$$

$$d\sigma_a = -kT\sum_{i=1}^{N}\Gamma_i\, d\ln a_{is} \qquad (T = \text{const.}) \tag{43}$$

where $a_{is} = a_i(z{=}0)$ is the "subsurface" value of activity a_i. From equations 29 and 34 one obtains

$$a_{is} = a_{i\infty}\exp(-z_i\Phi_s)\,, \tag{44}$$

The comparison between Equations 42 and 43 shows that the Gibbs adsorption equation can be expressed either in terms of σ, $\widetilde{\Gamma}_i$ and $a_{i\infty}$, or in terms of σ_a, Γ_i and a_{is}. Note that equations 42 and 44 are valid under *equilibrium* conditions, whereas equation 43 can be used also for the description of *dynamic* surface tension (Section 5.2.2) in the case of surfactant adsorption under diffusion control, assuming local equilibrium between adsorptions Γ_i and subsurface concentrations of the respective species.

The expression $\sigma_a = \sigma_0 - kTJ$, with J given in Table 2, can be used for description of both static and dynamic surface tension of ionic and nonionic surfactant solutions. The surfactant adsorption isotherms in this table can be used for both ionic and nonionic surfactants, with the only difference that in the case of ionic surfactant the adsorption constant K depends on the subsurface concentration of the inorganic counterions,[27] see Equation 48 below.

5.2.1.2.3 The effect of counterion binding

As an example, let us consider again the special case of SDS + NaCl solution. In this case, the Gibbs adsorption equation (1.70) takes the form

$$d\sigma_a = -kT(\Gamma_1\, d\ln a_{1s} + \Gamma_2\, d\ln a_{2s}) \tag{45}$$

where, as before, the indices "1" and "2" refer to the DS^- and Na^+ ions, respectively. The differentials in the right-hand side of Equation 45 are independent (one can vary

independently the concentrations of surfactant and salt), and moreover, $d\sigma_a$ is an exact (total) differential. Then, according to the Euler condition, the cross derivatives must be equal:[27]

$$\frac{\partial \Gamma_1}{\partial \ln a_{2s}} = \frac{\partial \Gamma_2}{\partial \ln a_{1s}} \tag{46}$$

A surfactant adsorption isotherm, $\Gamma_1 = \Gamma_1(a_{1s}, a_{2s})$, and a counterion adsorption isotherm, $\Gamma_2 = \Gamma_2(a_{1s}, a_{2s})$, are *thermodynamically compatible* only if they satisfy Equation 46. The counterion adsorption isotherm is usually taken in the form

$$\frac{\Gamma_2}{\Gamma_1} = \frac{K_2 a_{2s}}{1 + K_2 a_{2s}} \qquad \text{(Stern isotherm)} \tag{47}$$

where K_2 is a constant parameter. The latter equation, termed the *Stern isotherm*,[39] describes Langmuirian adsorption (binding) of counterions in the Stern layer. It can be proven that a sufficient condition Γ_2 form Equation 47 to satisfy the Euler's condition 46, together with one of the surfactant adsorption isotherms for Γ_1 in Table 2, is[27]

$$K = K_1(1 + K_2 a_{2s}) \tag{48}$$

where K_1 is another constant parameter. In other words, if K is expressed by Equation 48, the Stern isotherm 47 is thermodynamically compatible with every of the surfactant adsorption isotherms in Table 2. In analogy with Equation 3, the parameters K_1 and K_2 are related to the respective standard free energies of adsorption of surfactant ions and counterions $\Delta\mu_i^{(0)}$:

$$K_i = \frac{\delta_i}{\Gamma_\infty} \exp\left(\frac{\Delta\mu_i^{(0)}}{kT}\right) \qquad (i = 1, 2) \tag{49}$$

where δ_i stands for the thickness of the respective adsorption layer.

5.2.1.2.4 Dependence of adsorption parameter K on salt concentration

The physical meaning of Equation 48 can be revealed by chemical-reaction considerations. For simplicity, let us consider *Langmuir*-type adsorption, i.e., we treat the interface as a two-dimensional lattice. We will use the notation θ_0 for the fraction of the free sites in the lattice, θ_1 for the fraction of sites containing adsorbed surfactant ion S^-, and θ_2 for the fraction of sites containing the complex of an adsorbed surfactant ion + a bound counterion. Obviously,

one can write $\theta_0 + \theta_1 + \theta_2 = 1$. The adsorptions of surfactant ions and counterions can be expressed in the form:

$$\Gamma_1/\Gamma_\infty = \theta_1 + \theta_2 \; ; \qquad \Gamma_2/\Gamma_\infty = \theta_2 \tag{50}$$

Following Kalinin and Radke [119], we consider the "reaction" of adsorption of S^- ions:

$$A_0 + S^- = A_0S^- \tag{51}$$

where A_0 symbolizes an empty adsorption site. In accordance with the rules of the chemical kinetics one can express the rates of adsorption and desorption in the form:

$$r_{1,\mathrm{ads}} = K_{1,\mathrm{ads}}\theta_0\, c_{1\mathrm{s}} \; , \qquad r_{1,\mathrm{des}} = K_{1,\mathrm{des}}\theta_1 \tag{52}$$

where, as before, $c_{1\mathrm{s}}$ is the subsurface concentration of surfactant; $K_{1,\mathrm{ads}}$ and $K_{1,\mathrm{des}}$ are constants. In view of Equation 50 one can write $\theta_0 = (\Gamma_\infty - \Gamma_1)/\Gamma_\infty$ and $\theta_1 = (\Gamma_1 - \Gamma_2)/\Gamma_\infty$. Thus, with the help of Equation 52 we obtain the net adsorption flux of surfactant:

$$Q_1 \equiv r_{1,\mathrm{ads}} - r_{1,\mathrm{des}} = K_{1,\mathrm{ads}}c_{1\mathrm{s}}(\Gamma_\infty - \Gamma_1)/\Gamma_\infty - K_{1,\mathrm{des}}(\Gamma_1 - \Gamma_2)/\Gamma_\infty \tag{53}$$

Next, let us consider the reaction of counterion binding:

$$A_0S^- + M^+ = A_0SM \tag{54}$$

The rates of the direct and reverse reactions are, respectively,

$$r_{2,\mathrm{ads}} = K_{2,\mathrm{ads}}\theta_1\, c_{2\mathrm{s}} \; , \qquad r_{2,\mathrm{des}} = K_{2,\mathrm{des}}\theta_2 \tag{55}$$

where $K_{2,\mathrm{ads}}$ and $K_{2,\mathrm{des}}$ are the respective rate constants, and $c_{2\mathrm{s}}$ is the subsurface concentration of counterions. Having in mind that $\theta_1 = (\Gamma_1 - \Gamma_2)/\Gamma_\infty$ and $\theta_2 = \Gamma_2/\Gamma_\infty$, with the help of Equation 55 we deduce an expression for the adsorption flux of counterions:

$$Q_2 \equiv r_{2,\mathrm{ads}} - r_{2,\mathrm{des}} = K_{2,\mathrm{ads}}\, c_{2\mathrm{s}}(\Gamma_1 - \Gamma_2)/\Gamma_\infty - K_{2,\mathrm{des}}\,\Gamma_2/\Gamma_\infty \tag{56}$$

If we can assume that the reaction of counterion binding is much faster than the surfactant adsorption, then we can set $Q_2 \equiv 0$, and Equation 56 reduces to the Stern isotherm, Equation 47, with $K_2 \equiv K_{2,\mathrm{ads}}/K_{2,\mathrm{des}}$. Next, a substitution of Γ_2 from Equation 47 into Equation 53 yields[35]

$$Q_1 \equiv r_{1,\mathrm{ads}} - r_{1,\mathrm{des}} = K_{1,\mathrm{ads}}\, c_{1\mathrm{s}}(\Gamma_\infty - \Gamma_1)/\Gamma_\infty - K_{1,\mathrm{des}}(1 + K_2\, c_{2\mathrm{s}})^{-1}\,\Gamma_1/\Gamma_\infty \tag{57}$$

Equation 57 shows that the adsorption flux of surfactant is influenced by the subsurface concentration of counterions, $c_{2\mathrm{s}}$. At last, if there is equilibrium between surface and

subsurface, we have to set $Q_1 \equiv 0$ in Equation 57, and thus we obtain the Langmuir isotherm for an ionic surfactant:

$$Kc_{1s} = \Gamma_1/(\Gamma_\infty - \Gamma_1), \qquad \text{with} \qquad K \equiv (K_{1,ads}/K_{1,des})(1 + K_2\, c_{2s}) \tag{58}$$

Note that $K_1 \equiv K_{1,ads}/K_{1,des}$. This result demonstrates that the linear dependence of K on c_{2s} (Equation 48) can be deduced from the reactions of surfactant adsorption and counterion binding, Equations 51 and 54. (For $I < 0.1$ M we have $\gamma_\pm \approx 1$ and then activities and concentrations of the ionic species coincide.)

5.2.1.2.5 Comparison of theory and experiment

As illustration, we consider the interpretation of experimental isotherms by Tajima et al.[38,40,41] for the surface tension σ vs. SDS concentrations at eleven fixed concentrations of NaCl, see Figure 2. Processing the set of data for the interfacial tension $\sigma = \sigma(c_{1\infty}, c_{2\infty})$ as a function of the bulk concentrations of surfactant (DS^-) ions and Na^+ counterions, $c_{1\infty}$ and $c_{2\infty}$, one can determine the surfactant adsorption, $\Gamma_1(c_{1\infty}, c_{2\infty})$, the counterion adsorption, $\Gamma_2(c_{1\infty}, c_{2\infty})$, the surface potential, $\psi_s(c_{1\infty}, c_{2\infty})$, and the Gibbs elasticity $E_G(c_{1\infty}, c_{2\infty})$ for every desirable surfactant and salt concentrations.

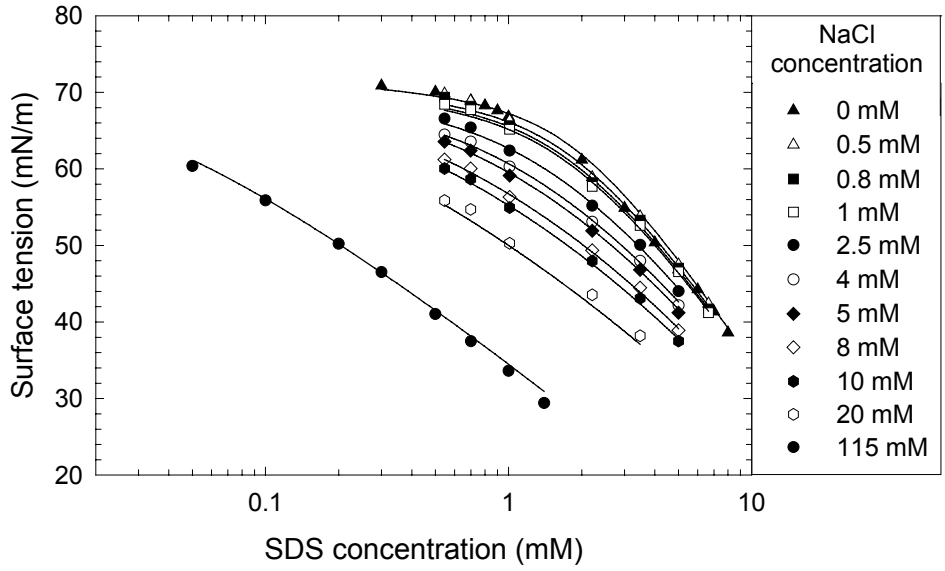

FIGURE 2. Plot of the surface tension σ vs. the concentration of SDS, $c_{1\infty}$, for 11 fixed NaCl concentrations. The symbols are experimental data by Tajima et al.[38,40,41] The lines represent the best fit[42] with the full set of equations specified in the text, involving the van der Waals isotherms of adsorption and surface tension (Table 2).

The theoretical dependence $\sigma = \sigma(c_{1\infty}, c_{2\infty})$ is determined by the following *full set of equations*: Equation 44 for i = 1,2; the Gouy equation 36, Equation 39 (with σ_d expressed by Equation 41 and J from Table 2), the Stern isotherm 47, and one surfactant adsorption isotherm from Table 2, say the van der Waals one. Thus we get a set of 6 equations for determining 6 unknown variables: σ, Φ_s, a_{1s}, a_{2s}, Γ_1 and Γ_2. (For $I < 0.1$ M the activities of the ions can be replaced by the respective concentrations.) The principles of the numerical procedure are described in Reference 27.

The theoretical model contains four parameters, β, Γ_∞, K_1 and K_2, whose values are to be obtained from the best fit of the experimental data. Note that all eleven curves in Figure 2 are fitted simultaneously.[42] In other words, the parameters β, Γ_∞, K_1 and K_2 are the same for all curves. The value of Γ_∞, obtained from the best fit of the data in Figure 2, corresponds to $1/\Gamma_\infty = 31$ Å^2. The respective value of K_1 is 82.2 m^3/mol, which in view of Equation 49 gives a standard free energy of surfactant adsorption $\Delta\mu_1^{(0)} = 12.3\ kT$ per DS^- ion, that is 30.0 kJ/mol. The determined value of K_2 is 8.8×10^{-4} m^3/mol, which after substitution in Equation 49 yields a standard free energy of counterion binding $\Delta\mu_2^{(0)} = 1.9\ kT$ per Na^+ ion, that is 4.7 kJ/mol. The value of the parameter β is positive, $2\beta\Gamma_\infty/kT = +2.89$, which indicates attraction between the hydrocarbon tails of the adsorbed surfactant molecules. However, this attraction is too weak to cause two-dimensional phase transition. The van der Waals isotherm predicts such transition for $2\beta\Gamma_\infty/kT > 6.75$.

Figure 3 shows calculated curves for the adsorptions of surfactant, Γ_1 (the full lines), and counterions, Γ_2 (the dotted lines), vs. the SDS concentration, $c_{1\infty}$. These lines represent the variation of Γ_1 and Γ_2 along the experimental curves, which correspond to the lowest and highest NaCl concentrations in Figure 2, viz. $c_{3\infty}$ = 0 and 115 mM. One sees that both Γ_1 and Γ_2 are markedly greater when NaCl is present in the solution. The highest values of Γ_1 for the curves in Figure 3 are 4.2×10^{-6} mol/m^2 and 4.0×10^{-6} mol/m^2 for the solutions with and without NaCl, respectively. The latter two values compare well with the saturation adsorptions measured by Tajima et al.[40,41] for the same system by means of the radiotracer method, viz. $\Gamma_1 = 4.3 \times 10^{-6}$ mol/m^2 and 3.2×10^{-6} mol/m^2 for the solutions with and without NaCl.

For the solution *without* NaCl the occupancy of the Stern layer, Γ_2/Γ_1 rises from 0.15 to 0.73 and then exhibits a tendency to level off. The latter value is consonant with data of other authors,[43-45] who have obtained values of Γ_2/Γ_1 up to 0.70 – 0.90 for various ionic surfactants; pronounced evidences for counterion binding have been obtained also in experiments with solutions containing surfactant micelles.[46-50] As it could be expected, both Γ_1 and Γ_2 are higher for the solution *with* NaCl. These results imply that the counterion adsorption (binding) should be always taken into account.

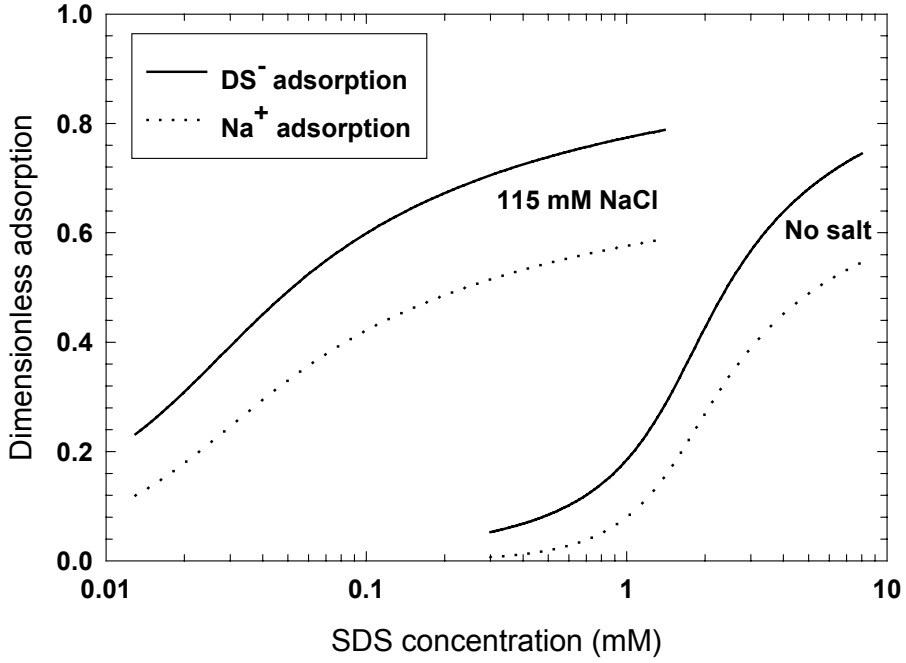

FIGURE 3. Plots of the dimensionless adsorptions of surfactant ions Γ_1/Γ_∞ (DS^-, the full lines), and counterions Γ_2/Γ_∞ (Na^+, the dotted lines), vs. the surfactant (SDS) concentration, $c_{1\infty}$. The lines are calculated[42] for NaCl concentrations 0 and 115 mM using parameter values determined from the best fit of experimental data (Figure 2).

The fit of the data in Figure 2 gives also the values of the surface electric potential, ψ_s. For the solutions with 115 mM NaCl the model predicts surface potentials varying in the range $|\psi_s|$ = 55–95 mV within the experimental interval of surfactant concentrations, whereas for the solution without salt the calculated surface potential is higher: $|\psi_s|$ = 150-180 mV (for SDS ψ_s has a negative sign). Thus it turns out that measurements of surface tension, interpreted by means of an appropriate theoretical model, provide a method for determining the surface potential ψ_s in a broad range of surfactant and salt concentrations. The described approach could be also applied to solve the inverse problem, viz. to process data for the

surface potential. In this way, the adsorption of surfactant on solid particles can be determined from the measured zeta-potential.[51]

5.1.2.2 DYNAMIC SURFACE TENSION

If the surface of an equilibrium surfactant solution is disturbed (expanded, compressed, renewed, etc.), the system will try to restore the equilibrium by exchange of surfactant between the surface and the subsurface layer (adsorption-desorption). The change of the surfactant concentration in the subsurface layer triggers a diffusion flux in the solution. In other words, the process of equilibration (relaxation) of an expanded adsorption monolayer involves two consecutive stages:

(i) diffusion of surfactant molecules from the bulk solution to the subsurface layer and

(ii) transfer of surfactant molecules from the subsurface to the adsorption layer; the rate of transfer is determined by the height of the kinetic barrier to adsorption.

(In the case of desorption the processes have the opposite direction.) Such interfacial expansions are typical for foam generation and emulsification. The rate of adsorption relaxation determines whether the formed bubbles / drops will coalesce upon collision, and in final reckoning – how large will be the foam volume and the emulsion drop-size.[52,53] Below we focus our attention on the relaxation time of surface tension, τ_σ, which characterizes the interfacial dynamics.

The overall rate of surfactant adsorption is controlled by the slowest stage. If it is stage (i), we deal with *diffusion control*, while if stage (ii) is slower, the adsorption occurs under *barrier (kinetic) control*. The next four subsections are dedicated to processes under diffusion control (which are the most frequently observed), whereas in Subsection 5.2.2.5 we consider adsorption under barrier control.

Various experimental methods for dynamic surface tension measurements are available. Their operational time-scales cover different time intervals.[54,55] Methods with a *shorter* characteristic operational time are the oscillating jet method,[56-58] the oscillating bubble method,[59-62] the fast-formed drop technique,[63,64] the surface wave techniques,[65-68] and the maximum bubble pressure method.[69-74] Methods of *longer* characteristic operational time are the inclined plate method,[75,76] the drop-weight/volume techniques,[77-80] the funnel[81] and overflowing cylinder[82] methods; the axisymmetric drop shape analysis (ADSA);[83,84] see References 54, 55 and 85 for a more detailed review.

In this section, devoted to dynamic surface tension, we consider mostly *nonionic* surfactant solutions. In Subsection 5.2.2.4 we address the more complicated case of *ionic* surfactants. We will restrict our considerations to the simplest case of *relaxation of an initial uniform interfacial dilatation*. The more complex case of simultaneous adsorption and dilatation is considered elsewhere.[54,70,74,82,85]

5.2.2.1 Adsorption under Diffusion Control

Here we consider a solution of a *nonionic* surfactant, whose concentration, $c_1 = c_1(z,t)$, depends on the position and time because of the diffusion process. (As before, z denotes the distance to the interface, which is situated in the plane $z = 0$.) Correspondingly, the surface tension, surfactant adsorption and the subsurface concentration of surfactant vary with time: $\sigma = \sigma(t)$, $\Gamma_1 = \Gamma_1(t)$, $c_{1s} = c_{1s}(t)$. The surfactant concentration obeys the equation of diffusion:

$$\frac{\partial c_1}{\partial t} = D_1 \frac{\partial^2 c_1}{\partial z^2} \qquad (z > 0,\ t > 0) \tag{59}$$

where D_1 is the diffusion coefficient of the surfactant molecules. The exchange of surfactant between the solution and its interface is described by the boundary conditions

$$c_1(0,t) = c_{1s}(t), \qquad \frac{d\Gamma_1}{dt} = D_1 \frac{\partial c_1}{\partial z}, \qquad (z = 0,\ t > 0) \tag{60}$$

The latter equation states that the rate of increase of the adsorption Γ_1 is equal to the diffusion influx of surfactant per unit area of the interface. Integrating Equation 59, along with 60, one can derive the equation of Ward and Tordai:[86]

$$\Gamma_1(t) = \Gamma_1(0) + \sqrt{\frac{D_1}{\pi}}\left[2c_{1\infty}\sqrt{t} - \int_0^t \frac{c_{1s}(\tau)}{\sqrt{t-\tau}}\,d\tau\right] \tag{61}$$

Solving Equation 61 together with some of the adsorption isotherms $\Gamma_1 = \Gamma_1(c_{1s})$ in Table 2, one can in principle determine the two unknown functions $\Gamma_1(t)$ and $c_{1s}(t)$. Since the relation $\Gamma_1(c_{1s})$ is nonlinear (except for the Henry isotherm), this problem, or its equivalent formulations, can be solved either numerically,[87] or by employing appropriate approximations.[70,88]

In many cases it is convenient to use asymptotic expressions for the functions $\Gamma_1(t)$, $c_{1s}(t)$ and $\sigma(t)$ for *short times* ($t\to 0$) and *long times* ($t\to\infty$). A general asymptotic expression for the short times can be derived from Equation 61 substituting $c_{1s} \approx c_{1s}(0) = \text{const.}$:

$$\Gamma_1(t) = \Gamma_1(0) + 2\sqrt{D_1/\pi}\,[c_{1\infty} - c_{1s}(0)]\sqrt{t} \qquad (t\to 0) \tag{62}$$

Analogous asymptotic expression can be obtained also for the long times, although the derivation is not so simple. Hansen[89] derived an useful asymptotics for the subsurface concentration:

$$c_{1s}(t) = c_{1\infty} - \frac{\Gamma_{1e} - \Gamma(0)}{\sqrt{\pi D_1 t}} \qquad (t\to\infty) \tag{63}$$

where Γ_{1e} is the equilibrium value of the surfactant adsorption. The validity of Hansen's equation 63 was confirmed in subsequent studies by other authors.[90,91]

Below we continue our review of the asymptotic expressions considering separately the cases of *small* and *large* initial perturbations.

5.2.2.2 Small Initial Perturbation

When the deviation from equilibrium is small, then the adsorption isotherm can be linearized:

$$\Gamma_1(t) - \Gamma_{1e} \approx \left(\frac{\partial\Gamma_1}{\partial c_1}\right)_e \left[c_{1s}(t) - c_e\right] \tag{64}$$

Here and hereafter the subscript "*e*" means that the respective quantity refers to the equilibrium state. The set of linear equations, 59, 60 and 64, has been solved by Sutherland.[92] The result, which describes the relaxation of a *small* initial interfacial dilatation, reads:

$$\frac{\sigma(t) - \sigma_e}{\sigma(0) - \sigma_e} = \frac{\Gamma_1(t) - \Gamma_{1e}}{\Gamma_1(0) - \Gamma_{1e}} = \exp\left(\frac{t}{\tau_\sigma}\right)\text{erfc}\left(\sqrt{\frac{t}{\tau_\sigma}}\right) \tag{65}$$

where

$$\tau_\sigma \equiv \frac{1}{D_1}\left(\frac{\partial\Gamma_1}{\partial c_1}\right)_e^2 \tag{66}$$

is the characteristic relaxation time of surface tension and adsorption, and

$$\mathrm{erfc}(x) \equiv \frac{2}{\sqrt{\pi}} \int_x^{\infty} \exp(-x^2)\, dx \tag{67}$$

is the so called complementary error function.[93,94] The asymptotics of the latter function for small and large values of the argument are:[93,94]

$$\mathrm{erfc}(x) = 1 - \frac{2}{\sqrt{\pi}} x + O(x^3) \quad \text{for } x << 1; \qquad \mathrm{erfc}(x) = \frac{\mathrm{e}^{-x^2}}{\sqrt{\pi}\, x}\left[1 + O\left(\frac{1}{x^2}\right)\right] \quad \text{for } x >> 1 \tag{68}$$

Combining Equations 65 and 68 one obtains the short-time and long-time asymptotics of the surface tension relaxation:

$$\frac{\sigma(t) - \sigma_e}{\sigma(0) - \sigma_e} = \frac{\Gamma_1(t) - \Gamma_{1e}}{\Gamma_1(0) - \Gamma_{1e}} = 1 - \frac{2}{\sqrt{\pi}} \sqrt{\frac{t}{\tau_\sigma}} + O\left[\left(\frac{t}{\tau_\sigma}\right)^{3/2}\right] \qquad (t << \tau_\sigma) \tag{69}$$

$$\frac{\sigma(t) - \sigma_e}{\sigma(0) - \sigma_e} = \frac{\Gamma_1(t) - \Gamma_{1e}}{\Gamma_1(0) - \Gamma_{1e}} = \sqrt{\frac{\tau_\sigma}{\pi t}} + O\left[\left(\frac{\tau_\sigma}{t}\right)^{3/2}\right] \qquad (t << \tau_\sigma) \tag{70}$$

Equation 70 is often used as a test to verify whether the adsorption process is under diffusion control: data for $\sigma(t)$ are plotted vs. $1/\sqrt{t}$ and it is checked if the plot complies with a straight line; moreover, the intercept of the line gives σ_e. We recall that Equations 69 and 70 are valid in the case of a *small* initial perturbation; alternative asymptotic expressions for the case of *large* initial perturbation are considered in the next subsection.

With the help of the thermodynamic equations 2 and 6 one derives

$$\frac{\partial \Gamma_1}{\partial c_1} = \frac{\partial \Gamma_1}{\partial \sigma} \frac{\partial \sigma}{\partial c_1} = \frac{\Gamma_1^2 kT}{c_1 E_G} \tag{71}$$

Thus Equation 66 can be expressed in an alternative form:[35]

$$\tau_\sigma = \frac{1}{D_1} \left(\frac{\Gamma_1^2 kT}{c_1 E_G}\right)_e^2 \tag{72}$$

Substituting E_G from Table 3 into Equation 72 one can obtain expressions for τ_σ corresponding to various adsorption isotherms. In the special case of Langmuir adsorption isotherm one can present Equation 72 in the form[35]

$$\tau_\sigma = \frac{1}{D_1} \frac{(K\Gamma_\infty)^2}{(1 + Kc_1)^4} = \frac{1}{D_1} \frac{(K\Gamma_\infty)^2}{\left(1 + E_G/(\Gamma_\infty kT)\right)^4} \qquad \text{(for Langmuir isotherm)} \tag{73}$$

Equation 73 visualizes the very strong dependence of the relaxation time τ_σ on the surfactant concentration c_1; in general, τ_σ can vary with many orders of magnitude as a function of c_1. Equation 73 shows also that high Gibbs elasticity corresponds to short relaxation time, and vice versa.

As a quantitative example let us take typical parameter values: K_1 = 15 m^3/mol, $1/\Gamma_\infty$ = 40 Å^2, $D_1 = 5.5 \times 10^{-6}$ cm^2/s and T = 298 K. Then with $c_1 = 6.5 \times 10^{-6}$ M, from Table 3 (Langmuir isotherm) and Equation 73 we calculate $E_G \approx 1.0$ mN/m and $\tau_\sigma \approx 5$ s. In the same way, for $c_1 = 6.5 \times 10^{-4}$ M we calculate $E_G \approx 100$ mN/m and $\tau_\sigma \approx 5 \times 10^{-4}$ s.

To directly measure the Gibbs elasticity E_G, or to precisely investigate the dynamics of surface tension, one needs an experimental method, whose characteristic time is smaller compared to τ_σ. Equation 73 and the latter numerical example show that when the surfactant concentration is higher, the experimental method should be faster.

5.2.2.3 Large Initial Perturbation

By definition, we have *large initial perturbation* when at the initial moment the interface is clean of surfactant:

$$\Gamma_1(0) = 0, \qquad c_{1s}(0) = 0 \tag{74}$$

In such case, the Hansen equation 63 reduces to

$$c_{1s}(t) = c_{1\infty} - \frac{\Gamma_{1e}}{\sqrt{\pi D_1 t}} \qquad (t \to \infty) \tag{75}$$

By substituting $c_{1s}(t)$ for c_1 in the Gibbs adsorption equation 2, and integrating, one obtains the long-time asymptotics of the surface tension of a nonionic surfactant solution after a large initial perturbation:

$$\sigma(t) - \sigma_e = \left(\frac{\Gamma_1^2 kT}{c_1}\right)_e \left(\frac{1}{\pi D_1 t}\right)^{1/2} \qquad \text{(large initial perturbation)} \tag{76}$$

with the help of Equation 72 one can bring Equation 76 into another form:

$$\sigma(t) - \sigma_e = E_G \left(\frac{\tau_\sigma}{\pi t}\right)^{1/2} \qquad \text{(large initial perturbation)} \tag{77}$$

where E_G is given in Table 3. It is interesting to note that Equation 77 is applicable to both nonionic and ionic surfactants with the only difference that for nonionics τ_σ is given by Equation 66, whereas for ionic surfactants the expression for τ_σ is somewhat longer, see References 35 and 95.

The above equations show that in the case of adsorption under diffusion control the long-lime asymptotics can be expressed in the form

$$\sigma = \sigma_e + S t^{-1/2} \tag{78}$$

In view of Equations 70 and 77, the slope S of the dependence σ vs. $t^{-1/2}$ is given by the expressions[95]

$$S_s = [\sigma(0) - \sigma_e]\left(\frac{\tau_\sigma}{\pi}\right)^{1/2} \qquad \text{(small perturbation)} \tag{79}$$

$$S_l = E_G\left(\frac{\tau_\sigma}{\pi}\right)^{1/2} \qquad \text{(large perturbation)} \tag{80}$$

As known, the surfactant adsorption Γ_1 monotonically increases with the rise of the surfactant concentration, c_1. In contrast, the slope S_l is a non-monotonic function of c_1: S_l exhibits a maximum at a certain concentration. To demonstrate that we will use the expression

$$S_l = \frac{\Gamma_1^2 kT}{c_1\sqrt{\pi D_1}} \tag{81}$$

which follows from Equations 76 and 78. In Equation 81 we substitute the expressions for c_1 stemming from the Langmuir and Volmer adsorption isotherms (Table 2 with $c_1 = a_{1s}$); the result reads

$$\widetilde{S}_l = \theta(1-\theta) \qquad \text{(for Langmuir isotherm)} \tag{82}$$

$$\widetilde{S}_l = \theta(1-\theta)\exp\left(-\frac{\theta}{1-\theta}\right) \qquad \text{(for Volmer isotherm)} \tag{83}$$

where θ and $\widetilde{S}_l$ are the dimensionless adsorption and slope coefficient:

$$\theta = \Gamma_{1e}/\Gamma_\infty, \qquad \widetilde{S}_l = \frac{S_l\sqrt{\pi D_1}}{kT\,K\,\Gamma_\infty^2} \tag{84}$$

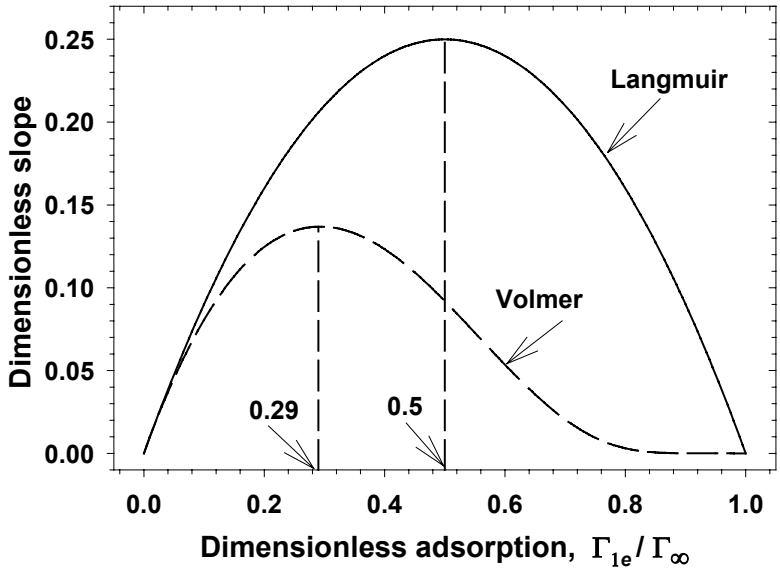

FIGURE 4. Plot of the dimensionless slope, $\widetilde{S}_l$, vs. the dimensionless equilibrium surfactant adsorption, $\theta = \Gamma_{1e}/\Gamma_\infty$, in accordance with Equations 82 and 83, corresponding to the cases of localized and non-localized adsorption.

Figure 4 compares the dependencies $\widetilde{S}_l(\theta)$ given by Equations 82 and 83: one sees that the former is symmetric and has a maximum at $\theta = 0.5$, whereas the latter is asymmetric with a maximum at $\theta \approx 0.29$. We recall that the Langmuir and Volmer isotherms correspond to *localized* and *non-localized* adsorption, respectively (see Section 5.2.1.1.2). Then Figure 4 shows that the symmetry / asymmetry of the plot $\widetilde{S}_l$ vs. θ provides a *test* for verifying whether the adsorption is localized or non-localized. (The practice shows that the fits of *equilibrium* surface tension isotherms do not provide such a test: theoretical isotherms corresponding to localized and non-localized adsorption are found to fit equally well surface tension data!)

From another viewpoint, the non-monotonic behavior of $S_l(\theta)$ can be interpreted as follows. Equation 80 shows that $S_l \propto E_G\sqrt{\tau_\sigma}$; then the non-monotonic behavior stems from the fact that E_G is an increasing function of c_1, whereas τ_σ is a decreasing function of c_1. This qualitative conclusion is valid also for the case of ionic surfactant, as demonstrated in the next section.

5.2.2.4 Generalization for Ionic Surfactants

In the case of ionic surfactants the dynamics of adsorption is more complicated because of the presence of a dynamic electric double layer. Indeed, the adsorption of surfactant at the interface creates surface charge, which is increasing in the course of the adsorption process. The charged interface repels the new-coming surfactant molecules, but attracts the conversely charged counterions (Figure 1); some of them bind to the surfactant headgroups thus decreasing the surface charge density and favoring the adsorption of new surfactant molecules. The theoretical description of the overall adsorption process involves the (electro)diffusion equations for the surfactant ions, counterions and coions, and the Poisson equation from electrodynamics. Different analytical and numerical approaches to the solution of this problem have been proposed.[13, 95-102] Below we describe an approach to the dynamics of ionic surfactant adsorption which is simpler both as a concept, and as a computer-program realization, but agrees very well with the experiment.

Two time scales can be distinguished in the adsorption process of ionic species. The first time-scale is characterized by the diffusion relaxation time of the electric double layer, $t_{\mathrm{edl}} = 1/(D_1 \kappa_{\mathrm{c}}^2 I)$, see Equations 32 and 34 above. It accounts for the interplay of electrostatic interactions and diffusion. The second scale is provided by the characteristic time of the used experimental method, t_{exp}, viz. the minimum interfacial age which can be achieved with the given method; typically $t_{\mathrm{exp}} \geq 5 \times 10^{-3}$ s. For example, if the diffusivity is $D_1 = 5.5 \times 10^{-10}$ m^2/s, for $I = 10^{-5}$ M and 10^{-2} M one calculates, correspondingly, $t_{\mathrm{edl}} = 1.7 \times 10^{-5}$ and 1.7×10^{-8} s. One sees that $\varepsilon \equiv t_{\mathrm{edl}} / t_{\mathrm{exp}}$ 1 is a small parameter. The presence of such small parameter implies the existence of two characteristic length scales: *inner* (in the EDL) $l_{\mathrm{in}} \equiv (D_1 t_{\mathrm{edl}})^{1/2}$ and outer (outside the EDL) $l_{\mathrm{out}} \equiv (D_1 t_{\mathrm{exp}})^{1/2}$. In fact, l_{in} characterizes the width of the layer in which the variation of the ionic concentrations is governed by the electric field, whereas l_{out} scales the width of the zone in which the concentrations of the species vary due to the diffusion. Next, one can apply the method of the matched inner and outer asymptotic expansions[103] to solve the problem. Without entering into mathematical details, here we outline the final results and the computational procedure, which is relatively simple:[104]

In the outer zone, where the electrical field is zero one obtains a generalized version of the Hansen equation 75 for all diffusing species:

$$c_{i,\mathrm{b}} = c_{i\infty} - \frac{\widetilde{\Gamma}_{i,e}}{\sqrt{\pi D_i t}} \tag{85}$$

where $c_{i,\mathrm{b}}$ is the concentration of the respective ion at the inner boundary of the outer zone, D_i is diffusion coefficient, and $\widetilde{\Gamma}_{i,e}$ is the total equilibrium adsorption of the respective species, see Equations 37 and 38. In Section 5.2.1.2.5 we specified the full set of equations which allow one to calculate all equilibrium parameters, supposedly the constants β, Γ_∞, K_1 and K_2 are determined from the best fit of experimental data – see the discussion related to Figure 2. (In the simpler case of nonionic surfactant the full set of equations reduces to a couple of corresponding adsorption and surface tension isotherms from Table 2, which enables one to calculate Γ_1 and σ for each given value of c_1.) The computational procedure for the dynamic problem is the following one:

1. One calculates $\Gamma_{i,e}$ using the full set of equations in Section 5.2.1.2.5;

2. Next, from Equation 85 one calculates $c_{i,\mathrm{b}}(t)$ for a set of values of t in the experimental time interval;

3. Further, in the full set of equations in Section 5.2.1.2.5 one replaces everywhere $c_{i\infty}$ with $c_{i,\mathrm{b}}(t)$; then, for each value of t, we solve this system of equations to determine the functions $\Gamma_i(t)$, $\Phi_s(t)$ and $\sigma(t)$. In the long-time limit one can determine also $S_l = \partial\sigma/\partial t^{-1/2}$.

The justification of this procedure can be accomplished by means of the method of the matched asymptotic expansions.[104]

Comparison of theory and experiment. To illustrate how the theory compares with the experiment, in Figure 5 we present five experimental curves for $\sigma(t)$ corresponding to five different surfactant concentrations, at fixed concentration of added electrolyte, 12 mM NaCl. The surfactant is sodium dodecyl-benzene-sulfonate (DDBS). (This specific sample was a technical product containing 82.6 wt% pure DDBS and 17.4 wt% Na_2SO_4.) The dynamic surface tension $\sigma(t)$ was measured by means of the fast formed drop (FFD) technique.[63,64] The method consists in a sudden formation of a drop at the orifice of a capillary by a quick breaking of a jet of surfactant solution which flows out of the capillary. Thus a fresh curved interface is formed at the capillary tip. The surfactant adsorbs at the immobile curved interface and, consequently, the surface tension and the pressure inside the drop decrease with time; the pressure is registered by means of a piezo-transducer, whose electric output can be

converted in terms of surface tension by using the Laplace equation of capillarity. In this way, the curves for $\sigma(t)$ in Figure 5 were obtained.[104] The capillary pressure was recorded every 0.1 s, which gives a large number of experimental points and provides a good statistics. In addition, equilibrium surface tension isotherms have been obtained and processed as explained in Section 5.2.1.2.5 to determine the parameters β, Γ_∞ , K_1, K_2, etc. The van der Waals isotherm (Table 2) has been employed.

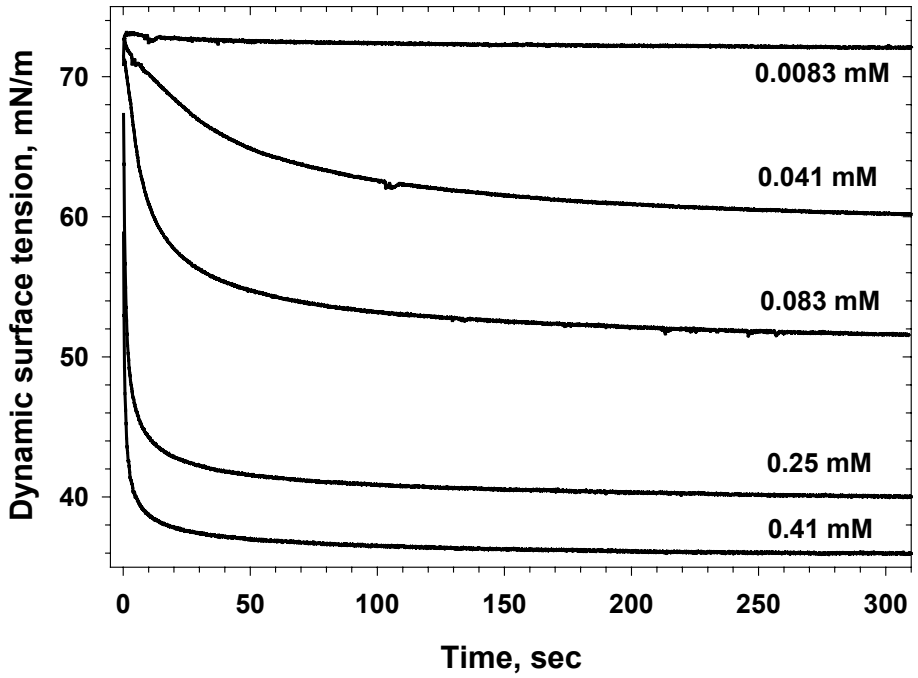

FIGURE 5. Experimental curves[104] for the relaxation of surface tension σ with time t for five fixed concentrations (denoted in the figure) of sodium dodecyl-benzene-sulfonate (DDBS). The solutions contain 12 mM added NaCl, and Na_2SO_4 whose concentration is 21 wt% of that of DDBS.

The long-time portions of the curves in Figure 5, plotted as σ vs. $t^{-1/2}$, comply very well with straight lines, whose slopes, S_l, are plotted in Figure 6a – the points. The theoretical curve for S_l is calculated using the procedure given after Equation 85. The curve is obtained using only the parameters of the equilibrium surface tension isotherm and the diffusion coefficients of the ionic species. One sees that the agreement between theory and experiment is excellent. (No adjustable parameters have been used to fit the dynamic data.) The plot in Figure 6a exhibits a maximum, in agreement with our expectations (see Section 5.2.2.3).

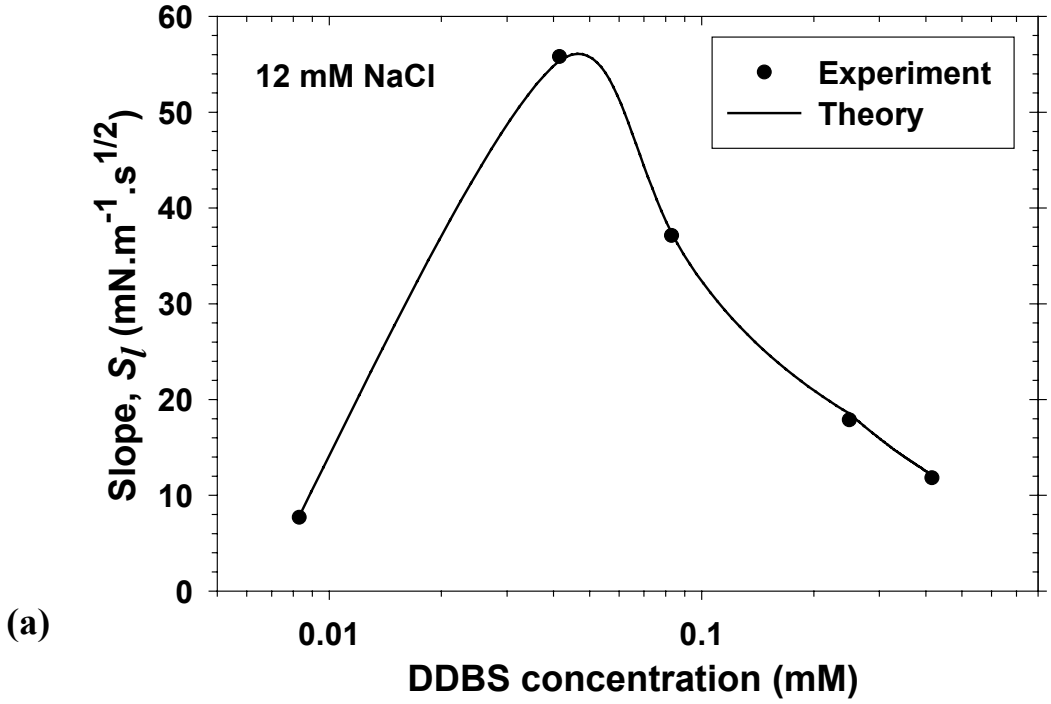

(a)

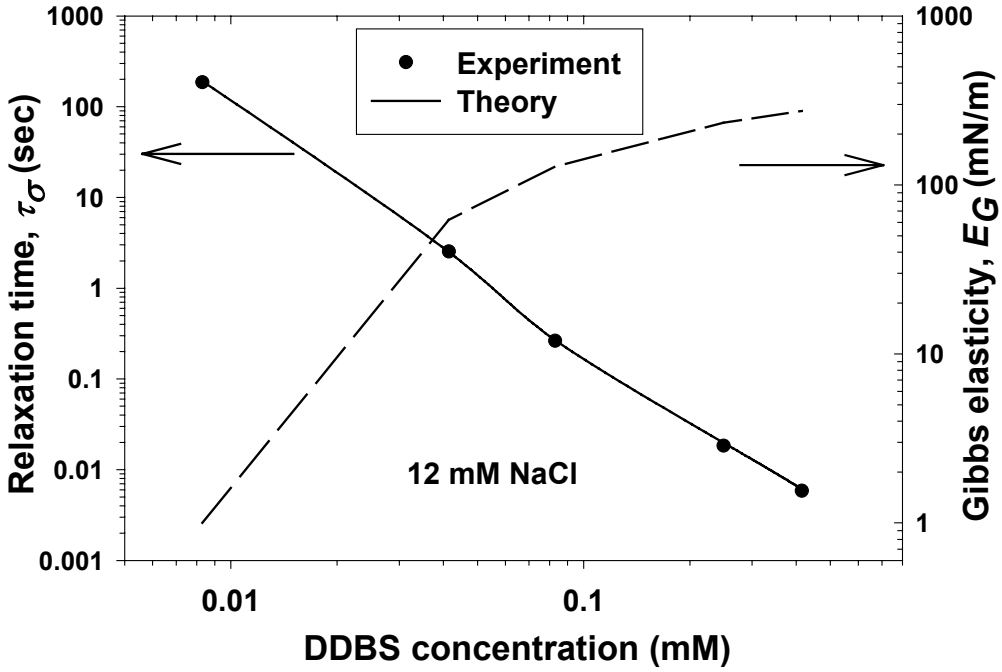

(b)

FIGURE 6. (a) Plot of the slope coefficient S_l vs. the surfactant (DDBS) concentration; the points are the values of S_l for the curves in Figure 5; the line is theoretical curve obtained using the procedure described after Equation 85 (no adjustable parameters). (b) Plots of the relaxation time τ_σ and the Gibbs elasticity E_G vs. the DDBS concentration; E_G is computed from the equilibrium surface tension isotherm; $\tau_\sigma = \pi(S_l/E_G)^2$ is calculated using the above values of S_l.

The comparison between theory and experiment could be carried out also in terms of the relaxation time of the surface tension, τ_σ. One can use the connection $\tau_\sigma = \pi (S_l/E_G)^2$, which follows from Equation 80. The Gibbs elasticity E_G is calculated from the van der Waals expression in Table 3. The results for τ_σ and E_G are shown in Figure 6b. One sees the wide range of variation of the characteristic relaxation time τ_σ, which varies with more than 4 orders of magnitude in the investigated range of concentrations. Moreover, one sees that for the higher surfactant concentrations, the so called "long-time" relaxation could be effectuated within 0.01–0.1 seconds. On the other hand, for the low surfactant concentrations the relaxation can be longer than 100 s. In part, this variation of the relaxation time t_σ with orders of magnitude is due to the strong variation of the surface elasticity E_G with the surfactant concentration, see the right-hand curve in Figure 6b.

5.2.2.5 Adsorption under Barrier Control

In general, the adsorption is under barrier (kinetic, transfer) control when the stage of surfactant transfer from the subsurface to the surface is much slower than the diffusion stage because of some kinetic barrier. The latter can be due to steric hindrance, spatial reorientation or conformational changes accompanying the adsorption of molecules, including destruction of the shells of oriented water molecules wrapping the surfactant hydrocarbon tail in water.[105] We will restrict our considerations to the case of pure barrier control, without double layer effects. In such case the surfactant concentration is uniform throughout the solution, c_1 = const., and the increase of the adsorption $\Gamma_1(t)$ is solely determined by the transitions of surfactant molecules over the adsorption barrier, separating subsurface from surface:

$$\frac{d\Gamma_1}{dt} = Q \equiv r_{\text{ads}}(c_1, \Gamma_1) - r_{\text{des}}(\Gamma_1) \tag{86}$$

r_{ads} and r_{des} are the rates of surfactant adsorption and desorption. The concept of barrier-limited adsorption originates from the works of Bond and Puls,[106] and Doss,[107] and has been further developed by other authors.[108-115] Table 5 summarizes some expressions for the total rate of adsorption under barrier control, Q. The quantities K_{ads} and K_{des} in Table 5 are the rate constants of adsorption and desorption, respectively. Their ratio is equal to the equilibrium constant of adsorption

$$K_{\text{ads}} / K_{\text{des}} = K\,, \tag{87}$$

Table 5. Rate of Surfactant Adsorption for Different Kinetic Models

Type of isotherm	Rate of reversible adsorption $Q = r_{\text{ads}}(c_1, \Gamma_1) - r_{\text{des}}(\Gamma_1)$
Henry	$Q = K_{\text{ads}}\, c_1 - K_{\text{des}}\Gamma_1/\Gamma_\infty$
Freundlich	$Q = K_{\text{ads}}\, K^{m-1}\, c_1^m - K_{\text{des}}\Gamma_1/\Gamma_\infty$
Langmuir	$Q = K_{\text{ads}}\, c_1\left(1 - \dfrac{\Gamma_1}{\Gamma_\infty}\right) - K_{\text{des}}\Gamma_1/\Gamma_\infty$
Frumkin	$Q = K_{\text{ads}} c_1\left(1 - \dfrac{\Gamma_1}{\Gamma_\infty}\right) - K_{\text{des}}\dfrac{\Gamma_1}{\Gamma_\infty}\exp\left(-\dfrac{2\beta\Gamma_1}{kT}\right)$
Volmer	$Q = K_{\text{ads}} c_1 - K_{\text{des}}\dfrac{\Gamma_1}{\Gamma_\infty - \Gamma_1}\exp\left(\dfrac{\Gamma_1}{\Gamma_\infty - \Gamma_1}\right)$
van der Waals	$Q = K_{\text{ads}} c_1 - K_{\text{des}}\dfrac{\Gamma_1}{\Gamma_\infty - \Gamma_1}\exp\left(\dfrac{\Gamma_1}{\Gamma_\infty - \Gamma_1} - \dfrac{2\beta\Gamma_1}{kT}\right)$

The parameters Γ_∞ and K are the same as in Tables 2–4. Setting $Q = 0$ (assuming equilibrium surface–subsurface), from each expression in Table 5 one deduces the respective equilibrium adsorption isotherm in Table 2. In addition, for $\beta = 0$ the expressions for Q related to the Frumkin and van der Waals model reduce, respectively, to the expressions for Q in the Langmuir and Volmer models. For $\Gamma_1 << \Gamma_\infty$ both the Frumkin and Langmuir expressions in Table 5 reduce to the Henry expression.

Substituting Q from Table 5 into Equation 86, and integrating, one can derive explicit expressions for the relaxation of surfactant adsorption:

$$\frac{\sigma(t) - \sigma_e}{\sigma(0) - \sigma_e} \approx \frac{\Gamma_1(t) - \Gamma_{1,e}}{\Gamma_1(0) - \Gamma_{1,e}} = \exp\left(-\frac{t}{\tau_\sigma}\right) \tag{88}$$

Equation 88 holds for $\sigma(t)$ only in the case of small deviations from equilibrium, whereas there is not such a restriction concerning $\Gamma_1(t)$; the relaxation time in Equation 88 is given by the expressions

$$\tau_\sigma = \left(K_{\mathrm{des}} / \Gamma_\infty\right)^{-1} \qquad \text{(Henry and Freundlich)} \qquad (89)$$

$$\tau_\sigma = \left(\frac{K_{\mathrm{des}}}{\Gamma_\infty} + \frac{K_{\mathrm{ads}} c_1}{\Gamma_\infty}\right)^{-1} \qquad \text{(Langmuir)} \qquad (90)$$

Equation 88 predicts that the perturbation of surface tension, $\Delta\sigma(t) = \sigma(t) - \sigma_e$, relaxes exponentially. This is an important difference with the cases of adsorption under diffusion and electro-diffusion control, for which $\Delta\sigma(t) \propto 1/\sqrt{t}$, cf. Equations 70, 76 and 78. Thus a test whether or not the adsorption occurs under purely barrier control is to plot data for $\ln[\Delta\sigma(t)]$ vs. t and to check if the plot complies with a straight line.

In the case of *ionic* surfactants the adsorption of surfactant ions is accompanied by binding of counterions. In addition, the concentrations of the ionic species vary across the electric double layer (even at equilibrium). These effects are taken into account in Equation 57, which can be used as an expression for Q in the case of Langmuirian barrier adsorption of an ionic surfactant.

In fact, a pure barrier regime of adsorption is not frequently observed. It is expected that the barrier becomes more important for substances of low surface activity and high concentration in the solution. Such adsorption regime was observed with propanol, pentanol, 1,6 hexanoic acid, etc. – see Reference 85 for details.

It may happen that the characteristic times of diffusion and transfer across the barrier are comparable. In such case we deal with *mixed* kinetic regime of adsorption. Insofar as the stages of diffusion and transfer are consecutive, the boundary conditions at the interface are

$$\frac{d\,\Gamma_1}{d\,t} = r_{\mathrm{ads}}(c_1, \Gamma_1) - r_{\mathrm{des}}(\Gamma_1) = D_1\left(\frac{\partial c_1}{\partial t}\right)_{z=0} \qquad (91)$$

The formal transition in Equation 91 from mixed to diffusion control of adsorption is not trivial and demands application of scaling and asymptotic expansions. The criterion for occurrence of adsorption under diffusion control (presence of equilibrium between subsurface and surface) is

$$\frac{a\,K_{\mathrm{des}}}{D_1}\left(\frac{\partial\,\Gamma_1}{\partial\,c_1}\right)_e >> 1 \qquad (92)$$

where a is a characteristic thickness of the diffusion layer.

An important difference between the regimes of diffusion and barrier control is in the form of the respective initial conditions. In the case of large initial deformations these are

$$\Gamma_1(0) = 0, \qquad c_{1s}(0) = 0 \qquad \text{(diffusion control)} \tag{93}$$

$$\Gamma_1(0) = 0, \qquad c_{1s}(0) = c_{1\infty} \qquad \text{(barrier control)} \tag{94}$$

Equation 93 reflects the fact that in diffusion regime the surface is always assumed to be equilibrated with the subsurface. In particular, if $\Gamma_1 = 0$, then one must have $c_{1s} = 0$. In contrast, Equation 94 stems from the presence of barrier: for time intervals shorter than the characteristic time of transfer, the removal of the surfactant from the interface ($\Gamma_1 = 0$) cannot affect the subsurface layer (because of the barrier) and then $c_{1s}(0) = c_{1\infty}$. This purely theoretical consideration implies that the effect of barrier could show up at the short times of adsorption, whereas at the long times the adsorption will occur under diffusion control.[116] The existence of barrier-affected adsorption regime at the short adsorption times could be confirmed or rejected by means of the fastest methods for measurement of dynamic surface tension.

5.3 CAPILLARY HYDROSTATICS AND THERMODYNAMICS

5.3.1 SHAPES OF FLUID INTERFACES

5.3.1.1 Laplace and Young Equations

A necessary condition for mechanical equilibrium of a fluid interface is the Laplace equation of capillarity[117-120]

$$2H\sigma = \Delta P \tag{95}$$

Here H is the local mean curvature of the interface and ΔP is the local jump of the pressure across the interface. If $z = z(x, y)$ is the equation of the interface in Cartesian coordinates, then H can be expressed in the form[120]

$$2H = \nabla_s \cdot \left[\frac{\nabla_s z}{\left(1 + |\nabla_s z|^2\right)^{1/2}} \right] \tag{96}$$

where ∇_s is the gradient operator in the plane xy. More general expressions for H can be found in the literature on differential geometry.[120-122] Equation 95, along with Equation 96, represents a second order partial differential equation which determines the shape of the fluid interface. The interface is bounded by a *three-phase contact line* at which the boundary conditions for the differential equation are formulated. The latter are the respective necessary conditions for mechanical equilibrium at the contact lines. When one of the three phases is solid (Figure 7(a)), the boundary condition takes the form of the Young[123] equation:

$$\sigma_{12} \cos \alpha = \sigma_{1s} - \sigma_{2s} \tag{97}$$

where α is the three-phase contact angle, σ_{12} is the tension of the interface between the fluid phases 1 and 2, whereas σ_{1s} and σ_{2s} are the tensions of the two fluid-solid interfaces. Insofar as the values of the three σ's are determined by the intermolecular forces, the contact angle α is a material characteristics of a given three phase system. However, when the solid is not smooth and chemically homogeneous, then the contact angle exhibits hysteresis, i.e., α has no defined equilibrium value.[6, 124] Contact angle hysteresis can be observed even with molecularly smooth and homogeneous interfaces under dynamic conditions.[125]

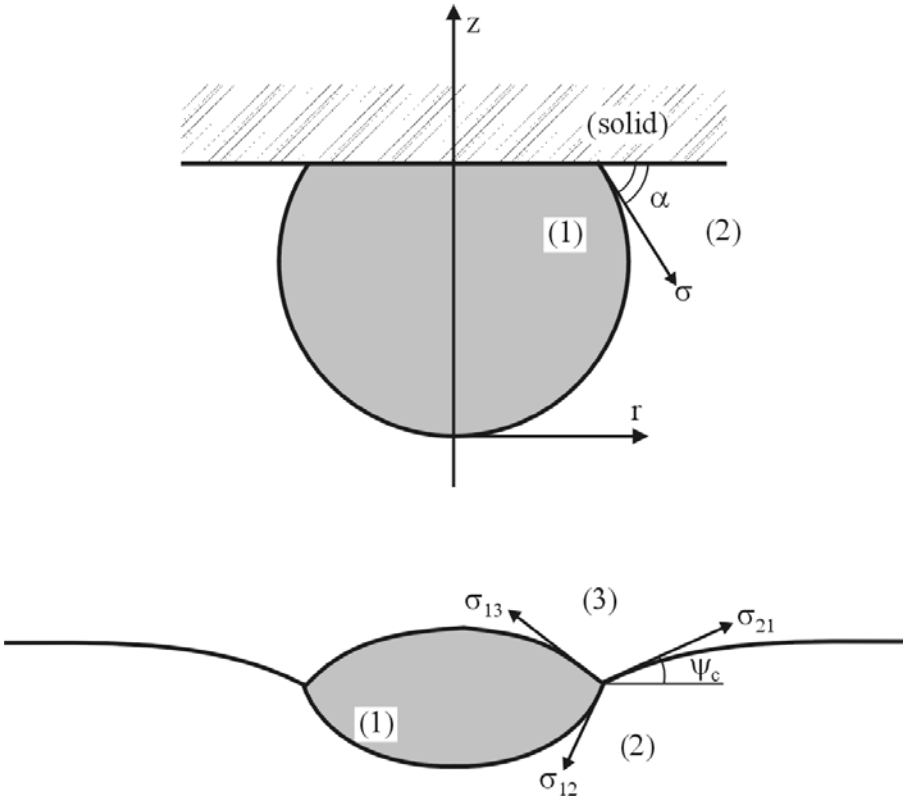

FIGURE 7. Sketch of fluid particle (1) attached to an interface. (a) Fluid particle attached to solid interface; α is the contact angle; σ is the interfacial tension of the boundary between the two fluid phases. (b) Fluid particle attached to a fluid interface; σ_{12}, σ_{13} and σ_{23} are the interfacial tensions between the respective phases; ψ_c is the slope angle of the outer meniscus at the contact line.

When all the three neighboring phases are fluid, then the boundary condition takes the form of the Neumann[126] vectorial triangle:

$$\sigma_{12}\,\boldsymbol{\nu}_{12} + \sigma_{13}\,\boldsymbol{\nu}_{13} + \sigma_{23}\,\boldsymbol{\nu}_{23} = 0 \tag{98}$$

(see Figure 7(b)); here $\boldsymbol{\nu}_{ik}$ is a unit vector, which is simultaneously normal to the contact line and tangential to the boundary between phases i and k. The Laplace, Young and Neumann equations can be derived as conditions for minimum of the free energy of the system;[35,120,127] the effect of the line tension can be also taken into account in Equations 97 and 98.[127]

In the special case of spherical interface $H = 1/R$, with R being the sphere radius, and Equation 95 takes its most popular form, $2\sigma/R = \Delta P$. In the case of axisymmetric meniscus (z – axis of symmetry, Figure 7) the Laplace equation reduces to either of the following two equivalent forms:[119,128]

$$\frac{1}{r}\frac{d}{dr}\left[\frac{rz'}{\left(1+z'^2\right)^{1/2}}\right]=\frac{\Delta P}{\sigma}, \qquad z=z(r) \tag{99}$$

$$-\frac{r''}{\left(1+r'^2\right)^{3/2}}+\frac{1}{r\left(1+r'^2\right)^{1/2}}=\frac{\Delta P}{\sigma}, \qquad r=r(z) \tag{100}$$

Two equivalent parametric forms of Laplace equation are often used for calculations:[119,128]

$$\frac{d\sin\varphi}{dr}+\frac{\sin\varphi}{r}=\frac{\Delta P}{\sigma}, \qquad \tan\varphi=\frac{dz}{dr} \tag{101}$$

or

$$\frac{d\varphi}{ds}=\frac{\Delta P}{\sigma}-\frac{\sin\varphi}{r}, \qquad \frac{dr}{ds}=\cos\varphi, \qquad \frac{dz}{ds}=\sin\varphi \tag{102}$$

Here, φ is the meniscus running slope angle (Figure 7(a)) and s is the arc length along the generatrix of the meniscus. Equation 102 is especially convenient for numerical integration, whereas Equation 101 may create numerical problems at the points with $\tan\varphi = \pm\infty$, like the particle equator in Figure 7(a). A generalized form of Equation 101, with account for the interfacial (membrane) bending elastic modulus, k_c,

$$\sigma\left(\frac{d\sin\varphi}{dr}+\frac{\sin\varphi}{r}\right)=\Delta P+\frac{k_c}{r}\cos\varphi\frac{d}{dr}\left\{r\cos\varphi\frac{d}{dr}\left[\frac{1}{r}\frac{d}{dr}(r\sin\varphi)\right]\right\} \tag{103}$$

serves for description of the axisymmetric configurations of real and model cell membranes.[35,129,130] The Laplace equation can be generalized to account also for the interfacial bending moment (spontaneous curvature), shear elasticity, etc., for review see References 35 and 129. The latter effects are physically important for systems or phenomena like capillary waves,[131] lipid membranes,[132,133] emulsions,[134] and microemulsions.[135]

5.3.1.2 Solutions of Laplace Equations for Menisci of Different Geometry

Very often the capillary menisci have rotational symmetry. In general, there are three types of axially symmetric menisci corresponding to the three regions denoted in Figure 8: (1) Meniscus meeting the axis of revolution, (2) Meniscus decaying at infinity, and (3) Meniscus confined between two cylinders, $0<R_1<r<R_2<\infty$. These three cases are separately considered below.

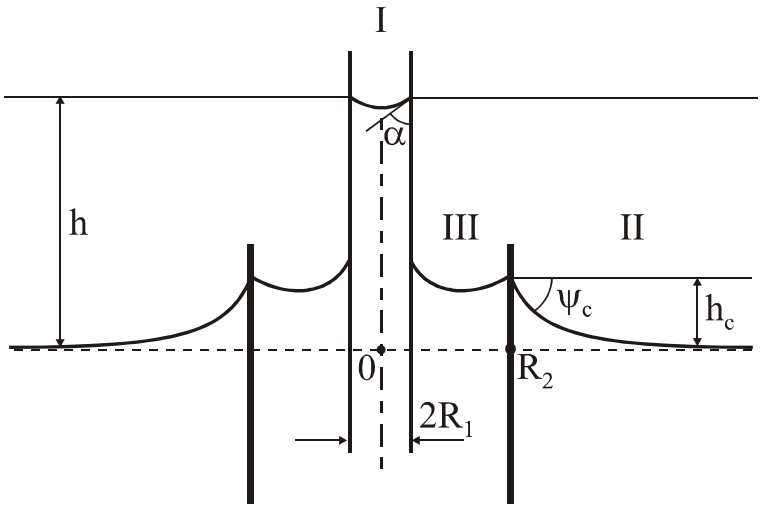

FUGURE 8. Capillary menisci formed around two coaxial cylinders of radii R_1 and R_2. (I) Meniscus meeting the axis of revolution; (II) meniscus decaying at infinity; (III) meniscus confined between the two cylinders. h denotes the capillary raise of the liquid in the inner cylinder; h_c is the elevation of meniscus II at the contact line $r = R_2$.

5.3.1.2.1 Meniscus meeting the axis of revolution

This includes the cases of a bubble/droplet under a plate (Figure 7(a)), the two surfaces of a floating lens (Figure 8(b)), and any kind of sessile or pendant droplets/bubbles. Such a meniscus is a part of a sphere when the effect of gravity is negligible, that is when

$$\Delta\rho\, g\, b^2 / \sigma << 1 \tag{104}$$

Here g is the gravity acceleration, $\Delta\rho$ is the difference in the mass densities of the lower and the upper fluid and b is a characteristic radius of the meniscus curvature. For example, if Equation 104 is satisfied with $b = R_1$ (see Figure 8), the raise, h, of the liquid in the capillary is determined by means of the equation[6]

$$h = (2\sigma\cos\alpha)/(\Delta\rho g R_1) \tag{105}$$

When the gravity effect is not negligible, the capillary pressure, ΔP, becomes dependent on the z-coordinate:

$$\Delta P = 2\sigma / b + \Delta\rho g z \tag{106}$$

Here b is the radius of curvature at the particle apex, where the two principal curvatures are equal (e.g., the bottom of the bubble in Figure 7(a)). Unfortunately, Equation 99, along with Equation 106, has no closed analytical solution. The meniscus shape can be exactly determined by numerical integration of Equation 102. Alternatively, various approximate

expressions are available.[128,136,137] For example, if the meniscus slope is small, $z'^2 << 1$, Equation 99 reduces to a linear differential equation of Bessel type, whose solution reads

$$z(r) = 2[I_0(qr) - 1]/(bq^2) \qquad q \equiv (\Delta\rho g/\sigma)^{1/2} \tag{107}$$

where $I_0(x)$ is the modified Bessel function of the first kind and zeroth order.[138,139] Equation 107 describes the shape of the lower surface of the lens in Figure 7(b); similar expression can be derived also for the upper lens surface.

5.3.1.2.2 Meniscus decaying at infinity

Examples are the outer menisci in Figures 7(b) and 8. In this case the action of gravity cannot be neglected insofar as the gravity keeps the interface flat far from the contact line. The capillary pressure is

$$\Delta P = \Delta\rho g z \tag{108}$$

As mentioned above, Equation 99, along with Equation 108, has no closed analytical solution. On the other hand, the region far from the contact line has always small slope, $z'^2 << 1$. In this region Equation 99 can be linearized, and then in analogy with Equation 107 one derives

$$z(r) = A\, K_0(qr) \qquad (z'^2 << 1) \tag{109}$$

where A is a constant of integration and $K_0(x)$ is the modified Bessel function of the second kind and zeroth order.[138,139] The numerical integration of Equation 102 can be carried out by using the boundary condition[47] $z'/z = -qK_1(qr)/K_0(qr)$ for some appropriately fixed $r << q^{-1}$ (see Equation 109). Alternatively, approximate analytical solutions of the problem are available.[128,137,140] In particular, Derjaguin[141] has derived an asymptotic formula for the elevation of the contact line at the outer surface of a thin cylinder,

$$h_c = -R_1 \sin\psi_c \ln[qR_1\gamma_e(1+\cos\psi_c)/4], \qquad (qR_1)^2 << 1 \tag{110}$$

where R_1 is the radius of the contact line, ψ_c is the meniscus slope angle at the contact line (Figure 8), q is defined by Equation 107 and $\gamma_e = 1.781\ 072\ 418...$is the constant of Euler-Masceroni.[139]

5.3.1.2.3 Meniscus confined between two cylinders ($0 < R_1 < r < R_2 < \infty$)

This is the case with the Plateau borders in real foams and emulsions, and with the model films in the Scheludko cell;[142,143] such is the configuration of the capillary bridges

(Figure 9(a)) and of the fluid particles pressed between two surfaces (Figure 9(b)). When the gravitational deformation of the meniscus cannot be neglected, the interfacial shape can be determined by numerical integration of Equation 102, or by iteration procedure.[144] When the meniscus deformation caused by gravity is negligible, analytical solution can be found as described below.

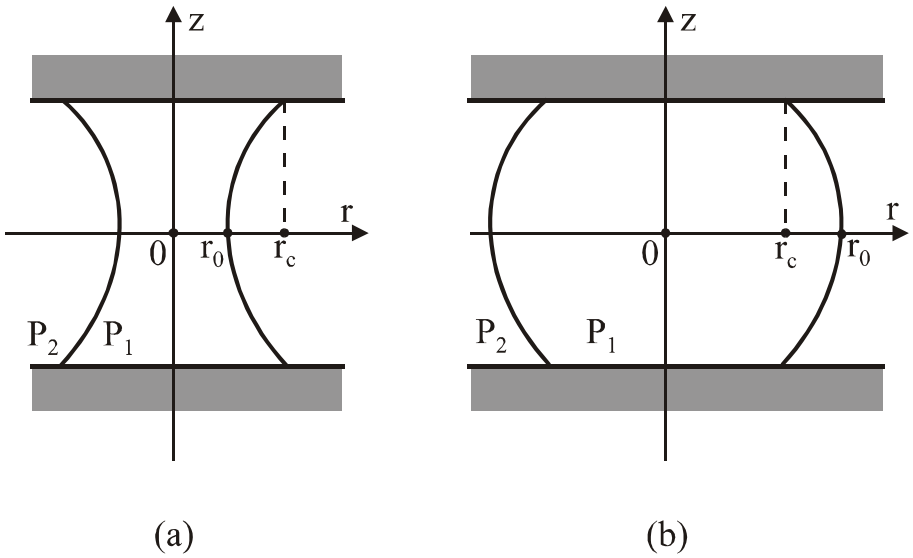

FIGURE 9. Concave (a) and convex (b) capillary bridges between two parallel plates. P_1 and P_2 denote the pressures inside and outside the capillary bridge, r_0 is the radius of its section with the midplane; r_c is the radius of the three-phase contact lines.

To determine the shape of the menisci depicted in Figures 9(a) and 9(b), one integrates Equation 101 from r_0 to r to derive

$$\frac{dz}{dr} = \frac{k_1\left(r^2 - r_0^2\right) + r_0}{\pm\left[\left(r^2 - r_0^2\right)\left(r_1^2 - r^2\right)\right]^{1/2}|k_1|}, \qquad k_1 \equiv \frac{P_1 - P_2}{2\sigma}, \qquad r_1 \equiv \left|\frac{1 - k_1 r_0}{k_1}\right| \tag{111}$$

The pressures in phases 1 and 2, P_1 and P_2, and r_0 are shown in Figure 9. Equation 111 describes curves, which after Plateau[118,119,145-147] are called "nodoid" and "unduloid," (see Figure 10). The nodoid (unlike the unduloid) has points with horizontal tangent, where $dz/dr = 0$. Then with the help of Equation 111 one can deduce that the meniscus generatrix is a part of *nodoid* if $k_1 r_0 \in (-\infty, 0) \cup (1, +\infty)$, while the meniscus generatrix is a part of *unduloid* if $k_1 r_0 \in (0, 1)$.

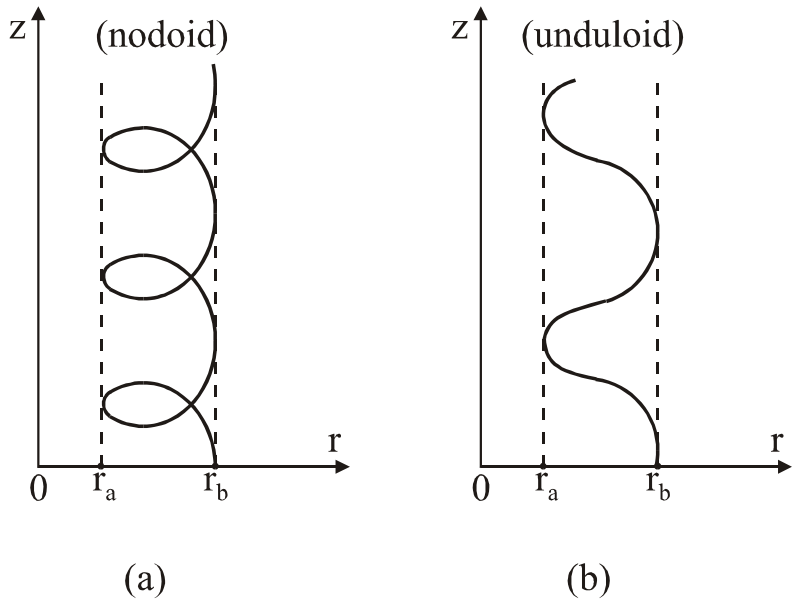

FIGURE 10. Typical shape of nodoid (a) and unduloid (b) Plateau curves. Note that the curves are confined between two cylinders of radii r_a and r_b.

In the special case, when $k_1 r_0 = 1$, the meniscus is spherical. In the other special case, $k_1 r_0 = 0$, the meniscus has the shape of *catenoid*, i.e.

$$z = \pm r_0 \ln\left\{ r/r_0 + \sqrt{(r/r_0)^2 - 1} \right\}, \qquad (k_1 = 0) \tag{112}$$

The meniscus has a "neck" (Figure 9(a)) when $k_1 r_0 \in (-\infty, 1/2)$; in particular, the generatrix is nodoid for $k_1 r_0 \in (-\infty, 0)$, catenoid for $k_1 r_0 = 0$, and unduloid for $k_1 r_0 \in (0, 1/2)$. For the configuration depicted in Figure 9(a) one has $r_1 > r_0$ (in Figure 10 $r_a = r_0$, $r_b = r_1$) and Equation 111 can be integrated to yield

$$z(r) = \pm\left\{ r_0 \mathrm{F}(\phi_1, q_1) + r_1 \operatorname{sgn} k_1 \left[\mathrm{E}(\phi_1, q_1) - \frac{1}{r r_1} \sqrt{(r^2 - r_0^2)(r_1^2 - r^2)} \right] \right\} \qquad (r_0 \le r \le r_1) \tag{113}$$

where sng$x$ denotes the sign of x, $q_1 = (1 - r_0^2 / r_1^2)^{1/2}$, $\sin\phi_1 = q_1^{-1}(1 - r_0^2 / r^2)^{1/2}$; $\mathrm{F}(\phi, q)$ and $\mathrm{E}(\phi, q)$ are the standard symbols for elliptic integrals of the first and the second kind.[138,139] A convenient method for computation of $\mathrm{F}(\phi, q)$ and $\mathrm{E}(\phi, q)$ is the method of the arithmetic-geometric mean (see Reference 138, Chapter 17.6).

The meniscus has a "haunch" (Figure 9(b)) when $k_1 r_0 \in (1/2, +\infty)$; in particular, the generatrix is unduloid for $k_1 r_0 \in (1/2, 1)$, circumference for $k_1 r_0 = 1$, and nodoid for

$k_1 r_0 \in (1, +\infty)$. For the configuration depicted in Figure 9(b) one has $r_0 > r_1$ (in Figure 10 $r_a = r_1$, $r_b = r_0$) and Equation 111 can be integrated to yield

$$z(r) = \mp\left[(r_0 - 1/k_1)\mathrm{F}(\phi_2, q_2) - r_0 \mathrm{E}(\phi_2, q_2)\right], \qquad (r_1 \le r \le r_0) \tag{114}$$

where $q_2 = (1 - r_1^2/r_0^2)^{1/2}$, $\sin\phi_2 = q_2^{-1}(1 - r^2/r_0^2)^{1/2}$. Additional information about the shapes, stability and nucleation of capillary bridges, and for the capillary-bridge forces between particles, can be found in Chapter 11 of Reference 35.

5.3.1.3 Gibbs-Thomson Equation

The dependence of the capillary pressure on the interfacial curvature leads to a difference between the chemical potentials of the components in small droplets (or bubbles) and in the large bulk phase. This effect is the driving force of phenomena like nucleation[148,149] and Ostwald ripening (see Section 5.3.1.4 below). Let us consider the general case of a multicomponent two-phase system; we denote the two phases by α and β. Let phase α be a liquid droplet of radius R. The two phases are supposed to coexist at equilibrium. Then one can derive[4,5,150,151]

$$\left(\mu_i^\beta\right)_R - \left(\mu_i^\beta\right)_{R=\infty} = \left(\mu_i^\alpha\right)_R - \left(\mu_i^\alpha\right)_{R=\infty} = V_i^\alpha \frac{2\sigma}{R} \tag{115}$$

where μ is chemical potential, V_i is partial volume, the superscripts denote phase and the subscripts denote component. Equation 31 is derived under the following assumptions. When β is a gaseous phase, it is assumed that the partial volume of each component in the gas is much larger than its partial volume in the liquid α; this is fulfilled far enough from the critical point.[151] When phase β is liquid, it is assumed that $P^\beta(R) = P^\beta(R{=}\infty)$, where P denotes pressure.

When phase β is an ideal gas, Equation 115 yields[4,5,150,151]

$$\frac{P_i^\beta(R)}{P_i^\beta(\infty)} = \exp\left(\frac{2\sigma V_i^\alpha}{R\ kT}\right) \tag{116}$$

where $P_i^\beta(R)$ and $P_i^\beta(\infty)$ denote respectively the equilibrium vapor pressure of component i in the droplet of radius R and in a large liquid phase of the same composition. Equation 116 shows that the equilibrium vapor pressure of a droplet increases with the decrease of the droplet size. (For a bubble, instead of a droplet, R must be changed to $-R$ in the right-hand

side of Equation 116 and the tendency becomes the opposite.) Equation 116 implies that in an aerosol of polydisperse droplets the larger droplets will grow and the smaller droplets will diminish down to complete disappearance.

The small droplets are "protected" against disappearance when phase α contains a non-volatile component. Then instead of Equation 116 one has

$$\frac{P_i^{\beta}(R)}{P_i^{\beta}(\infty)} = \frac{1 - X(R)}{1 - X(\infty)} \exp\left(\frac{2\sigma V_i^{\alpha}}{RkT}\right) \tag{117}$$

where X denotes the molar fraction of the non-volatile component in phase α; for $X(R) = X(\infty)$ Equation 117 reduces to Equation 116. Setting the left-hand side of Equation 117 equal to 1, one can determine the value $X(R)$ needed for a liquid droplet of radius R, surrounded by the gas phase β, to coexist at equilibrium with a large ($R = \infty$) liquid phase α of composition $X(\infty)$.

When both phases α and β are liquid, Equation 115 yields

$$\frac{X_i^{\beta}(R)}{X_i^{\beta}(\infty)} = \exp\left(\frac{2\sigma V_i^{\alpha}}{RkT}\right) \tag{118}$$

where $X_i^{\beta}(R)$ denotes the equilibrium molar fraction of component i in phase β coexisting with a droplet of radius R, and $X_i^{\beta}(\infty)$ denotes the value of $X_i^{\beta}(R)$ for $R \to \infty$, i.e., for phase β coexisting with a large phase α of the same composition as the droplet. In the case of an oil-in-water emulsion X_i^{β} can be the concentration of the oil dissolved in the water. In particular, Equation 118 predicts that the large emulsion droplets will grow and the small droplets will diminish. This phenomenon is called Ostwald ripening (see the next section). If the droplets (phase α) contain a component, which is insoluble in phase β, the small droplets will be protected against complete disappearance; a counterpart of Equation 117 can be derived:

$$\frac{X_i^{\beta}(R)}{X_i^{\beta}(\infty)} = \frac{1 - X(R)}{1 - X(\infty)} \exp\left(\frac{2\sigma V_i^{\alpha}}{RkT}\right) \tag{119}$$

where X denotes the equilibrium concentration in phase α of the component which is insoluble in phase β. Setting the left-hand side of Equation 119 equal to 1, one can determine the value $X(R)$ needed for an emulsion droplet of radius R, surrounded by the continuous phase β, to coexist at equilibrium with a large ($R = \infty$) liquid phase α of composition $X(\infty)$.

5.3.1.4 Kinetics of Ostwald Ripening in Emulsions

The Ostwald ripening is observed when the substance of the emulsion droplets (we will call it component 1) exhibits at least minimal solubility in the continuous phase, β. As discussed above, the chemical potential of this substance in the larger droplets is lower than in the smaller droplets, see Equation 115. Then a diffusion transport of component 1 from the smaller toward the larger droplets will take place. Consequently, the size distribution of the droplets in the emulsion will change with time. The kinetic theory of Ostwald ripening was developed by Lifshitz and Slyozov,[152] Wagner[153] and further extended and applied by other authors.[154-157] The basic equations of this theory are the following.

The volume of an emulsion droplet grows (or diminishes) due to the molecules of component 1 supplied (or carried away) by the diffusion flux across the continuous medium. The balance of component 1 can be presented in the form[157]

$$\frac{4\pi}{3}\frac{d}{dt}R^3(t) = 4\pi DRV_1\left[c_m(t) - c_{eq}(R)\right] \tag{120}$$

where t is time, D is the diffusivity of component 1 in the continuous phase, V_1 is the volume per molecule of component 1, c_m is the number-volume concentration of component 1 in the continuous medium far away from the droplets surfaces and $c_{eq}(R)$ is the respective equilibrium concentration of the same component for a droplet of radius R as predicted by the Gibbs-Thomson equation. Note that Equation 120 is rigorous only for a diluted emulsion, in which the interdroplet concentration levels off at a constant value, $c = c_m$, around the middle of the space between each two droplets. Some authors[155] add in the right-hand side of Equation 120 also terms accounting for the convective mass transfer (in the case of moving droplets) and thermal contribution to the growth rate.

Since the theory is usually applied to droplets of diameter not smaller than micrometer (which are observable by optical microscope), the Gibbs-Thomson equation, Equation 118, can be linearized to yield[157]

$$c_{eq}(R) \approx c_\infty(1 + b/R), \qquad b \equiv 2\sigma V_1/(kT) \tag{121}$$

with c_∞ being the value of c_{eq} for flat interface. With $\sigma = 50$ mN/m, $V_1 = 100$ Å^3, and $T = 25^\circ$C one estimates $b = 2.5$ nm. The latter value justifies the linearization of Gibbs-Thomson equation for droplets of micrometer size.

Let $f(R,t)$ be the size distribution function of the emulsion droplets such that $f(R,t)\,dR$ is the number of particles per unit volume in the size range from R to $(R+dR)$. The balance of the number of particles in the system reads

$$df\,dR = \left(j\,dt\right)|_R - \left(j\,dt\right)|_{R+dR}\,, \qquad \left(j \equiv f\,dR/dt\right) \tag{122}$$

The term in the left-hand side of Equation 122 expresses the change of the number of droplets whose radius belongs to the interval $[R, R+\mathrm{d}R]$ during a time period dt; the two terms in the right-hand side represent the number of the incoming and outgoing droplets in the size interval $[R, R+dR]$ during time period dt. Dividing both sides of Equation 122 by $(dR\,dt)$ one obtains the so called continuity equation in the space of sizes:[153-157]

$$\frac{\partial f}{\partial t} + \frac{\partial j}{\partial R} = 0 \tag{123}$$

One more equation is needed to determine c_m. In a closed system this can be the total mass balance of component 1:

$$\frac{d}{dt}\left[c_m(t) + \frac{4\pi}{3}\int_0^\infty \mathrm{d}R\,R^3 f(R,t)\right] = 0 \tag{124}$$

The first and the second terms in the brackets express the amount of component 1 contained in the continuous phase and in the droplets, respectively. This expression is appropriate for diluted emulsions when c_m is not negligible compared to the integral in the brackets.

Alternatively, in opened systems and in concentrated emulsions one can use a mean field approximation based on Equation 121 to obtain the following equation for c_m:

$$c_m(t) = c_\infty\left[1 + \frac{b}{R_m(t)}\right], \qquad R_m(t) \equiv \frac{\int_{R_0}^\infty dR\,R f(R,t)}{\int_{R_0}^\infty dR\,f(R,t)} \tag{125}$$

where R_0 is a lower limit of the experimental distribution, typically $R_0 \approx 1\,\mu\mathrm{m}$ as smaller droplets cannot be observed optically. The estimates show that the neglecting of the integrals over the interval $0 < R < R_0$ in Equation 125 does not affect significantly the value of R_m. One sees that Equation 125 treats each emulsion droplet as being surrounded by droplets of average radius R_m, which provide a medium concentration c_m in accordance with the Gibbs-Thomson equation, Equation 121. From Equations 120-123 and 125 one can derive a simple expression for the flux j:

$$j(R,t) = Q\left(\frac{1}{RR_m} - \frac{1}{R^2}\right) f(R,t), \qquad Q \equiv Dbc_\infty V_1 \tag{126}$$

In calculations one uses the set of Equations 120, 123 and 124 or 125 to determine the distribution $f(R,t)$ at known distribution $f(R,0)$ at the initial moment $t = 0$. In other words, the theory predicts the evolution of the system at given initial state. From a computational viewpoint it is convenient to calculate $f(R,t)$ in a finite interval $R_0 \le R < R_{\max}$ (see Figure 11). The problem can be solved numerically by discretization: the interval $R_0 \le R < R_{\max}$ is subdivided into small portions of length δ, the integrals are transformed into sums and the problem is reduced to solving a linear set of equations for the unknown functions $f_k(t) \equiv f(R_k, t)$, where $R_k = R_0 + k\delta$, $k = 1,2,...$.

In practice, the emulsions are formed in the presence of surfactants. At concentrations above the critical micellization concentration (CMC) the swollen micelles can serve as carriers of oil between the emulsion droplets of different size. In other words, surfactant micelles can play the role of mediators of the Ostwald ripening. Micelle-mediated Ostwald ripening has been observed in solutions of nonionic surfactants.[158-160] In contrast, it was found that the micelles do not mediate the Ostwald ripening in undecane-in-water emulsions at the presence of an *ionic* surfactant (SDS).[161] It seems that the surface charge due to the adsorption of ionic surfactant (and the resulting double layer repulsion) prevents the contact of micelles with the oil drops, which is a necessary condition for micelle-mediated Ostwald ripening.

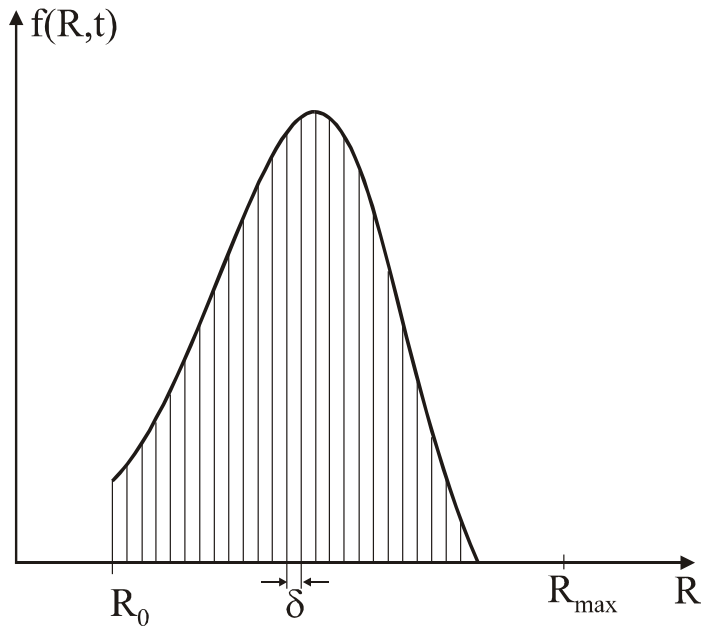

FIGURE 11. Sketch of the droplet size distribution function, $f(R,t)$ vs. the droplet radius R at a given moment t. δ is the length of the mesh used when solving the problem by discretization.

5.3.2 THIN LIQUID FILMS AND PLATEAU BORDERS

5.3.2.1 Membrane and Detailed Models of a Thin Liquid Film

Thin liquid films can be formed between two colliding emulsion droplets or between the bubbles in a foam. Formation of thin films accompanies the particle-particle and particle-wall interactions in colloids. From a *mathematical* viewpoint a film is thin when its thickness is much smaller than its lateral dimension. From a *physical* viewpoint a liquid film formed between two macroscopic phases is *thin* when the energy of interaction between the two phases across the film is not negligible. The specific forces causing the interactions in a thin liquid film are called *surface forces*. Repulsive surface forces stabilize thin films and dispersions, whereas attractive surface forces cause film rupture and coagulation. This section is devoted to the *macroscopic* (hydrostatic and thermodynamic) theory of thin films, while the *molecular* theory of surface forces is reviewed in Section 5.4 below.

In Figure 12 a sketch of plane-parallel liquid film of thickness h is presented. The liquid in the film contacts with the bulk liquid in the *Plateau border*. The film is symmetrical, i.e., it is formed between two *identical* fluid particles (drops, bubbles) of internal pressure P_0. The more complex case of non-symmetrical and curved films is reviewed elsewhere.[162-164]

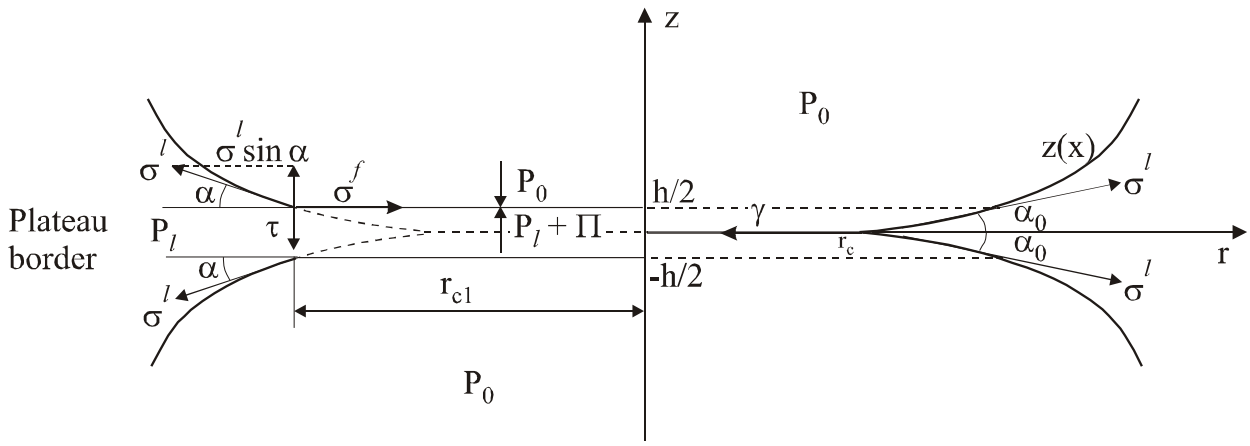

FIGURE 12. The detailed and membrane models of a thin liquid film (on the left- and right-hand side, respectively).

Two different, but supplementary, approaches (models) are used in the macroscopic description of a thin liquid film. The first of them, the "membrane approach", treats the film as a membrane of zero thickness and one tension, γ, acting tangentially to the membrane (see the right-hand side of Figure 12). In the "detailed approach", the film is modeled as a

homogeneous liquid layer of thickness h and surface tension σ^f. The pressure P_0 in the fluid particles is larger than the pressure, P_l, of the liquid in the Plateau border. The difference

$$P_c = P_0 - P_l \tag{127}$$

represents the capillary pressure of the liquid meniscus. By making the balance of the forces acting on a plate of unit width along the y-axis and height h placed normally to the film at $-h/2 < z < h/2$ (Figure 12) one derives the Rusanov[165] equation:

$$\gamma = 2\sigma^f + P_c h \tag{128}$$

Equation 128 expresses a condition for equivalence between the membrane and detailed models with respect to the lateral force. To derive the normal force balance one considers a parcel of unit area from the film surface in the detailed approach. Since the pressure in the outer phase P_0 is larger than the pressure inside the liquid, P_l, the mechanical equilibrium at the film surface is ensured by the action of an additional *disjoining* pressure, $\Pi(h)$ representing the surface force per unit area of the film surfaces[166]

$$\Pi(h) = P_0 - P_l = P_c \tag{129}$$

(see Figure 12). Note that Equation 129 is satisfied only at equilibrium; at non-equilibrium conditions the viscous force can also contribute to the force balance per unit film area. In general, the disjoining pressure, Π, depends on the film thickness, h. A typical $\Pi(h)$-isotherm is depicted in Figure 13 (for details see Section 5.4 below). One sees that the equilibrium condition, $\Pi = P_c$, can be satisfied at three points shown in Figure 13. Point 1 corresponds to a film, which is stabilized by the double layer repulsion; sometimes such a film is called the "primary film" or "common black film". Point 3 corresponds to unstable equilibrium and cannot be observed experimentally. Point 2 corresponds to a very thin film, which is stabilized by the short range repulsion; such a film is called the "secondary film" or "Newton black film". Transitions from common to Newton black films are often observed with foam films.[167-170] Note that $\Pi > 0$ means repulsion between the film surfaces, whereas $\Pi < 0$ corresponds to attraction.

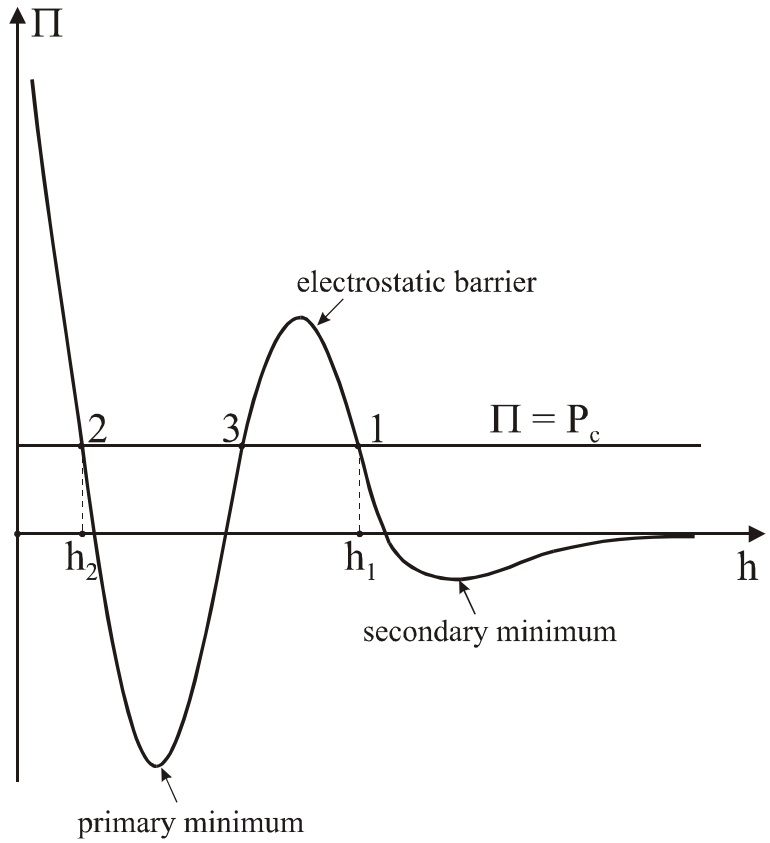

FIGURE 13. Sketch of a disjoining pressure isotherm of the DLVO type, Π vs. h. The intersection points of the Π(h)-isotherm with the line Π = P_c correspond to equilibrium films: $h = h_1$ (primary film), $h=h_2$ (secondary film). Point 3 corresponds to unstable equilibrium.

5.3.2.2 Thermodynamics of Thin Liquid Films

In the framework of the membrane approach the film can be treated as a single surface phase, whose Gibbs-Duhem equation reads:[162,171]

$$d\gamma = -s^f dT - \sum_{i=1}^{k} \Gamma_i d\mu_i \tag{130}$$

where γ is the film tension, T is temperature, s^f is excess entropy per unit area of the film, Γ_i and μ_i are the adsorption and the chemical potential of the i-th component. The Gibbs-Duhem equations of the liquid phase (l) and the outer phase (o) read

$$dP_\chi = s_v^\chi dT + \sum_{i=1}^{k} n_i^\chi d\mu_i, \qquad \chi = l,o \tag{131}$$

where s_v^χ and n_i^χ are entropy and number of molecules per unit volume, and P_χ is pressure ($\chi = l, o$). The combination of Equations 127 and 131 provides an expression for dP_c. Let us

multiply this expression by h and to subtract the result from the Gibbs-Duhem equation of the film, Equation 130. The result reads:

$$d\gamma = -\widetilde{s}\,dT + h\,dP_c - \sum_{i=1}^{k} \widetilde{\Gamma}_i\, d\mu_i \tag{132}$$

where

$$\widetilde{s} = s^f + (s_\nu^o - s_\nu^l)h, \qquad \widetilde{\Gamma}_i = \Gamma_i + (n_i^o - n_i^l)h, \qquad i = 1,...,k \tag{133}$$

An alternative derivation of the same equations is possible.[172,173] Imagine two equidistant planes separated at a distance h. The volume confined between the two planes is thought to be filled with the bulk liquid phase (l). Taking surface excesses with respect to the bulk phases one can derive Equations 132 and 133 with $\widetilde{s}$ and $\widetilde{\Gamma}_i$ being the excess surface entropy and adsorption ascribed to the surfaces of this liquid layer.[172,173] A comparison between Equations 132 and 130 shows that there is one additional differential in Equation 132. It corresponds to one supplementary degree of freedom connected with the choice of the parameter h. To specify the model one needs an additional equation to determine h. For example, let this equation be

$$\widetilde{\Gamma}_1 = 0 \tag{134}$$

Equation 134 requires h to be the thickness of a liquid layer from phase (l), containing the same amount of component 1 as the real film. This thickness is called the thermodynamic thickness of the film.[173] It can be on the order of the real film thickness if component 1 is chosen in an appropriate way, say the solvent in the film phase.

From Equations 129, 132 and 134 one obtains[172]

$$d\gamma = -\widetilde{s}\,dT + h\,d\Pi - \sum_{i=2}^{k} \widetilde{\Gamma}_i\, d\mu_i \tag{135}$$

A corollary of Equation 135 is the Frumkin[174] equation

$$\left(\frac{\partial \gamma}{\partial \Pi}\right)_{T,\mu_2,...,\mu_k} = h \tag{136}$$

Equation 136 predicts a rather weak dependence of the film tension γ on the disjoining pressure, Π, for equilibrium thin films (small h). By means of Equations 128 and 129 Equation 135 can be transformed to read[173]

$$2d\sigma^f = -\tilde{s}dT - \Pi dh - \sum_{i=2}^{k} \tilde{\Gamma}_i d\mu_i \tag{137}$$

From Equation 137 one can derive the following useful relations[172]

$$2\left(\frac{\partial \sigma^f}{\partial h}\right)_{T,\mu_2,\ldots,\mu_k} = -\Pi \tag{138}$$

$$\sigma^f(h) = \sigma^l + \frac{1}{2}\int_h^\infty \Pi(h)dh \tag{139}$$

with σ^l being the surface tension of the bulk liquid. Equation 139 allows calculation of the film surface tension when the disjoining pressure isotherm is known.

Note that the above thermodynamic equations are, in fact, corollaries from the Gibbs-Duhem equation of the membrane approach Equation 130. There is an equivalent and complementary approach, which treats the two film surfaces as separate surface phases with their own fundamental equations;[165,175,176] thus for a flat symmetric film one postulates.

$$dU^f = TdS^f + 2\sigma^f dA + \sum_{i=1}^{k} \mu_i dN_i^f - \Pi A dh, \tag{140}$$

where A is area; U^f, S^f and N_i^f are excess internal energy, entropy and number of molecules ascribed to the film surfaces. Compared with the fundamental equation of a simple surface phase,[5] Equation 140 contains an additional term, $\Pi A dh$, which takes into account the dependence of the film surface energy on the film thickness. Equation 140 provides an alternative thermodynamic definition of disjoining pressure:

$$\Pi = -\frac{1}{A}\left(\frac{\partial U^f}{\partial h}\right) \tag{141}$$

5.3.2.3 The Transition Zone between Thin Film and Plateau Border

5.3.2.3.1 Macroscopic description

The thin liquid films formed in foams or emulsions exist in a permanent contact with the bulk liquid in the Plateau border, encircling the film. From a macroscopic viewpoint, the boundary between film and Plateau border is treated as a three-phase contact line: the line, at which the two surfaces of the Plateau border (the two concave menisci sketched in Figure 12) intersect

at the plane of the film (see the right-hand side of Figure 12). The angle, α_0, subtended between the two meniscus surfaces, represents the thin film contact angle. The force balance at each point of the contact line is given by Equation 98 with $\sigma_{12} = \gamma$ and $\sigma_{13} = \sigma_{23} = \sigma^l$. The effect of the line tension, κ, can be also taken into account. For example, in the case of symmetrical flat film with circular contact line, like those depicted in Figure 12, one can write[176]

$$\gamma + \frac{\kappa}{r_c} = 2\sigma^l \cos\alpha_0 \tag{142}$$

where r_c is the radius of the contact line.

There are two film surfaces and two contact lines in the detailed approach (see the left-hand side of Figure 12). They can be treated thermodynamically as linear phases and an one-dimensional counterpart of Equation 140 can be postulated:[176]

$$dU^L = TdS^L + 2\widetilde{\kappa}dL + \sum_i \mu_i dN_i^L + \tau dh \tag{143}$$

Here U^L, S^L and N_i^L are linear excesses, $\widetilde{\kappa}$ is the line tension in the detailed approach and

$$\tau = \frac{1}{L}\left(\frac{\partial U^L}{\partial h}\right) \tag{144}$$

is a one-dimensional counterpart of the disjoining pressure (see Equation 141). The quantity τ, called the *transversal tension*, takes into account the interaction between the two contact lines. The general force balance at each point of the contact line can be presented in the form of the following vectorial sum[162]

$$\boldsymbol{\sigma}_i^f + \boldsymbol{\sigma}_i^l + \boldsymbol{\sigma}_i^\kappa + \boldsymbol{\tau}_i = \mathbf{0} \quad , \quad i = 1, 2 \tag{145}$$

The vectors taking part in Equation 145 are depicted in Figure 14, where $\left|\boldsymbol{\sigma}_i^\kappa\right| = \widetilde{\kappa}_i / r_{ci}$. For the case of a flat symmetric film (Figure 12) the tangential and normal projections of Equation 145, with respect to the plane of the film, read:

$$\sigma^f + \frac{\widetilde{\kappa}}{r_{c1}} = \sigma^l \cos\alpha \tag{146}$$

$$\tau = \sigma^l \sin\alpha \tag{147}$$

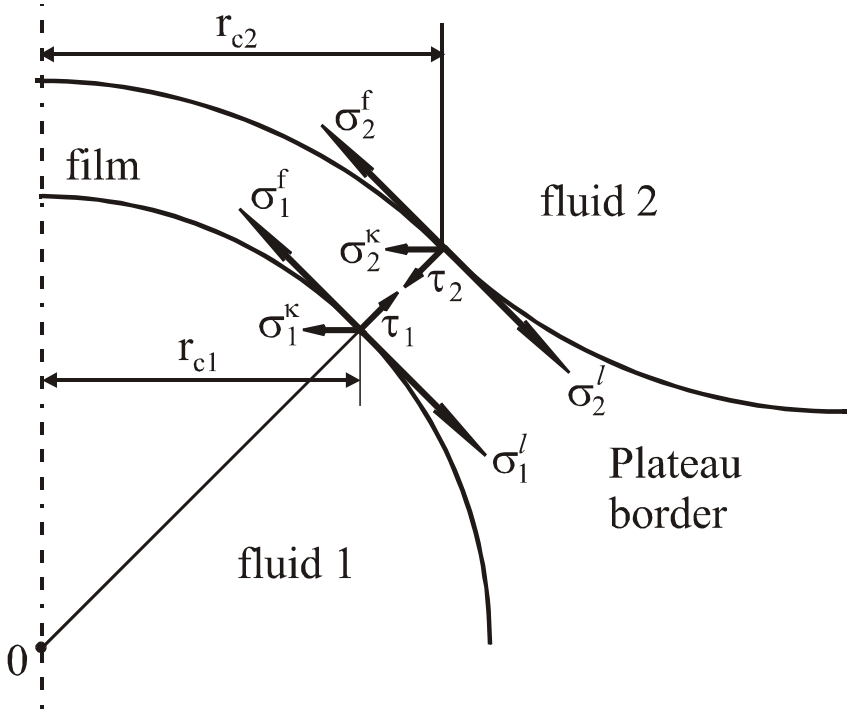

FIGURE 14. The force balance in each point of the two contact lines representing the boundary between a spherical film and the Plateau border (see Equation 145).

Note that in general $\alpha \neq \alpha_0$ (see Figure 12). Besides, both α_0 and α can depend on the radius of the contact line due to line tension effects. In the case of straight contact line from Equations 139 and 146 one derives[173]

$$\cos\alpha\big|_{r_{c1}=\infty} = \frac{\sigma^f}{\sigma^l} = 1 + \frac{1}{2\sigma^l}\int_h^\infty \Pi(h)\,dh \tag{148}$$

Since $\cos\alpha \leq 1$, the surface tension of the film must be less than the bulk solution surface tension, $\sigma^f < \sigma^l$, and the integral term in Equation 148 must be negative in order for a nonzero contact angle to be formed. Hence, the contact angle, α, and the transversal tension, τ (see Equation 147), are integral effects of the long-range *attractive* surface forces acting in the transition zone between the film and Plateau border, where $h > h_1$ (see Figure 13).

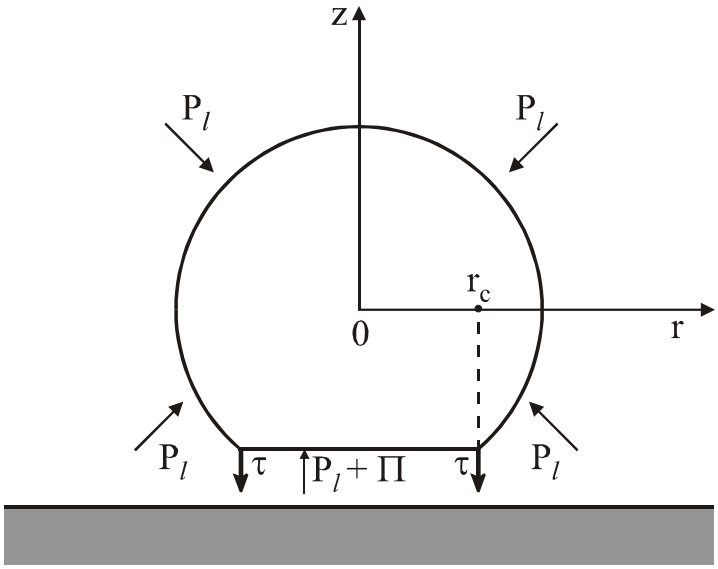

FIGURE 15. Sketch of the forces exerted on a fluid particle (bubble, drop, vesicle) attached to a solid surface: Π is disjoining pressure, τ is transversal tension, P_l is the pressure in the outer liquid phase.

In the case of a fluid particle attached to a surface (Figure 15) the integral of the pressure $P_l = P_0 - \Delta\rho g z$ over the particle surface equals the buoyancy force, F_b, which at equilibrium is counterbalanced by the disjoining-pressure and transversal-tension forces:[162,177]

$$2\pi r_{c1}\tau = F_b + \pi r_{c1}^2 \Pi \tag{149}$$

F_b is negligible for bubbles of diameter smaller than c.a. 300 μm. Then the forces due to τ and Π counterbalance each other. Hence, at equilibrium the role of the repulsive disjoining pressure is to keep the film thickness uniform, whereas the role of the attractive transversal tension is to keep the bubble (droplet) attached to the surface. In other words, the particle sticks to the surface at its contact line where the long-range attraction prevails (see Figure 13), whereas the repulsion predominates inside the film, where $\Pi = P_c > 0$. Note that this conclusion is valid not only for particle-wall attachment, but also for particle-particle interaction. For zero contact angle τ is also zero (Equation 147) and the particle will rebound from the surface (the other particle), unless some additional external force keeps it attached.

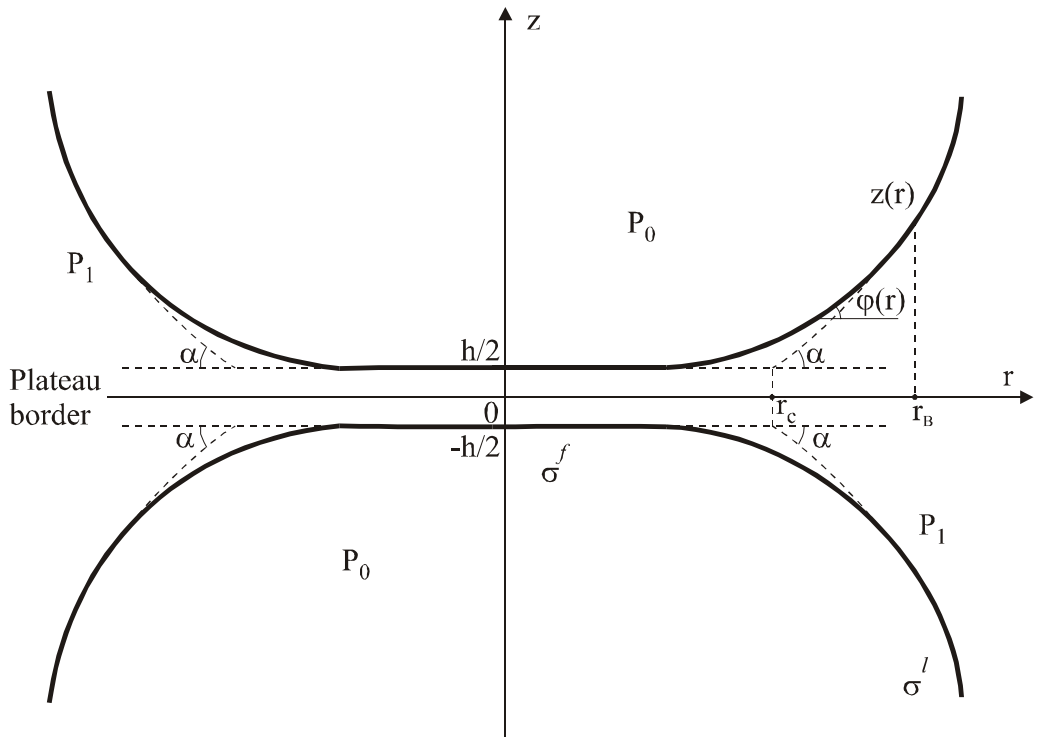

FIGURE 16 Liquid film between two attached fluid particles (bubbles, drops, vesicles). The solid lines represent the actual interfaces, whereas the dashed lines show the extrapolated interfaces in the transition zone between the film and the Plateau border.

5.3.2.3.2 Micromechanical description

From a microscopic viewpoint, the transition between the film surface and the meniscus is smooth, as depicted in Figure 16. As the film thickness increases across the transition zone, the disjoining pressure decreases and tends to zero at the Plateau border (see Figures 13 and 16). Respectively, the surface tension varies from σ^f for the film to σ^l for the Plateau border.[178,179] By using local force balance considerations, one can derive the equations governing the shape of the meniscus in the transition zone; in the case of axial symmetry (depicted in Figure 16), these equations read:[179]

$$\frac{d}{dr}\left(\sigma\sin\varphi\right)+\frac{1}{r}\sigma(r)\sin\varphi(r)=P_c-\Pi\left(h(r)\right) \tag{150}$$

$$-\frac{d}{dz}\left(\sigma\cos\varphi\right)+\frac{1}{r}\sigma(r)\sin\varphi(r)=P_c,\qquad \tan\varphi(r)=\frac{dz}{dr} \tag{151}$$

where $\varphi(r)$ and $h(r) = 2z(r)$ are the running meniscus slope angle and thickness of the gap. Equations 150 and 151 allow calculation of the three unknown functions, $z(r)$, $\varphi(r)$ and $\sigma(r)$, provided that the disjoining pressure, $\Pi(h)$, is known from the microscopic theory. By eliminating P_c between Equations 150 and 151 one can derive[179]

$$\frac{d\sigma}{dz} = -\Pi\big(h(r)\big)\cos\varphi(r) \tag{152}$$

This result shows that the hydrostatic equilibrium in the transition region is ensured by simultaneous variation of σ and Π. Equation 152 represents a generalization of Equation 138 for a film of uneven thickness and axial symmetry. Generalization of Equations 150–152 for the case of more complicated geometry is also available.[162,163]

For the Plateau border we have $z >> h$, $\Pi \to 0$, $\sigma \to \sigma^{l} = \text{const.}$, and both Equations 150 and 151 reduce to Equation 101 with $\Delta P = P_c$. The macroscopic contact angle, α, is defined as the angle at which the *extrapolated* meniscus, obeying Equation 101, meets the *extrapolated* film surface (see the dashed line in Figure 16). The real surface, shown by solid line in Figure 16, differs from this *extrapolated* (idealized) profile, because of the interactions between the two film surfaces, which is taken into account in Equation 150, but not in Equation 101. To compensate for the difference between the real and idealized system, the line and transversal tensions are ascribed to the contact line in the macroscopic approach. In particular, the line tension makes up for the differences in surface tension and running slope angle:[179]

$$\frac{\widetilde{\kappa}}{r_c} = \int_0^{r_B}\left[\left(\frac{\sigma\sin^2\varphi}{r\cos\varphi}\right)^{\text{real}} - \left(\frac{\sigma\sin^2\varphi}{r\cos\varphi}\right)^{\text{idealized}}\right]dr \tag{153}$$

whereas τ compensates for the differences in surface forces (disjoining pressure):

$$\tau = \frac{1}{r_c}\int_0^{r_B}\Big[(\Pi)^{\text{id}} - \Pi(r)\Big]r\,dr \tag{154}$$

where

$$(\Pi)^{\text{id}} = P_c \qquad \text{for} \quad 0 < r < r_c$$
$$(\Pi)^{\text{id}} = 0 \qquad \text{for} \quad r > r_c$$

The superscripts "real" and "idealized" in Equation 69 mean that the quantities in the respective parentheses must be calculated for the real and idealized meniscus profiles; the latter coincide for $r > r_B$ (Figure 16). Results for $\tilde{\kappa}$ and τ calculated by means of Equations 153 and 154 can be found in Reference 180.

In conclusion, it should be noted that the width of the transition region between a thin liquid film and Plateau border is usually very small[178] - below 1 μm. That is why the optical measurements of the meniscus profile give information about the thickness of the Plateau border in the region $r > r_B$ (Figure 16). Then if the data are processed by means of the Laplace equation (Equation 101), one determines the contact angle, α, as discussed above. In spite of being a purely macroscopic quantity, α characterizes the magnitude of the surface forces inside the thin liquid film, as implied by Equation 148. This has been pointed out by Derjaguin[181] and Princen and Mason.[182]

5.3.2.4 Methods for Measuring Thin Film Contact Angles

Prins[183] and Clint *et al.*[184] developed a method of contact angle measurement for macroscopic flat foam films formed in a glass frame in contact with a bulk liquid. They measured the jump in the force exerted on the film at the moment, when the contact angle is formed. Similar experimental setup was used by Yamanaka[185] for measurement of the velocity of motion of the three-phase contact line.

An alternative method, which can be used in both equilibrium and dynamic measurements with vertical macroscopic films, was developed by Princen and Frankel.[186,187] They determined the contact angle from the data for diffraction of a laser beam refracted by the Plateau border.

In the case of microscopic films, especially appropriate are the interferometric methods: light beams reflected or refracted from the liquid meniscus interfere and create fringes, which in turn give information about the shape of the liquid surfaces. The fringes are usually formed in the vicinity of the contact line, which provides a high precision of the extrapolation procedure used to determine the contact angle (see Figure 16). One can distinguish several interference techniques depending on how the interference pattern is

created. In the usual interferometry the fringes are due to interference of beams reflected from the upper and lower meniscus. This technique can be used for contact angle measurements with foam films,[144,188-190] emulsion films,[191,192] and adherent biological cells.[130] The method is applicable for not-too-large contact angles ($\alpha < 8° - 10°$); for larger meniscus slopes the region of fringes shrinks and the measurements are not possible.

The basic principle of the differential interferometry consists of an artificial splitting of the original image into two equivalent and overlapping images (see Françon[193] or Beyer[194]). Thus interferometric measurements are possible with meniscus surfaces of larger slope. The differential interferometry in transmitted light was used by Zorin *et al*.[195,196] to determine the contact angles of wetting and free liquid films. This method is applicable when the whole system under investigation is transparent to the light.

Differential interferometry in reflected light allows measurement of the shape of the upper reflecting surface. This method was used by Nikolov *et al*.[177,197-199] to determine the contact angle, film and line tension of foam films formed at the top of small bubbles floating at the surface of ionic and nonionic surfactant solutions. An alternative method is the holographic interferometry applied by Picard *et al*.[200,201] to study the properties of bilayer lipid membranes in solution. Film contact angles can be also determined from the Newton rings of liquid lenses, which spontaneously form in films from micellar surfactant solutions.[144]

Contact angles can be also determined by measuring several geometrical parameters characterizing the profile of the liquid meniscus and processing them by using the Laplace equation (Equation 101).[202,203] The computer technique allows processing of many experimental points from meniscus profile and automatic digital image analysis.

Contact angles of microscopic particles against another phase boundary can be determined interferometrically, by means of a film trapping technique (FTT).[204,205] It consists in capturing of μm-sized particles, emulsion drops and biological cells in thinning free foam films or wetting films. The interference pattern around the entrapped particles allows one to reconstruct the meniscus shape, to determine the contact angles, and to calculate the particle-to-interface adhesion energy.[204,205]

5.3.3 LATERAL CAPILLARY FORCES BETWEEN PARTICLES ATTACHED TO INTERFACES

5.3.3.1 Particle-Particle Interactions

The origin of the lateral capillary forces between particles captive at a fluid interface is the deformation of the interface, which is supposed to be flat in the absence of particles. The larger the interfacial deformation, the stronger the capillary interaction. It is known that two similar particles floating on a liquid interface attract each other[206-208] (see Figure 17(a)). This attraction appears because the liquid meniscus deforms in such a way that the gravitational potential energy of the two particles decreases when they approach each other. Hence the origin of this force is the particle weight (including the Archimedes force).

A force of capillary attraction appears also when the particles (instead of being freely floating) are partially immersed in a liquid layer on a substrate[209-211] (see Figure 17(b)). The deformation of the liquid surface in this case is related to the wetting properties of the particle surface, i.e., to the position of the contact line and the magnitude of the contact angle, rather than to gravity.

To distinguish between the capillary forces in the case of floating particles and in the case of partially immersed particles on a substrate, the former are called lateral *flotation* forces and the latter, lateral *immersion* forces.[208,211] These two kinds of force exhibit similar dependence on the interparticle separation but very different dependencies on the particle radius and the surface tension of the liquid (see References 35 and 212 for comprehensive reviews). The flotation and immersion forces can be both attractive (Figures 17(a) and 17(b)) and repulsive (Figures 17(c) and 17(d)). This is determined by the signs of the meniscus slope angles ψ_1 and ψ_2 at the two contact lines: the capillary force is attractive when $\sin\psi_1 \sin\psi_2 > 0$ and repulsive when $\sin\psi_1 \sin\psi_2 < 0$. In the case of flotation forces $\psi > 0$ for *light* particles (including bubbles) and $\psi < 0$ for *heavy* particles. In the case of immersion forces between particles protruding from an aqueous layer $\psi > 0$ for *hydrophilic* particles and $\psi < 0$ for *hydrophobic* particles. When $\psi = 0$ there is no meniscus deformation and, hence, there is no capillary interaction between the particles. This can happen when the weight of the particles is too small to create significant surface deformation (Figure 17(e)).

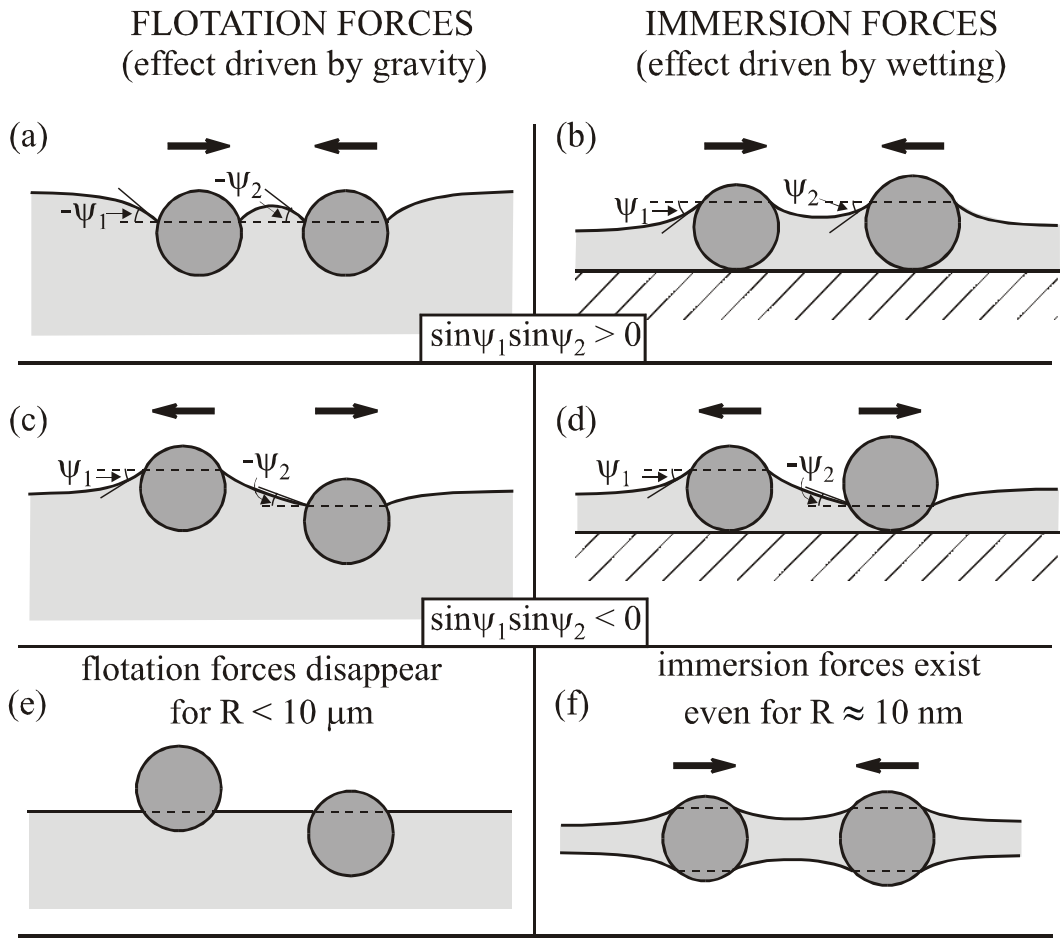

FIGURE 17. Flotation (a, c, e) and immersion (b, d, f) lateral capillary forces between two particles attached to fluid interface: (a) and (b) are two similar particles; (c) is a light and a heavy particle; (d) is a hydrophilic and a hydrophobic particle; (e) is small floating particles that do not deform the interface; (f) is small particles captured in a thin liquid film deforming the interfaces due to the wetting effects.

The immersion force appears not only between particles in wetting films (Figures 17(b) (d)), but also in symmetric fluid films (Figure 17(f)). The theory provides the following asymptotic expression for calculating the lateral capillary force between two particles of radii R_1 and R_2 separated by a center-to-center distance L: [35,207-212]

$$F = 2\pi\sigma Q_1 Q_2 q \mathrm{K}_1(qL)\left[1 + O\left(q^2 R_k^2\right)\right] \qquad r_k << L \tag{155}$$

where σ is the liquid-fluid interfacial tension, r_1 and r_2 are the radii of the two contact lines and $Q_k = r_k \sin\psi_k$ ($k = 1, 2$) is the "capillary charge" of the particle;[208,211] in addition

$$\begin{aligned} q^2 &= \Delta\rho g/\sigma \qquad (\text{in thick film}) \\ q^2 &= (\Delta\rho q - \Pi')/\sigma \qquad (\text{in thin films}) \end{aligned} \tag{156}$$

Here, $\Delta\rho$ is the difference between the mass densities of the two fluids, and Π' is the derivative of the disjoining pressure with respect to the film thickness; $K_1(x)$ is the modified Bessel function of the first order. The asymptotic form of Equation 155 for $qL << 1$ ($q^{-1} = 2.7$ mm for water),

$$F = 2\pi\sigma Q_1 Q_2 / L \qquad r_k << L << q^{-1} \tag{157}$$

looks like a two-dimensional analogue of Coulomb's law, which explains the name "capillary charge" of Q_1 and Q_2. Note that the immersion and flotation forces exhibit the same functional dependence on the interparticle distance, see Equations 155 and 157. On the other hand, their different physical origin results in different magnitudes of the "capillary charges" of these two kinds of capillary force. In this aspect they resemble the electrostatic and gravitational forces, which obey the same power law, but differ in the physical meaning and magnitude of the force constants (charges, masses). In the special case when $R_1 = R_2 = R$ and $r_k << L << q^{-1}$ one can derive[211,212]

$$\begin{aligned} F &\propto \left(R^6/\sigma\right)\mathrm{K}_1(qL) \quad \text{for flotation force} \\ F &\propto \sigma R^2 \mathrm{K}_1(qL) \quad \text{for immersion force} \end{aligned} \tag{158}$$

Hence, the flotation force decreases, while the immersion force increases, when the interfacial tension σ increases. Besides, the flotation force decreases much more strongly with the decrease of R than the immersion force. Thus $F_{\text{flotation}}$ is negligible for $R < 10\,\mu$m, whereas $F_{\text{immersion}}$ can be significant even when $R = 10$ nm. This is demonstrated in Figure 18 where the two types of capillary interaction are compared for a wide range of particle sizes. The values of the parameters used are: particle mass density $\rho_p = 1.05$ g/cm^3, surface tension $\sigma = 72$ mN/m, contact angle $\alpha = 30°$, interparticle distance $L = 2R$, and thickness of the non-disturbed planar film $l_0 = R$. The drastic difference in the magnitudes of the two types of capillary forces is due to the different deformation of the water-air interface. The small floating particles are too light to create substantial deformation of the liquid surface, and the lateral capillary forces are negligible (Figure 17(e)). In the case of immersion forces the particles are restricted in the vertical direction by the solid substrate. Therefore, as the film becomes thinner, the liquid surface deformation increases, thus giving rise to a strong interparticle attraction.

As seen in Figure 18, the immersion force can be significant between particles whose radii are larger than few nanometers. It has been found to promote the growth of two-

dimensional crystals from colloid particles,[213-216] viruses and globular proteins.[217-223] Such two-dimensional crystals have found various applications: for nanolithography,[224] microcontact printing,[225] as nanostructured materials in photo-electrochemical cells,[226] for photocatalitic films,[227] photo- and electro-luminescent semiconductor materials,[228] as samples for electron microscopy of proteins and viruses,[229] as immunosensors,[230] etc. (for reviews see References 35 and 231).

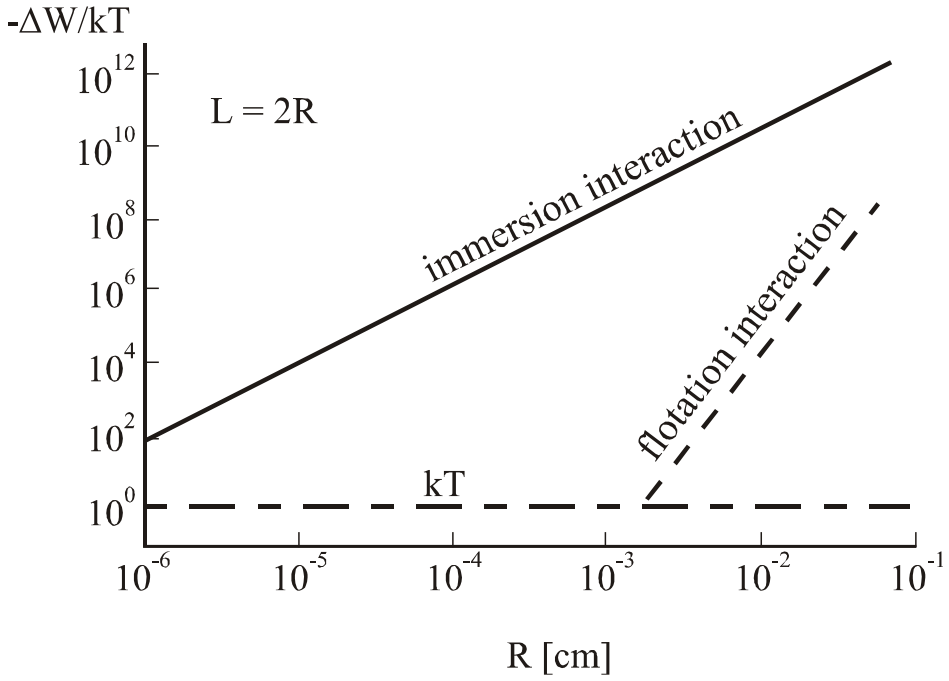

FIGURE 18. Plot of the capillary interaction energy in *kT* units, $\Delta W/kT$, vs. the radius, *R*, of two similar particles separated at a center-to-center distance $L = 2R$.

In the case of interactions between inclusions in lipid bilayers (Figure 19) the elasticity of the bilayer interior must also be taken into account. The calculated energy of capillary interaction between integral membrane proteins turns out to be of the order of several *kT*.[133] hence, this interaction can be a possible explanation of the observed aggregation of membrane proteins.[133,232-234] The lateral capillary forces have been calculated also for the case of particles captured in a *spherical* (rather than planar) thin liquid film or vesicle.[235]

Lateral capillary forces between vertical cylinders or between spherical particles have been measured by means of sensitive electromechanical balance,[236] piezo-transduser balance[237] and torsion micro-balance.[238] Good agreement between theory and experiment has been established.[237,238]

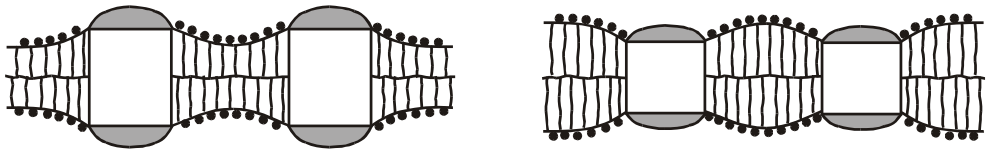

(a) (b)

FIGURE 19. Inclusions (say, membrane proteins) in a lipid bilayer: the thickness of the inclusion can be greater (a) or smaller (b) than the thickness of the (nondisturbed) lipid bilayer. In both cases, the overlap of the deformations around the inclusions leads to an attraction between them (see References 35 and 133).

As already mentioned, the weight of μm-sized and sub-μm floating particles is not sufficient to deform the fluid interface and to bring about capillary force between the particles (Figure 17(e)). However, the situation changes if the contact line at the particle surface has *undulated* or *irregular* shape (Figure 20(a)). This may happen when the particle surface is rough, angular or heterogeneous. In such cases, the contact line sticks to an edge or to the boundary between two domains of the heterogeneous surface. The undulated contact line induces undulations in the surrounding fluid interface.[231,239-241] Let $z = \zeta(x,y)$ be the equation describing the interfacial shape around such isolated particle. Using polar coordinates (r, φ) in the xy-plane, one can express the interfacial shape as a Fourier expansion:

$$\zeta(r,\varphi) = \sum_{m=1}^{\infty} r^{-m} \left(A_m \cos m\varphi + B_m \sin m\varphi\right) \tag{159}$$

where r is the distance from the particle centre, A_m and B_m are coefficients. In analogy with electrostatics, Equation 159 can be interpreted as a multipole expansion: the terms with m = 1, 2, 3, ... , play the role of capillary "dipoles", "quadrupoles", "hexapoles", etc.[231,240,241] The term with m = 0 (capillary "charge") is missing since there is no axisymmetric contribution to the deformation (negligible particle weight). Moreover, the dipolar term with m = 2 is also absent because it is annihilated by a spontaneous rotation of the floating particle around a horizontal axis.[240] Therefore, the leading term becomes the quadrupolar one, with m = 2. The interaction between capillary quadrupoles has been investigated theoretically.[240,241] This interaction is non-monotonic: attractive at long distances, but repulsive at short distances. Expressions for the rheological properties (surface dilatational and shear elasticity and yield stress) of Langmuir monolayers from angular particles have been derived.[35,241] "Mesoscale"

capillary multipoles have been experimentally realized by Bowden et al.,[242,243] by appropriate hydrophobization or hydrophilization of the sides of floating plates.

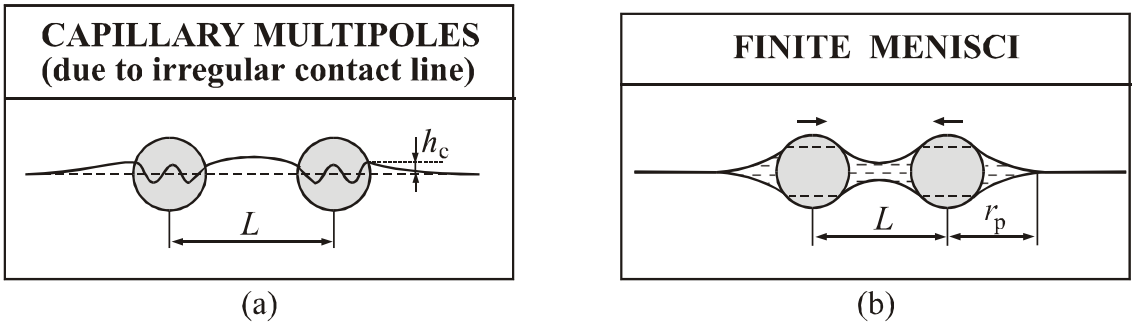

FIGURE 20. Special types of immersion capillary forces: (a) The contact line attachment to an irregular edge on the particle surface produces undulations in the surrounding fluid interface, which give rise to lateral capillary force between the particles. (b) When the size of particles, entrapped in a liquid film, is much greater than the non-perturbed film thickness, the meniscus surfaces meet at a finite distance, r_p; in this case, the capillary interaction begins at $L \leq 2r_p$.

At last, let us consider another type of capillary interactions – between particles surrounded by *finite* menisci. Such interactions appear when μm-sized or sub-μm particles are captured in a liquid film of much smaller thickness (Figure 20(b)).[244-247] If such particles are approaching each other, the interaction begins when the menisci around the two particles overlap, $L < 2r_p$ in Figure 20(b). The capillary force in this case is non-monotonic: initially the attractive force increases with the increase of interparticle distance, then it reaches a maximum and further decays.[247] In addition, there are hysteresis effects: the force is different on approach and separation at distances around $L = 2r_p$.[247]

5.3.3.2 Particle-Wall Interactions

The overlap of the meniscus around a floating particle with the meniscus on a vertical wall gives rise to a particle-wall interaction, which can be both repulsive and attractive. An example for a controlled meniscus on the wall is shown in Figure 21, where the "wall" is a hydrophobic Teflon barrier whose position along the vertical can be precisely varied and adjusted.

Two types of boundary conditions at the wall are analyzed theoretically:[35,248] fixed contact line (Figure 21) or, alternatively, fixed contact angle. In particular, the lateral

capillary force exerted on the particle depicted in Figure 21 is given by the following asymptotic expression:[35,248]

$$F = -\pi\sigma q\left[2Q_2 He^{-qx} + r_2 He^{-qx} - 2Q_2^2 \mathrm{K}_1(qx)\right] \tag{160}$$

Here, Q_2 and r_2 are the particle capillary charge and contact line radius, H characterizes the position of the contact line on the wall with respect to the nondisturbed horizontal liquid surface (Figure 21); x is the particle-wall distance; q is defined by Equation 156 (thick films). The first term in the right-hand side of Equation 160 expresses the gravity force pushing the particle to slide down over the inclined meniscus on the wall; the second term originates from the pressure difference across the meniscus on the wall; the third term expresses the so-called capillary image force, that is the particle is repelled by its mirror image with respect to the wall surface.[35,248]

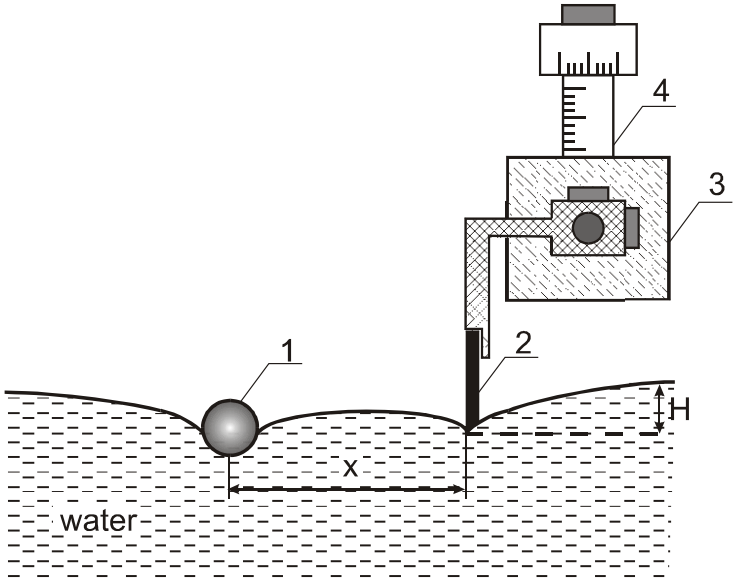

FIGURE 21. Experimental setup for studying the capillary interaction between a floating particle (1) and a vertical hydrophobic plate (2) separated at a distance, x. The edge of the plate is at a distance, H, lower than the level of the horizontal liquid surface far from the plate; (3) and (4) are micrometric table and screw (see References 249 and 250 for details).

Static[249] and dynamic[250] measurements with particles near walls have been carried out. In the static measurements the equilibrium distance of the particle from the wall (the distance at which $F = 0$) has been measured and a good agreement with the theory has been established.[249]

In the dynamic experiments[250] knowing the capillary force F (from Equation 160), and measuring the particle velocity, $\dot{x}$, one can determine the drag force, F_d:

$$F_d = m\ddot{x} - F, \qquad F_d \equiv 6\pi\eta R_2 f_d \dot{x} \tag{161}$$

where R_2, m and $\ddot{x}$ are the particle radius, mass and acceleration, η is the viscosity of the liquid and f_d is the drag coefficient. If the particle were in the bulk liquid, f_d would be equal to 1 and F_d would be given by the Stokes formula. In general, f_d differs from unity because the particle is attached to the interface. The experiment[250] gives f_d varying between 0.68 and 0.54 for particle contact angle varying from 49° to 82°; the data are in good quantitative agreement with the hydrodynamic theory of the drag coefficient.[251] In other words, the less the depth of particle immersion, the less the drag coefficient, as could be expected. However, if the floating particle is heavy enough, it deforms the surrounding liquid surface; the deformation travels together with the particle, thus increasing f_d several times.[250] The addition of surfactant strongly increases f_d. The latter effect can be used to measure the surface viscosity of adsorption monolayers from low molecular weight surfactants,[252] which is not accessible to the standard methods for measurement of surface viscosity.

In the case of *protein* adsorption layers, the surface elasticity is so strong that the particle (Figure 21) is arrested in the adsorption film. Nevertheless, with heavier particles and at larger meniscus slopes, it is possible to break the protein adsorption layer. Based on such experiments, a method for determining surface elasticity and yield stress has been developed.[253]

5.4 SURFACE FORCES

5.4.1 DERJAGUIN APPROXIMATION

The excess surface free energy per unit area of a plane-parallel film of thickness h is[14,254]

$$f(h) = \int_h^\infty \Pi(h)dh \tag{162}$$

where, as before, Π denotes disjoining pressure. Derjaguin[255] derived an approximate formula, which expresses the energy of interaction between two spherical particles of radii R_1 and R_2 through integral of $f(h)$:

$$U(h_0) = \frac{2\pi R_1 R_2}{R_1 + R_2} \int_{h_0}^{\infty} f(h)\, dh \tag{163}$$

Here h_0 is the shortest distance between the surfaces of the two particles (see Figure 22). In the derivation of Equation 163 it is assumed that the interaction between two parcels from the particle surfaces, separated at the distance h, is approximately the same as that between two similar parcels in a plane-parallel film. This assumption is correct when the range of action of the surface forces and the distance h_0 are small compared to the curvature radii R_1 and R_2. It has been established, both experimentally[34] and theoretically,[256] that Equation 163 provides a good approximation in the range of its validity.

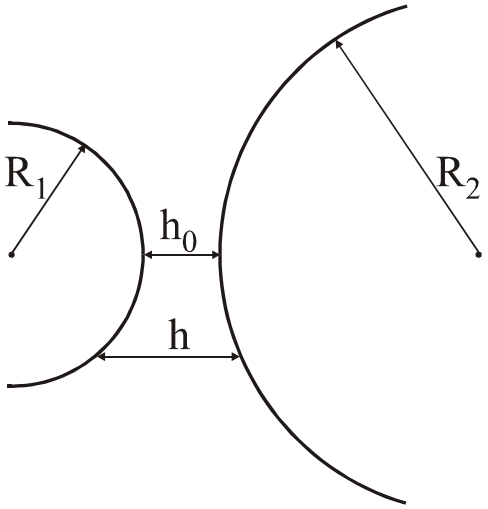

FIGURE 22. Two spherical particles of radii R_1 and R_2; the shortest and the running surface-to-surface distances are denoted by h_0 and h, respectively.

Equation 163 can be generalized for smooth surfaces of arbitrary shape (not necessarily spheres). For that purpose, the surfaces of the two particles are approximated with paraboloids in the vicinity of the point of closest approach ($h = h_0$). Let the principle curvatures at this point be c_1 and c_1' for the first particle, and c_2 and c_2' for the second particle. Then the generalization of Equation 163 reads:[254]

$$U(h_0) = \frac{2\pi}{\sqrt{C}} \int_{h_0}^{\infty} f(h)\, dh \tag{164}$$

$$C \equiv c_1 c_1' + c_2 c_2' + (c_1 c_2 + c_1' c_2') \sin^2 \omega + (c_1 c_2' + c_1' c_2) \cos^2 \omega$$

where ω is the angle subtended between the directions of the principle curvatures of the two approaching surfaces. For two spheres one has $c_1 = c_1' = 1/R_1$, $c_2 = c_2' = 1/R_2$, and Equation 164 reduces to Equation 163.

For two cylinders of radii r_1 and r_2 crossed at angle ω one has $c_1 = c_2 = 0$; $c_1' = 1/r_1$, $c_2' = 1/r_2$ and Equation 164 yields

$$U(h_0) = \frac{2\pi\sqrt{r_1 r_2}}{\sin\omega}\int_{h_0}^{\infty} f(h)\,dh \tag{165}$$

Equation 165 is often used in connection to the experiments with the surface force apparatus,[34,257] in which the interacting surfaces are two crossed cylindrical mica sheets. The divergence in Equation 165 for $\omega = 0$ reflects the fact that the axes of the two infinitely long cylinders are parallel for $\omega = 0$ and thus the area of the interaction zone becomes infinite.

The main features of the Derjaguin approximation are the following: (1) It is applicable to any type of force law (attractive, repulsive, oscillatory), if the range of the forces is much smaller than the particles radii and (2) It reduces the problem for interactions between particles to the simpler problem for interactions in plane-parallel films.

5.4.2 VAN DER WAALS SURFACE FORCES

The van der Waals interaction between molecules *i* and *j* obeys the law:

$$u_{ij}(r) = -\frac{\alpha_{ij}}{r^6} \tag{166}$$

where u_{ij} is the potential energy of interaction, r is the distance between the two molecules, and α_{ij} is a constant characterizing the interaction. In fact, the van der Waals forces represent an averaged dipole-dipole interaction, which is a superposition of three main terms: (1) orientation interaction: interaction between two permanent dipoles;[258] (2) induction interaction: interaction between one permanent dipole and one induced dipole;[259] (3) dispersion interaction: interaction between two induced dipoles.[260] The theory yields:[34]

$$\alpha_{ij} = \frac{1}{(4\pi\varepsilon_0)^2}\left[\frac{p_i^2 p_j^2}{3kT} + \left(p_i^2\alpha_{oj} + p_j^2\alpha_{0i}\right) + \frac{3\alpha_{0i}\alpha_{0j}h_p\nu_i\nu_j}{2(\nu_i+\nu_j)}\right] \tag{167}$$

where p_i and α_{i0} are molecular dipole moment and electronic polarizability; h_p is the Planck constant; and ν_i is the orbiting frequency of the electron in the Bohr atom.

For van der Waals interactions between molecules in a gas phase, the orientation interaction can yield from 0% (nonpolar molecules) up to 70% (molecules of large permanent dipole moment, like H_2O) of the value of α_{ij}; the contribution of the induction interaction in α_{ij} is usually low, about 5 to 10%; the contribution of the dispersion interaction might be between 24% (water) and 100% (nonpolar hydrocarbons); for numerical data, see Reference 34.

According to the *microscopic* theory by Hamaker,[261] the van der Waals interaction between two macroscopic bodies can be found by integration of Equation 166 over all couples of molecules, followed by subtraction of the interaction energy at infinite separation between the bodies. The result depends on the geometry of the system. For a plane-parallel film from component 3 located between two semiinfinite phases composed from components 1 and 2, the van der Waals interaction energy per unit area and the respective disjoining pressure, stemming from Equation 166, are:[261]

$$f_{\mathrm{vw}} = -\frac{A_{\mathrm{H}}}{12\pi h^2}, \qquad \Pi_{\mathrm{vw}} = -\frac{\partial f_{\mathrm{vw}}}{\partial h} = -\frac{A_{\mathrm{H}}}{6\pi h^3} \tag{168}$$

where, as usual, h is the thickness of the film and A_{H} is the compound Hamaker constant:[14]

$$A_{\mathrm{H}} = A_{33} + A_{12} - A_{13} - A_{23} \qquad \left(A_{ij} = \pi^2 \rho_i \rho_j \alpha_{ij}, \;\; i,j = 1,2,3\right) \tag{169}$$

A_{ij} is the Hamaker constant of components i and j; ρ_i and ρ_j are the molecular number densities of phases i and j built up from components i and j, respectively. If A_{ii} and A_{jj} are known, one can calculate A_{ij} by using the Hamaker approximation

$$A_{ij} = \left(A_{ii} A_{jj}\right)^{1/2} \tag{170}$$

In fact, Equation 170 is applicable to the dispersion contribution in the van der Waals interaction.[34]

When components 1 and 2 are identical, A_{H} is positive (see Equation 169), therefore, the van der Waals interaction between identical bodies, in any medium, is always attractive. Besides, two dense bodies (even if nonidentical) will attract each other when placed in medium 3 of low density (gas, vacuum). When the phase in the middle (component 3) has intermediate Hamaker constant between those of bodies 1 and 2, A_{H} can be negative and the van der Waals disjoining pressure can be repulsive (positive). Such is the case of an aqueous film between mercury and gas.[262]

Lifshitz et al.[263,264] developed an alternative approach to the calculation of the Hamaker constant A_{H} in condensed phases, called the *macroscopic* theory. The latter is not limited by the assumption for pairwise additivity of the van der Waals interaction (see also References 34, 254 and 265). The Lifshitz theory treats each phase as a continuous medium characterized by a given uniform dielectric permittivity, which is dependent on the frequency, ν, of the propagating electromagnetic waves. For the symmetric configuration of two identical phases *"i"* interacting across a medium *"j"*, the macroscopic theory provides the expression[34]

$$A_{\mathrm{H}} \equiv A_{iji} = A_{iji}^{(\nu=0)} + A_{iji}^{(\nu>0)} = \frac{3}{4} kT \left(\frac{\varepsilon_i - \varepsilon_j}{\varepsilon_i + \varepsilon_j}\right)^2 + \frac{3h_{\mathrm{p}}\nu_{\mathrm{e}}\left(n_i^2 - n_j^2\right)^2}{16\sqrt{2}\left(n_i^2 + n_j^2\right)^{3/2}} \tag{171}$$

where ε_i and ε_j are the dielectric constants of phases i and j; n_i and n_j are the respective refractive indices for visible light; as usual, h_p is the Planck constant; ν_e is the main electronic absorption frequency which is $\approx 3.0\times10^{15}$ Hz for water and the most organic liquids.[34] The first term in the right-hand side of Equation 171, $A_{iji}^{(\nu=0)}$, is the so called zero-frequency term, expressing the contribution of the orientation and induction interactions. Indeed, these two contributions to the van der Waals force represent electrostatic effects. Equation 171 shows that the zero-frequency term can never exceed $\frac{3}{4}kT \approx 3\times10^{-21}$ J. The last term in Equation 171, $A_{iji}^{(\nu>0)}$, accounts for the dispersion interaction. If the two phases, i and j, have comparable densities (as for emulsion systems, say oil-water-oil), then $A_{iji}^{(\nu>0)}$ and $A_{iji}^{(\nu=0)}$ are comparable by magnitude. If one of the phases, i or j, has a low density (gas, vacuum), one obtains $A_{iji}^{(\nu>0)} >> A_{iji}^{(\nu=0)}$. In the latter case, the Hamaker's microscopic approach may give comparable $A_{iji}^{(\nu>0)}$ and $A_{iji}^{(\nu=0)}$ in contradiction to the Lifshitz macroscopic theory, which is more accurate for condensed phases.

A geometrical configuration, which is important for disperse systems, is the case of two spheres of radii R_1 and R_2 interacting across a medium (component 3). Hamaker[261] has derived the following expression for the van der Waals interaction energy between two spheres:

$$U(h_0) = -\frac{A_H}{12}\left(\frac{y}{x^2+xy+x} + \frac{y}{x^2+xy+x+y} + 2\ln\frac{x^2+xy+x}{x^2+xy+x+y}\right) \tag{172}$$

where

$$x = h_0 / 2R_1, \qquad y = R_2 / R_1 \le 1 \tag{173}$$

and h_0 is the same as in Figure 22. For $x << 1$ Equation 172 reduces to

$$U(h_0) \approx -\frac{A_H}{12}\frac{y}{(1+y)x} = -\frac{2\pi R_1 R_2}{R_1+R_2}\frac{A_H}{12\pi h_0} \tag{174}$$

Equation 174 can be also derived by combining Equation 168 with the Derjaguin approximation (Equation 163). It is worthwhile noting, that the logarithmic term in Equation 172 can be neglected only if $x << 1$. For example, even when $x = 5\times10^{-3}$, the contribution of the logarithmic term amounts to about 10% of the result (for $y = 1$); consequently, for larger values of x this term must be retained.

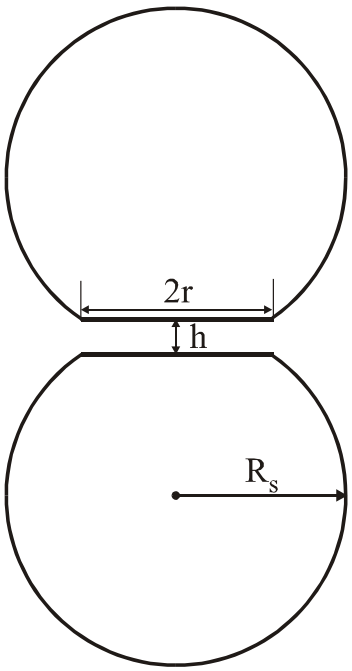

FIGURE 23. Thin film of radius r and thickness h formed between two attached fluid particles; the spherical part of the particle surface has radius R_s.

Another geometrical configuration, which corresponds to two colliding deformable emulsion droplets, is sketched in Figure 23. In this case the interaction energy is given by the expression[266]

$$U(h,r) = -\frac{A_{\mathrm{H}}}{12}\left[\frac{3}{4} + \frac{R_s}{h} + 2\ln\left(\frac{h}{R_s}\right) + \frac{r^2}{h^2} - \frac{2r^2}{R_s h}\right] \qquad (h, r << R_s) \qquad (175)$$

where h and r are the thickness and the radius of the flat film formed between the two deformed drops, respectively. R_s is the radius of the spherical part of the drop surface (see Figure 23). Equation 175 is a truncated series expansion; the exact formula, which is more voluminous, can be found in Reference 266. Expressions for U for other geometrical configurations are also available.[35,265]

The asymptotic behavior of the dispersion interaction at large intermolecular separations does not obey Equation 166; instead $u_{ij} \propto 1/r^7$ due to the electromagnetic retardation effect established by Casimir and Polder.[267] Various expressions have been proposed to account for this effect in the Hamaker constant.[265]

The orientation and induction interactions are electrostatic effects, so they are not subjected to electromagnetic retardation. Instead, they are subject to Debye screening due to the presence of electrolyte ions in the liquid phases. Thus for the interaction across an electrolyte solution the screened Hamaker constant is given by the expression[34,268]

$$A_{\mathrm{H}} = 2\kappa h\, A_0 e^{-2\kappa h} + A_d \qquad (176)$$

where A_0 denotes the contribution of orientation and induction interaction into the Hamaker constant and A_d is the contribution of the dispersion interaction; κ is the Debye screening parameter: $\kappa = \kappa_c I^{1/2}$ (see Equation 34).

5.4.3 ELECTROSTATIC SURFACE FORCES

5.4.3.1 Two Identically Charged Planes

First we consider the electrostatic (double layer) interaction between two identical charged plane parallel surfaces across solution of symmetrical *Z*:*Z* electrolyte. The charge of a counterion (i.e., ion with charge opposite to that of the surface) is $-Ze$, whereas the charge of a coion is $+Ze$ ($Z = \pm 1, \pm 2, ...$) with e being the elementary charge. If the separation between the two planes is very large, the number concentration of both counterions and coions would be equal to its bulk value, n_0, in the middle of the film. However, at finite separation, h, between the surfaces the two electric double layers overlap and the counterion and coion concentrations in the middle of the film, n_{10} and n_{20}, are no longer equal. Since the solution inside the film is supposed to be in electrochemical (Donnan) equilibrium with the bulk electrolyte solution of concentration n_0, one can write[269] $n_{10} n_{20} = n_0^2$, or alternatively

$$n_{10} = n_0 / \sqrt{m}, \qquad n_{20} = n_0 \sqrt{m}, \qquad m \equiv n_{20} / n_{10} \tag{177}$$

As pointed out by Langmuir,[270] the electrostatic disjoining pressure, Π_{el}, can be identified with the excess osmotic pressure in the middle of the film:

$$\Pi_{el} = kT\left(n_{10} + n_{20} - 2n_0\right) = n_0 kT\left(m^{1/4} - m^{-1/4}\right)^2 \tag{178}$$

Equation 178 demonstrates that for two identically charged surfaces Π_{el}, is always positive, i.e., corresponds to repulsion between the surfaces. In general, one has $0 < m \leq 1$, because the coions are repelled from the film due to the interaction with the film surfaces. To find the exact dependence of Π_{el} on the film thickness, h, one solves the Poisson-Boltzmann equation for the distribution of the electrostatic potential inside the film. The solution provides the following connection between Π_{el} and h for symmetric electrolytes:[254,271]

$$\Pi_{el} = 4n_0 kT \cot^2 \theta, \qquad \kappa h = 2\mathrm{F}(\varphi, \theta) \sin\theta \tag{179}$$

where $F(\varphi, \theta)$ is an elliptic integral of the first kind, and φ is related with θ as follows:

$$\cos\varphi = (\cot\theta)/\sinh(Z\Phi_s/2) \qquad \text{(fixed surface potential } \Phi_s) \tag{180}$$

$$\tan\varphi = (\tan\theta)\sinh(Z\Phi_\infty/2) \qquad \text{(fixed surface charge } \sigma_s) \tag{181}$$

$$\cosh(Z\Phi_\infty) = 1 + \frac{1}{2}\left(\frac{Ze\sigma_s}{\varepsilon\varepsilon_0 kT\kappa}\right)^2, \qquad \Phi_s \equiv \frac{e\psi_s}{kT} \tag{182}$$

Here, Φ_s is the dimensionless surface potential and Φ_∞ is the value of Φ_s for $h \to \infty$. Equation 179 expresses the dependence $\Pi_{el}(h)$ in a parametric form: $\Pi_{el}(\theta)$, $h(\theta)$. Fixed surface potential or charge means that Φ_s or σ_s does not depend on the film thickness h. The latter is important to be specified when integrating $\Pi(h)$ or $f(h)$ (in accordance with Equations 162 to 165) to calculate the interaction energy.

In principle, it is possible neither the surface potential nor the surface charge to be constant.[272] In such case a condition for *charge regulation* is applied, which in fact represents the condition for dynamic equilibrium of the counterion exchange between the Stern and diffuse parts of the electric double layer. As discussed in Section 5.2.1.2.3, the Stern layer itself can be considered as a Langmuirian adsorption layer of counterions. One can relate the maximum possible surface charge density (due to all surface ionizable groups) to Γ_1 in Equation 47: $\sigma_{max} = Ze\Gamma_1$. Likewise, the effective surface charge density, σ_s, which is smaller by magnitude than σ_{max} (because some ionizable groups are blocked by adsorbed counterions) can be expressed as $\sigma_s = Ze(\Gamma_1 - \Gamma_2)$. Then, with the help of Equation 44, the Stern isotherm (Equation 47) can be represented in the form

$$\frac{\sigma_{max} - \sigma_s}{\sigma_{max}} = \left[1 + (K_2 I)^{-1} \exp(Z\Phi_s)\right]^{-1} \tag{183}$$

The product $Z\Phi_s$ is always positive. At high surface potential, $Z\Phi_s \to \infty$, from Equation 183 one obtains $\sigma_s \to \sigma_{max}$, that is no blocking of surface ionizable by adsorbed counterions.

When the film thickness is large enough ($\kappa h \geq 1$) the difference between the regimes of constant potential, constant charge and charge regulation becomes negligible, i.e., the usage of each of them leads to the same results for $\Pi_{el}(h)$.[14]

When the dimensionless electrostatic potential in the middle of the film

$$\Phi_m = \frac{e}{kT}\psi_m = -\frac{1}{2Z}\ln m \tag{184}$$

is small enough (the film thickness, h, is large enough), one can suppose that $\Phi_m \approx 2\Phi_1(h/2)$, where Φ_1 is the dimensionless electric potential at a distance $h/2$ from the surface (of the film) when the other surface is removed at infinity. Since

$$Z\Phi_1(h/2) = 4\,\mathrm{e}^{-\kappa h/4}\tanh(Z\Phi_s/4) \tag{185}$$

from Equations 178, 184 and 185 one obtains a useful asymptotic formula[273]

$$\Pi_{\text{el}} \approx n_0 kTZ^2\Phi_m^2 \approx 64 n_0 kT\left(\tanh\frac{Z\Phi_s}{4}\right)^2 e^{-\kappa h} \tag{186}$$

It is interesting to note, that when Φ_s is large enough, the hyperbolic tangent in Equation 186 is identically 1, and Π_{el} (as well as f_{el}) becomes independent of the surface potential (or charge). Equation 186 can be generalized for the case of 2:1 electrolyte (bivalent counterion) and 1:2 electrolyte (bivalent coion):[274]

$$\Pi_{\text{el}} = 432 n_{(2)} kT\left(\tanh\frac{v_{i:j}}{4}\right)^2 \text{e}^{-\kappa h} \tag{187}$$

where $n_{(2)}$ is the concentration of the bivalent ions, the subscript "*i:j*" takes value "2:1" or "1:2", and

$$v_{2:1} = \ln\left[3/\left(1+2\text{e}^{-\Phi_s}\right)\right], \qquad v_{1:2} = \ln\left[\left(2\text{e}^{\Phi_s}+1\right)/3\right] \tag{188}$$

5.4.3.2 Two Nonidentically Charged Planes

Contrary to the case of two identically charged surfaces, which always repel each other (see Equation 178), the electrostatic interaction between two plane-parallel surfaces of different potentials, ψ_{s1} and ψ_{s2}, can be either repulsive or attractive.[254,275] Here, we will restrict our considerations to the case of low surface potentials, when the Poisson-Boltzmann equation can be linearized. In spite of being not too general quantitatively, this case exhibits qualitatively all features of the electrostatic interaction between different surfaces.

If $\psi_{s1} = \text{const.}$, and $\psi_{s2} = \text{const.}$, then the disjoining pressure at constant surface potential reads:[254]

$$\Pi_{\text{el}}^{\psi} = \frac{\varepsilon\varepsilon_0\kappa^2}{2\pi}\frac{2\psi_{s1}\psi_{s2}\cosh\kappa h - \left(\psi_{s1}^2+\psi_{s2}^2\right)}{\sinh^2\kappa h} \tag{189}$$

When the two surface potentials have opposite signs, i.e., when $\psi_{s1}\psi_{s2} < 0$, Π_{el}^{ψ} is negative for all h and corresponds to electrostatic attraction (see Figure 24(a)). This result could have been anticipated, since two charges of opposite sign attract each other. More interesting is the case, when $\psi_{s1}\psi_{s2} > 0$, but $\psi_{s1} \neq \psi_{s2}$. In the latter case, the two surfaces repel each other for $h > h_0$, whereas they attract each other for $h < h_0$ (Figure 24(a)); h_0 is determined by the equation $\kappa h_0 = \ln\left(\psi_{s2}/\psi_{s1}\right)$; $\psi_{s2} > \psi_{s1}$. In addition, the electrostatic repulsion has a maximum value of:

$$\Pi_{\text{el}}^{\psi}(\max) = \frac{\varepsilon\varepsilon_0\kappa^2}{2\pi}\psi_{s1}^2 \quad \text{at} \quad h_{\max} = \frac{1}{\kappa}\text{arccosh}\frac{\psi_{s2}}{\psi_{s1}}, \qquad \psi_{s2} > \psi_{s1} \tag{190}$$

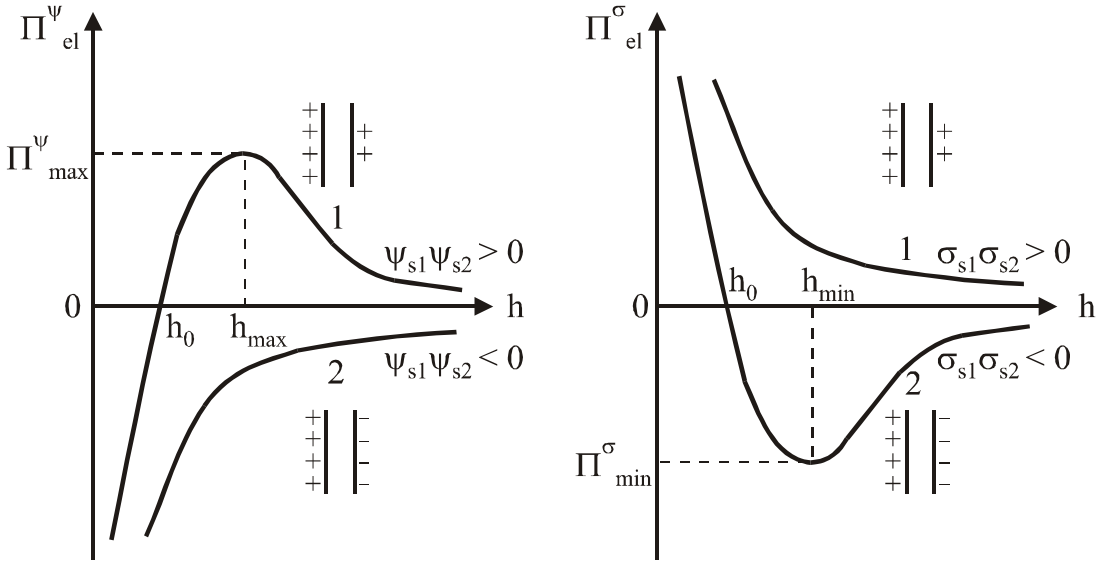

FIGURE 24. Electrostatic disjoining pressure at (a) fixed surface potential, $\Pi_{\rm el}^{\psi}$, and (b) fixed surface charge density, $\Pi_{\rm el}^{\sigma}$, both of them plotted vs. the film thickness h. ψ_{s1} and ψ_{s2} are the potentials of the two surfaces; σ_{s1} and σ_{s2} are the respective surface charge densities.

Similar electrostatic disjoining pressure isotherm has been used to interpret the experimental data for aqueous films on mercury.[147] It is worthwhile noting, that $\Pi_{\rm el}^{\psi}(\max)$ depends only on ψ_{s1}, i.e., the maximum repulsion is determined by the potential of the surface of lower charge.

If σ_{s1} = const., and σ_{s2} = const., then instead of Equation 189 one has[254]

$$\Pi_{\rm el}^{\sigma}(h) = \frac{1}{2\varepsilon\varepsilon_0}\frac{2\sigma_{s1}\sigma_{s2}\cosh\kappa h + \sigma_{s1}^2 + \sigma_{s2}^2}{\sinh^2\kappa h} \tag{191}$$

When $\sigma_1\sigma_2 > 0$ Equation 191 yields $\Pi_{\rm el}^{\sigma} > 0$ for every h (see Figure 24(b)). However, when $\sigma_1\sigma_2 < 0$, $\Pi_{\rm el}^{\sigma}$ is repulsive for small thickness, $h < h_0$ and attractive for larger separations, $h > h_0$; h_0 is determined by the equation $\kappa h_0 = \ln(-\sigma_{s2}/\sigma_{s1})$; $|\sigma_{s2}| > |\sigma_{s1}|$. The electrostatic disjoining pressure in this case has a minimum value

$$\Pi_{\rm el}^{\sigma}(\min) = \frac{1}{\varepsilon\varepsilon_0}\sigma_{s1}\sigma_{s2}, \qquad \text{at} \qquad h_{\min} = \frac{1}{\kappa}\operatorname{arccosh}\left(-\frac{\sigma_{s2}}{\sigma_{s1}}\right) \tag{192}$$

Finally, it should be noted, that all curves depicted in Figures 24(a) and (b) decay exponentially at $h \to \infty$. An asymptotic expression for Z:Z electrolytes, which generalizes Equation 186, holds:[254,273]

$$\Pi_{\mathrm{el}}(h) = 64 n_0 kT \gamma_1 \gamma_2 \mathrm{e}^{-\kappa h}, \qquad \gamma_k \equiv \tanh\left(\frac{Ze\psi_{sk}}{4kT}\right), \; k = 1,2 \tag{193}$$

Equation 193 is valid for both low and high surface potentials, if only $\exp(-\kappa h)$ 1.

5.4.3.3 Two Charged Spheres

When the electric double layers are thin compared with the particle radii (κ^{-1} R_1, R_2) and the gap between the particles is small (h_0 R_1, R_2), one can use Equation 193 in conjunction with the Derjaguin approximation, Equations 162 and 163. The result for the energy of electrostatic interaction between two spheres reads:

$$U_{\mathrm{el}}(h_0) = \frac{128\pi R_1 R_2}{\kappa^2 (R_1 + R_2)} n_0 kT \gamma_1 \gamma_2 \mathrm{e}^{-\kappa h} \tag{194}$$

Equation 194 is valid for any surface potentials ψ_{s1} and ψ_{s2} but only for $\exp(\kappa h)$ 1. Complementary expressions, which are valid for every h R_1,R_2, but for small surface potentials, can be derived by integrating Equations 189 and 191, instead of Equation 193. In this way, for $\psi_{s1} = \text{const.}$ and $\psi_{s2} = \text{const.}$, one can derive:[276]

$$U_{\mathrm{el}}^{\psi}(h_0) = \frac{\pi\varepsilon\varepsilon_0 R_1 R_2}{R_1 + R_2}\left[(\psi_{s1} + \psi_{s2})^2 \ln\left(1 + \mathrm{e}^{-\kappa h_0}\right) + (\psi_{s1} - \psi_{s2})^2 \ln\left(1 - \mathrm{e}^{-\kappa h_0}\right)\right] \tag{195}$$

or alternatively, for $\sigma_{s1} = \text{const.}$ and $\sigma_{s2} = \text{const.}$ one obtains[277]

$$U_{\mathrm{el}}^{\sigma}(h_0) = \frac{-\pi R_1 R_2}{\varepsilon\varepsilon_0 \kappa^2 (R_1 + R_2)}\left[(\sigma_{s1} + \sigma_{s2})^2 \ln\left(1 - \mathrm{e}^{-\kappa h_0}\right) + (\sigma_{s1} - \sigma_{s2})^2 \ln\left(1 + \mathrm{e}^{-\kappa h_0}\right)\right] \tag{196}$$

The range of validity of the different approximations involved in the derivations of Equations 194 to 196 is discussed in the book of Russel et al.[278]

As mentioned above, Equations 194 to 196 hold for h_0 R. In the opposite case, when h_0 is comparable to or larger than the particle radius R, one can use the equation[14]

$$U_{\mathrm{el}}(h_0) = \frac{4\pi\varepsilon\varepsilon_0 \psi_s^2 R^2}{2R + h_0} \mathrm{e}^{-\kappa h_0} \tag{197}$$

stemming from the theory of Debye and Hückel[279] for two identical particles. Equation 197 was derived by using the superposition approximation (valid for weak overlap of the two electric double layers) and the linearized Poisson-Boltzmann equation. A simple approximate

formula, representing in fact interpolation between Equations 197 and 195 (the latter for $R_1 = R_2 = R$), has been derived by McCartney and Levine[280]

$$U_{\mathrm{el}}^{\psi}(h_0) = 4\pi\varepsilon\varepsilon_0 R\psi_s^2 \frac{R + h_0}{2R + h_0} \ln\left(1 + \frac{Re^{-\kappa h_0}}{R + h_0}\right) \tag{198}$$

Equation 198 has the advantage to give a good approximation for every h_0 provided that the Poisson-Boltzmann equation can be linearized. Similar expressions for the energy of electrostatic interaction between two deformed droplets or bubbles (Figure 23) can be derived.[266]

5.4.4 DLVO THEORY

The first quantitative theory of interactions in thin liquid films and dispersions is the DLVO theory called after the names of the authors: Derjaguin and Landau[281] and Verwey and Overbeek.[273] In this theory, the total interaction is supposed to be a superposition of van der Waals and double layer interactions. In other words, the total disjoining pressure and the total interaction energy are presented in the form:

$$\Pi = \Pi_{\mathrm{vw}} + \Pi_{\mathrm{el}}, \qquad U = U_{\mathrm{vw}} + U_{\mathrm{el}} \tag{199}$$

A typical curve, Π vs. h, exhibits a maximum representing a barrier against coagulation, and two minima, called primary and secondary minimum (see Figure 13); the U vs. h curve has a similar shape. The primary minimum appears if strong short-range repulsive forces (e.g., steric forces) are present. With small particles, the depth of the secondary minimum is usually small ($U_{\min} < kT$). If the particles cannot overcome the barrier, coagulation (flocculation) does not take place, and the dispersion is stable due to the electrostatic repulsion, which gives rise to the barrier. With larger colloidal particles ($R > 0.1$ μm) the secondary minimum could be deep enough to cause coagulation and even formation of ordered structures of particles.[282]

By addition of electrolyte or by decreasing the surface potential of the particles, one can suppress the electrostatic repulsion and thus decrease the height of the barrier. According to DLVO theory, the critical condition determining the onset of rapid coagulation is

$$U(h_{\max}) = 0, \qquad \left.\frac{dU}{dh}\right|_{h_{\max}} = 0 \tag{200}$$

where $h = h_{\max}$ denotes the position of the barrier.

By using Equation 174 for U_{vw} and Equation 194 for U_{el} one derives from Equations 199 and 200 the following criterion for the threshold of rapid coagulation of identical particles ($R_1 = R_2 = R$; $\gamma_1 = \gamma_2 = \gamma$):

$$\frac{\kappa^6}{n_0^2} = \left[\frac{768\pi}{A_H} kT \mathrm{e}^{-1} \tanh^2\left(\frac{Ze\psi_s}{4kT} \right) \right]^2 \tag{201}$$

For a $Z{:}Z$ electrolyte, substituting $\kappa^2 = (2Z^2e^2n_0)/(\varepsilon_0\varepsilon kT)$ into Equation 201, one obtains:

$$n_0(\text{critical}) \propto \frac{1}{Z^6} \tanh^4\left(\frac{Ze\psi_s}{4kT} \right) \tag{202}$$

When ψ_s is high enough, the hyperbolic tangent equals 1 and Equation 202 yields $n_0(\text{critical}) \propto Z^{-6}$ which is, in fact, the empirical rule established earlier by Schulze[283] and Hardy.[284]

5.4.5 NON-DLVO SURFACE FORCES

After 1980, a number of surface forces have been found out which are not taken into account by conventional DLVO theory. They are considered separately below.

5.4.5.1 Ion Correlation Forces

As shown by Debye and Hückel,[279] due to the strong electrostatic interaction between the ions in a solution, the positions of the ions are correlated in such a way that a counterion atmosphere appears around each ion, thus screening its Coulomb potential. The energy of formation of the counterion atmospheres gives a contribution to the free energy of the system called correlation energy.[23] The correlation energy affects also a contribution to the osmotic pressure of the electrolyte solution, which can be presented in the form[23]

$$\Pi_{osm} = kT \sum_{i=1}^{k} n_i - \frac{kT\kappa^2}{24\pi} \tag{203}$$

The first term in the right-hand side of the Equation 117 corresponds to an ideal solution, whereas the second term takes into account the effect of electrostatic interactions between the ions (the same effect is accounted for thermodynamically by the activity coefficient, see Equation 31).

The expression for Π_{el} in the DLVO theory (Equation 178) obviously corresponds to an ideal solution, the contribution of the ionic correlations being neglected. Hence, in a more general theory, instead of Equation 199 one writes:

$$\Pi = \Pi_{vw} + \Pi_{el} + \Pi_{cor} \tag{204}$$

where Π_{cor} is the contribution of the ionic correlations to the disjoining pressure. The theory of Π_{cor} takes into account the following effects: (1) the different ionic concentration (and hence the different Debye screening) in the film compared to that in the bulk solution; (2) the energy of deformation of the counterion atmosphere due to the image forces; (3) the energy of the long-range correlations between charge-density fluctuations in the two opposite electric double layers. For calculating Π_{cor} both numerical solutions[285,286] and analytical expressions[287,288] have been obtained. For example, in the case when the electrolyte is symmetrical (Z:Z) and $\exp(-\kappa h) \quad 1$ one can use the asymptotic formula[287]

$$\Pi_{cor} = \Pi_{el} \frac{Z^2 e^2 \kappa}{16\pi\varepsilon\varepsilon_0 kT}\left(\ln 2 + 2I_C\right) + O\left(e^{-\kappa h}\right) \tag{205}$$

where Π_{el} is the conventional DLVO electrostatic disjoining pressure,

$$I_C = \frac{1}{2}(1+J)\ln 2 + \frac{2-2z^3+z}{2z\left(2z^2-1\right)^2} - \frac{1}{2}(1-J)\ln\left(z+z^2\right)$$

$$- \frac{\sqrt{z^2-1}}{z}\left[1+J+4\left(2z^2-1\right)^{-3}\right]\arctan\sqrt{\frac{z-1}{z+1}}$$

$$J \equiv \frac{2z^2-3}{\left(2z^2-1\right)^3}, \qquad z \equiv \left[1+\left(\frac{e\sigma_s}{2\varepsilon\varepsilon_0 kT\kappa}\right)^2\right]^{1/2}$$

The results for the case of symmetric electrolytes are the following. Π_{cor} is negative and corresponds to attraction, which can be comparable by magnitude with Π_{vw}. In the case of 1:1 electrolyte Π_{cor} is usually small correction to Π_{el}. In the case of 2:2 electrolyte, however, the situation can be quite different: the attractive forces, $\Pi_{cor} + \Pi_{vw}$, prevails over Π_{el} and the total disjoining pressure, Π, becomes negative. The effect of Π_{cor} is even larger in the presence of ions of higher valence. Thus, the ion-correlation attraction could be the explanation for the sign inversion of the second virial coefficient, β_2, of micellar surfactant solutions (from $\beta_2 > 0$ to $\beta_2 < 0$, measured by light scattering) when the Na^+ ions are replaced by Al^{3+} ions at fixed total ionic strength (see Figure 31 in Reference 289). Short-range net attractive ion-correlation forces have been measured by Marra[290,291] and Kjellander et al.[292,293] between highly charged anionic bilayer surfaces in $CaCl_2$ solutions. These forces are believed to be responsible for the strong adhesion of some surfaces (clay and bilayer membranes) in the presence of divalent counterions.[34,292,294] On the other hand, Kohonen et al.[295] measured a monotonic repulsion between two mica surfaces in 4.8×10^{-3} M solution of $MgSO_4$. Additional work is necessary to verify the theoretical predictions and to clarify the physical significance of the ion-correlation surface force.

Note that the theory predicts ion-correlation attraction not only across water films with overlapping electric double layers, but also across *oily* films intervening between two water phases. In the latter case, Π_{cor} is not zero because the ions belonging to the two outer double layers interact across the thin dielectric (oil) film. The theory for such a film[296] predicts that Π_{cor} is negative (attractive) and strongly dependent on the dielectric permittivity of the oil film; Π_{cor} can be comparable by magnitude with Π_{vw}; $\Pi_{el} = 0$ in this case.

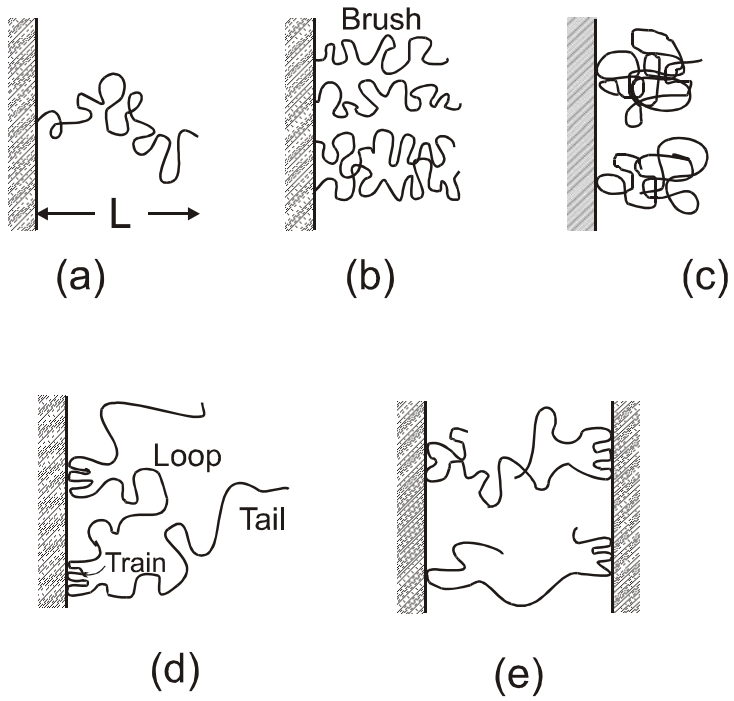

FIGURE 25. Polymeric chains adsorbed at an interface: (a) terminally anchored polymer chain of mean end-to-end distance *L*; (b) a brush of anchored chains; (c) adsorbed (but not anchored) polymer coils; (d) configuration with a loop, trains and tails; (e) bridging of two surfaces by adsorbed polymer chains.

5.4.5.2 Steric Interaction

5.4.5.2.1 Physical background

The steric interaction between two surfaces appears when chain molecules, attached at some point(s) to a surface, dangle out into the solution (see Figure 25). When two such surfaces approach each other, the following effects take place:[34,297-299] (1) The entropy decreases due to the confining of the dangling chains which results in a repulsive osmotic force known as *steric* or *overlap* repulsion. (2) In a poor solvent, the segments of the chain molecules attract each other; hence the overlap of the two approaching layers of polymer molecules will be accompanied with some *intersegment attraction*; the latter can prevail for small overlap, however at the distance of larger overlap it becomes negligible compared with the osmotic

repulsion. (3) Another effect, known as the *bridging attraction*, occurs when two opposite ends of chain molecule can attach (adsorb) to the opposite approaching surfaces, thus forming a bridge between them (see Figure 25(e)).

Steric interaction can be observed in foam or emulsion films stabilized with nonionic surfactants or with various polymers, including proteins. The usual nonionic surfactants molecules are anchored (grafted) to the liquid interface by their hydrophobic moieties. When the surface concentration of adsorbed molecules is high enough, the hydrophilic chains are called to form a brush (Figure 25(b)). The coils of macromolecules, like proteins, can also adsorb at a liquid surface (Figure 25(c)). Sometimes the configurations of the adsorbed polymers are very different from the statistical coil: loops, trains, and tails can be distinguished (Figure 25(d)).

The osmotic pressure of either dilute or concentrated polymer solutions can be expressed in the form:[300]

$$\frac{P_{\text{osm}}}{nkT} = \frac{1}{N} + \frac{1}{2}nv + \frac{1}{3}n^2 w + \ldots \tag{206}$$

Here N is the number of segments in the polymer chain, n is the number segment density, v and w account for the pair and triplet interactions, respectively, between segments. In fact, v and w are counterparts of the second and third virial coefficients in the theory of imperfect gases;[11] v and w can be calculated if information about the polymer chain and the solvent is available:[278]

$$w^{1/2} = \bar{v}m / N_{\text{A}}, \qquad v = w^{1/2}\left(1 - 2\chi\right) \tag{207}$$

where $\bar{v}$ (m^3/kg) is the specific volume per segment, m (kg/mol) is the molecular weight per segment, N_{A} is the Avogadro number and χ is the Flory parameter. The latter depends on both the temperature and the energy of solvent-segment interaction. Then, v can be zero (see Equation 207) for some special temperature, called the *theta temperature*. The solvent at the theta temperature is known as the *theta solvent* or *ideal solvent*. The theta temperature in polymer solutions is a counterpart of the Boil temperature in imperfect gases: this is the temperature at which the intermolecular (intersegment) attraction and repulsion are exactly counterbalanced. In a good solvent, however, the repulsion due mainly to the excluded volume effect dominates the attraction and $v > 0$. In contrast, in a poor solvent the intersegment attraction prevails, so $v < 0$.

5.4.5.2.2 Thickness of the polymer adsorption layer

The steric interaction between two approaching surfaces appears when the film thickness becomes of the order of, or smaller than $2L$ where L is the mean-square end-to-end distance of the hydrophilic portion of the chain. If the chain was entirely extended, then L would be equal

to *Nl* with *l* being the length of a segment; however, due to the Brownian motion $L < Nl$. For an anchored chain, like that depicted in Figure 25(a), in a theta solvent, L can be estimated as:[278]

$$L \approx L_0 \equiv l\sqrt{N} \tag{208}$$

In a good solvent $L > L_0$, whereas in a poor solvent $L < L_0$. In addition, L depends on the surface concentration, Γ, of the adsorbed chains, i.e., L is different for an isolated molecule and for a brush (see Figures 25(a) and (b)). The mean field approach[278,301] applied to polymer solutions provides the following equation for calculating L

$$\widetilde{L}^3 - \left(1 + \frac{1}{9}\widetilde{\Gamma}^2\right)\widetilde{L}^{-1} = \frac{1}{6}\widetilde{v} \tag{209}$$

where $\widetilde{L}$, $\widetilde{\Gamma}$ and $\widetilde{v}$ are the dimensionless values of L, Γ and v defined as follows:

$$\widetilde{L} = L/\left(l\sqrt{N}\right), \qquad \widetilde{\Gamma} = \Gamma N\sqrt{w}/l, \qquad \widetilde{v} = v\Gamma N^{3/2}/l \tag{210}$$

For an isolated adsorbed molecule $(\widetilde{\Gamma} = 0)$ in an ideal solvent $\left(\widetilde{v} = 0\right)$ Equation 209 predicts $\widetilde{L} = 1$, i.e., $L = L_0$.

5.4.5.2.3 Overlap of adsorption layers

We now consider the case of terminally anchored chains, like those depicted in Figures 25(a) and (b). Dolan and Edwards[302] calculated the steric interaction free energy per unit area, *f*, as a function on the film thickness, *h*, in a theta solvent:

$$f(h) = \Gamma kT\left[\frac{\pi^2}{3}\frac{L_0^2}{h^2} - \ln\left(\frac{8\pi}{3}\frac{L_0^2}{h^2}\right)\right] \quad \text{for} \quad h < L_0\sqrt{3} \tag{211}$$

$$f(h) = 4\Gamma kT\exp\left(-\frac{3h^2}{2L_0^2}\right) \qquad \text{for} \quad h > L_0\sqrt{3} \tag{212}$$

where L_0 is the end-to-end distance as defined by Equation 208. The boundary between the power-law regime ($f \propto 1/h^2$) and the exponential decay regime is at $h = L_0\sqrt{3} \approx 1.7\,L_0$, the latter being slightly less than $2L_0$, which is the intuitively expected onset of the steric overlap. The first term in the right-hand side of Equation 211 comes from the osmotic repulsion between the brushes, which opposes the approach of the two surfaces; the second term is negative and accounts effectively for the decrease of the elastic energy of the initially extended chains when the thickness of each of the two brushes, pressed against each other, decreases.

In the case of good solvent the disjoining pressure $\Pi = -df/dh$ can be calculated by means of Alexander-de Gennes theory as:[303,304]

$$\Pi(h) = kT\Gamma^{3/2}\left[\left(\frac{2L_g}{h}\right)^{9/4} - \left(\frac{h}{2L_g}\right)^{3/4}\right] \quad \text{for} \quad h < 2L_g, \qquad L_g = N\left(\Gamma l^5\right)^{1/3} \tag{213}$$

where L_g is the thickness of a brush in a good solvent.[305] The positive and the negative terms in the right-hand side of Equation 213 correspond to osmotic repulsion and elastic attraction. The validity of Alexander-de Gennes theory was experimentally confirmed by Taunton et al.[306] who measured the forces between two brush layers grafted on the surfaces of two crossed mica cylinders.

In the case of adsorbed molecules, like these in Figure 25(c), which are not anchored to the surface, the measured surface forces depend significantly on the rate of approaching of the two surfaces.[307,308] The latter effect can be attributed to the comparatively low rate of exchange of polymer between the adsorption layer and the bulk solution. This leads to a hysteresis of the surface force: different interaction on approach and separation of the two surfaces.[34] In addition, one can observe two regimes of steric repulsion: (1) weaker repulsion at larger separations due to the overlap of the tails (Figure 25(d)) and (2) stronger repulsion at smaller separations indicating overlap of the loops.[309]

5.4.5.3 Oscillatory Structural Forces

5.4.5.3.1 Origin of the structural forces

Oscillatory structural forces appear in two cases: (1) in thin films of pure solvent between two smooth *solid* surfaces; (2) in thin liquid films containing colloidal particles (including macromolecules and surfactant micelles). In the first case, the oscillatory forces are called the *solvation forces*;[34,310] they are important for the short-range interactions between solid particles and dispersions. In the second case, the structural forces affect the stability of foam and emulsion films as well as the flocculation processes in various colloids. At higher particle concentrations, the structural forces stabilize the liquid films and colloids.[311-315] At lower particle concentrations, the structural forces degenerate into the so called *depletion attraction*, which is found to destabilize various dispersions.[316,317]

In all cases, the oscillatory structural forces appear when monodisperse spherical (in some cases ellipsoidal or cylindrical) particles are confined between the two surfaces of a thin film. Even one "hard wall" can induce ordering among the neighboring molecules. The oscillatory structural force is a result of overlap of the structured zones at two approaching surfaces.[318-321] A simple connection between density distribution and structural force is given by the contact value theorem:[34,321,322]

$$\Pi_{os}(h) = kT\left[n_s(h) - n_s(\infty)\right] \tag{214}$$

where Π_{os} is the disjoining pressure component due to the oscillatory structural forces, $n_s(h)$ is the particle number density in the subsurface layer as a function of the distance between the walls, h. Figure 26 illustrates the variation of n_s with h and the resulting disjoining pressure, Π_{os}. One sees that in the limit of very small separations, as the last layer of particles is eventually squeezed out, $n_s \to 0$ and

$$\Pi_{os}(h) \to -kT n_s(\infty) \quad \text{for} \quad h \to 0 \tag{215}$$

In other words, at small separations Π_{os} is negative (attractive). Equation 215 holds for both solvation forces and colloid structural forces. In the latter case, Equation 215 represents the osmotic pressure of the colloid particles and the resulting attractive force is known as the depletion force (Section 5.4.5.3.3 below).

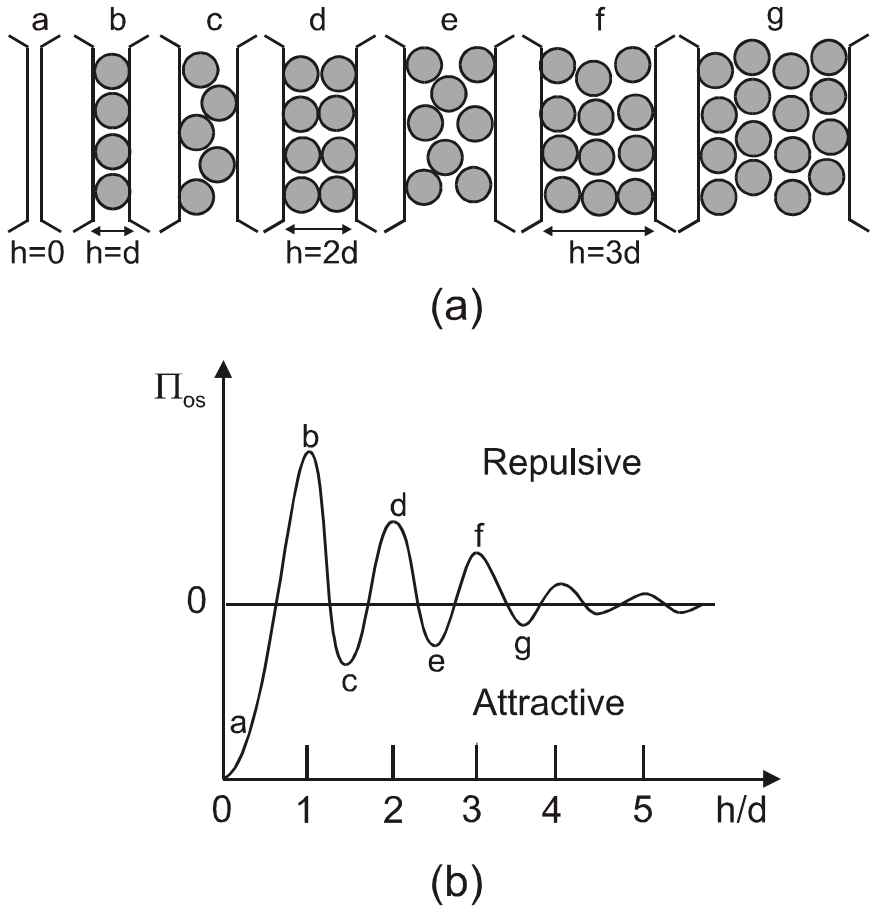

FIGURE 26. (a) Sketch of the consecutive stages of the thinning of a liquid film containing spherical particles; (b) plot of the related oscillatory structural component of disjoining pressure, Π_{os}, vs. the film thickness h (see Reference 34 for details).

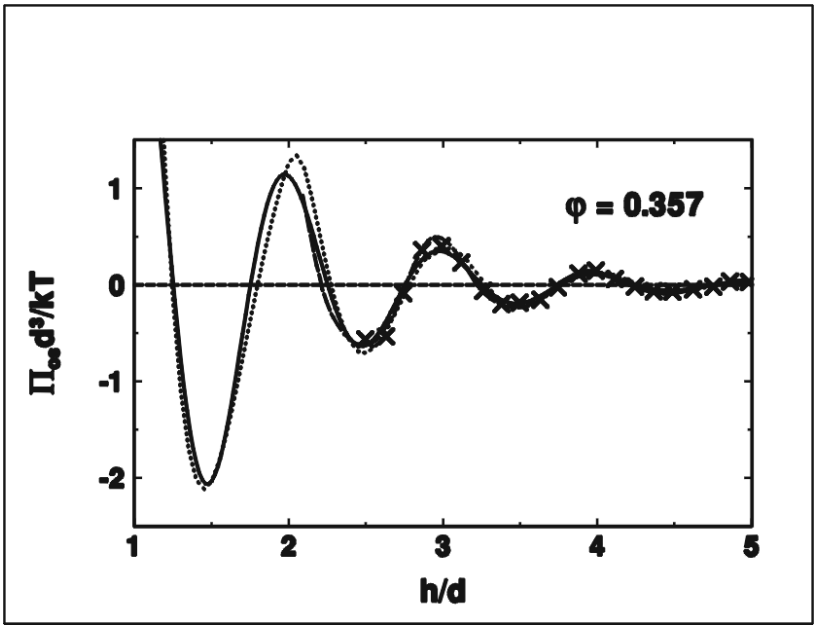

FIGURE 27. Dimensionless oscillatory disjoining pressure, $\Pi_{os}d^3/kT$, plotted vs. *h/d*. The solid curve calculated from Equation 216 is compared to the theories by Henderson[323] (the dotted curve), Kjellander and Sarman[326] (the dashed curve), and Karlström[329] (the **x** points). (From Kralchevsky, P.A. and Denkov, N.D., *Chem. Phys Lett.*, 240, 385, 1995. With permission.)

It is worthwhile noting that the wall can induce structuring in the neighboring fluid only if the magnitude of the surface roughness is negligible compared with the particle diameter, *d*. Indeed, when surface irregularities are present, the oscillations are smeared out and oscillatory structural force does not appear. If the film surfaces are fluid, the role of the surface roughness is played by the interfacial fluctuation capillary waves, whose amplitude (usually between 1 and 5 Å) is comparable to the diameter of the solvent molecules. That is why oscillatory solvation forces (due to structuring of solvent molecules) are observed only with liquid films, which are confined between smooth solid surfaces.[34] In order for structural forces to be observed in foam or emulsion films, the diameter of the colloidal particles must be much larger than the amplitude of the surface corrugations.[315]

The period of the oscillations is, in fact, always about the particle diameter.[34,315] In this aspect, the structural forces are appropriately called the "volume exclusion forces" by Henderson,[323] who derived an explicit (though rather complex) formula for calculating these forces.

A semiempirical formula for the oscillatory structural component of disjoining pressure was proposed[324]

$$\Pi_{os}(h) = P_0 \cos\left(\frac{2\pi h}{d_1}\right)\exp\left(\frac{d^3}{d_1^2 d_2} - \frac{h}{d_2}\right) \quad \text{for} \quad h > d$$
$$= -P_0 \qquad \text{for } 0 < h < d \tag{216}$$

where d is the diameter of the hard spheres, d_1 and d_2 are the period and the decay length of the oscillations which are related to the particle volume fraction, ϕ, as follows[324]

$$\frac{d_1}{d} = \sqrt{\frac{2}{3}} + 0.237\Delta\phi + 0.633(\Delta\phi)^2; \qquad \frac{d_2}{d} = \frac{0.4866}{\Delta\phi} - 0.420 \tag{217}$$

Here $\Delta\phi = \phi_{max} - \phi$ with $\phi_{max} = \pi/(3\sqrt{2})$ being the value of ϕ at close packing. P_0 is the particle osmotic pressure determined by means of Carnahan-Starling formula[325]

$$P_0 = nkT\frac{1 + \phi + \phi^2 - \phi^3}{(1-\phi)^3}, \qquad n = \frac{6\phi}{\pi d^3} \tag{218}$$

where n is the particle number density. It is clear that for $h < d$, when the particles are expelled from the slit into the neighboring bulk suspension, Equation 216 describes the depletion attraction. On the other hand, for $h > d$ the structural disjoining pressure oscillates around P_0 as defined by Equation 218 in agreement with the finding of Kjellander and Sarman.[326] The finite discontinuity of Π_{os} at $h = d$ is not surprising as, at this point, the interaction is switched over from oscillatory to depletion regime.

It is interesting to note that in an oscillatory regime the concentration dependence of Π_{os} is dominated by the decay length d_2 in the exponent (see Equations 216 and 217). Roughly speaking, for a given distance h, the oscillatory disjoining pressure Π_{os} increases five times when ϕ is increased 10%.[324]

The contribution of the oscillatory structural forces to the interaction free energy per unit area of the film can be obtained by integrating Π_{os}:

$$f_{os}(h) = \int_h^\infty \Pi_{os}(h')dh' = F(h) \qquad \text{for } h \geq d$$
$$= F(d) - P_0(d-h) \qquad \text{for } 0 \leq h \leq d \tag{219}$$
$$F(h) \equiv \frac{P_0 d_1 \exp\left[\left(d^3/d_1^2 d_2\right) - \left(h/d_2\right)\right]}{4\pi^2 + \left(d_1/d_2\right)^2}\left[\frac{d_1}{d_2}\cos\left(\frac{2\pi h}{d_1}\right) - 2\pi\sin\left(\frac{2\pi h}{d_2}\right)\right]$$

It should be noted that Equations 216 and 219 refer to hard spheres of diameter d. In practice, however, the interparticle potential can be "soft" because of the action of some long-range forces. If such is the case, one can obtain an estimation of the structural force by introducing an effective hard-core diameter[314]

$$d(T) = \left[\frac{3}{4\pi} \beta_2(T) \right]^{1/3} \tag{220}$$

where β_2 is the second virial coefficient in the virial expansion of the particle osmotic pressure: $P_{osm}/(nkT) = 1 + \beta_2 n/2 + \ldots$. When the particles are ionic surfactant micelles (or other electrically charged particles), the diameter of the effective hard sphere can be approximated as $d \approx d_H + 2\kappa^{-1}$, where the Debye screening length κ^{-1}, involves contributions from both the background electrolyte and the counterions dissociated from the micelles:[312,313,327,328]

$$\kappa^2 = \frac{e^2}{\varepsilon_0 \varepsilon KT} \left[2\,(\mathrm{CMC} + I_a) + (C_s - \mathrm{CMC})\alpha_d \right] \tag{221}$$

Here, d_H is the micelle hydrodynamic diameter (usually measured by dynamic light scattering); as before, CMC stands for the critical micellization concentration, C_s is the total concentration of ionic surfactant; I_a is the ionic strength due to added inorganic electrolyte (if any), and α_d is the degree of ionization of the micelle surface ionizable groups (non-neutralized by bound counterions).

In Figure 27 a curve calculated from Equation 216 is compared with the predictions of other studies. The dotted line is calculated by means of the Henderson theory.[323] The theoretical curve calculated by Kjellander and Sarman[316] for $\phi = 0.357$ and $h > 2$ by using the anisotropic Percus-Yevick approximation is shown by the dashed line; the crosses represent grand canonical Monte Carlo simulation results due to Karlström.[329] We proceed now with separate descriptions of solvation, depletion and colloid structural forces.

5.4.5.3.2 Oscillatory solvation forces

When the role of hard spheres, like those depicted in Figure 26, is played by the molecules of solvent, the resulting volume exclusion force is called the *oscillatory solvation force*, or sometimes when the solvent is water, *oscillatory hydration force*.[34] The latter should be distinguished from the *monotonic* hydration force, which has different physical origin and is considered separately in Section 5.4.5.4 below.

Measurement of the oscillatory solvation force became possible after the precise surface force apparatus had been constructed.[34] This apparatus allowed to measure the surface forces in thin liquid films confined between mica (or modified mica) surfaces and in this way to check the validity of the DLVO theory down to thickness of about 5 Å and even smaller. The experimental results with non-aqueous liquids of both spherical (CCl_4) or cylindrical (linear alkanes) molecules showed that at larger separations the DLVO theory is satisfied, whereas at separations on the order of several molecular diameters an oscillatory force is superimposed over the DLVO force law. In aqueous solutions, oscillatory forces were

observed at higher electrolyte concentrations with periodicity of 0.22 to 0.26 nm, about the diameter of the water molecule.[34] As mentioned above, the oscillatory solvation forces can exist only between smooth solid surfaces.

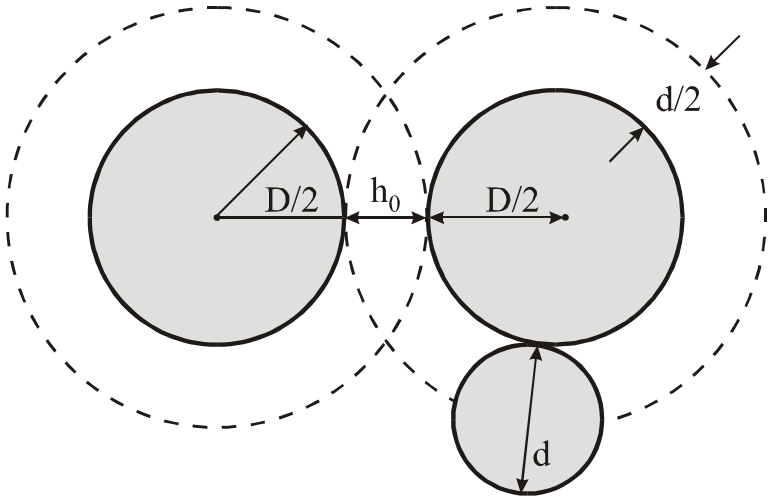

FIGURE 28. Overlap of the depletion zones around two particles of diameter *D* separated at a surface-to-surface distance h_0; the smaller particles have diameter *d*.

5.4.5.3.3 Depletion forces

Bondy[330] observed coagulation of rubber latex in presence of polymer molecules in the disperse medium. Asakura an Oosawa[316] published a theory, which attributed the observed interparticle attraction to the overlap of the depletion layers at the surfaces of two approaching colloidal particles (see Figure 28). The centers of the smaller particles, of diameter, *d*, cannot approach the surface of a bigger particle (of diameter *D*) at a distance shorter than *d*/2, which is the thickness of the depletion layer. When the two depletion layers overlap (Figure 28), some volume between the large particles becomes inaccessible for the smaller particles. This gives rise to an osmotic pressure, which tends to suck out the solvent between the bigger particles, thus forcing them against each other. The total depletion force experienced by one of the bigger particles is[316]

$$F_{\text{dep}} = -kTnS(h_0) \tag{222}$$

where the effective depletion area is

$$\begin{aligned} S(h_0) &= \frac{\pi}{4}(2D + d + h_0)(d - h_0) \quad \text{for } 0 \le h_0 \le d \\ S(h_0) &= 0 \qquad\qquad\qquad\qquad\quad \text{for } d \le h_0 \end{aligned} \tag{223}$$

Here, h_0 is the shortest distance between the surfaces of the larger particles, and *n* is the number density of the smaller particles. By integrating Equation 222 one can derive an

expression for the depletion interaction energy between the two larger particles, $U_{dep}(h_0)$. For $D \gg d$ this expression reads:

$$U_{dep}(h_0)/kT \approx -\frac{3}{2}\phi\frac{D}{d^3}(d-h_0)^2 \qquad 0 \le h_0 \le d \tag{224}$$

where $\phi = \pi nd^3/6$ is the volume fraction of the small particles. The maximum value of U_{dep} at $h_0 = 0$ is $U_{dep}(0)/kT \approx -3\phi D/(2d)$. For example, if $D/d = 50$ and $\phi = 0.1$, then $U_{dep}(0) = 7.5\,kT$. This depletion attraction turns out to be large enough to cause flocculation in dispersions. De Hek and Vrij[317] studied systematically the flocculation of sterically stabilized silica suspensions in cyclohexane by polystyrene molecules. Patel and Russel[331] investigated the phase separation and rheology of aqueous polystyrene latex suspensions in the presence of polymer (Dextran T-500). The stability of dispersions is often determined by the competition between electrostatic repulsion and depletion attraction.[332] An interplay of steric repulsion and depletion attraction was studied theoretically by van Lent *et al*.[333] for the case of polymer solution between two surfaces coated with anchored polymer layers. Joanny *et al*.[334] and Russel *et al*.[278] re-examined the theory of depletion interaction by taking into account the internal degrees of freedom of the polymer molecules; their analysis confirmed the earlier results of Asakura and Oosawa.[316]

In the case of plane-parallel films the depletion component of disjoining pressure is

$$\begin{aligned} \Pi_{dep}(h) &= -nkT \qquad h < d \\ \Pi_{dep}(h) &= 0 \qquad\quad h > d \end{aligned} \tag{225}$$

which is similar to Equation 215. This is not surprising because in both case we are dealing with the excluded volume effect. Evans and Needham[335] succeeded to measure the depletion energy of two interacting bilayer surfaces in a concentrated Dextran solution; their results confirm the validity of Equation 225.

The depletion interaction is present always when a film is formed from micellar surfactant solution; the micelles play the role of the smaller particles. At higher micellar concentrations, the volume exclusion interaction becomes more complicated: it follows the oscillatory curve depicted in Figure 26. In this case only, the first minimum (that at $h \to 0$) corresponds to the conventional depletion force.

5.4.5.3.4 Colloid structural forces

In the beginning of the 20th century, Johnott[336] and Perrin[337] observed that soap films decrease their thickness by several stepwise transitions. The phenomenon was called *stratification*. Bruil and Lyklema[338] and Friberg et al.[339] studied systematically the effect of ionic surfactants and electrolytes on the occurrence of the stepwise transitions. Keuskamp and Lyklema[340] anticipated that some oscillatory interaction between the film surfaces must be

responsible for the observed phenomenon. Kruglyakov et al.[341,342] reported the existence of stratification with emulsion films.

The experimental results obtained called for some theoretical interpretation. Some authors[342,343] suggested that a possible explanation of the phenomenon can be the formation of lamella liquid-crystal structure inside the film. Such lamellar micelles are observed to form in surfactant solutions, but at concentrations much higher than those used in the experiments with stratifying films. The latter fact makes the lamella-liquid-crystal explanation problematic. Nikolov et al.[311,312,344] observed stratification not only with micellar surfactant solutions but also with latex suspensions. The heights of the step-wise changes in the film thickness were approximately equal to the diameter of the spherical particles, contained in the foam film.[311-315,345]

The experimental observations show that stratification is always observed when spherical colloidal particles are present in the film at a sufficiently high volume fraction; therefore, a realistic explanation can be that the stepwise transitions are manifestations of the oscillatory structural forces. The role of the "hard spheres" this time is played by the colloidal particles rather than by the solvent molecules. The mechanism of stratification was studied theoretically in Reference 346, where the appearance and expansion of black spots in the stratifying films were described as being a process of condensation of vacancies in a colloid crystal of ordered micelles within the film.

Two pronounced effects with stratifying films deserve to be mentioned: (1) The increase of electrolyte ionic strength, I_a, leads to smoother and faster thinning of the foam films from ionic surfactant solutions. When I_a becomes high enough, the stepwise transitions disappear.[312] This can be explained by suppression of the oscillatory structural forces due to decrease of the effective micelle volume fraction because of shrinkage of the counterion atmospheres (see Equation 221). (2) In the case of nonionic surfactant micelles, an increase of temperature leads to a similar effect - disappearance of the stepwise character of the film thinning.[314] This can be attributed to the change of the intermicellar interaction from being repulsive to being attractive with an increase of temperature.[347] The electrolyte and temperature dependence of the colloid structural forces provides a tool for the control of the stability of dispersions.

Oscillatory structural forces due to micelles[328] and microemulsion droplets[348] were directly measured by means of a surface force balance. The application of interference methods to free vertical stratifying films, containing 100 nm latex particles, showed that the particles form a colloid crystal structure of hexagonal packing inside the films.[349] Structuring of latex particles, analogous to stratification, was observed also in wetting films.[350] The measured contact angles of stratifying emulsion films, containing surfactant micelles, were found to agree well with Equation 219 (see also Equation 148).[192] Theoretical modeling of the

oscillatory force and the stepwise film thinning by means of the integral equations of statistical mechanics[351] and numerical simulations[352,353] has been carried out.

5.4.5.4 Repulsive Hydration and Attractive Hydrophobic Forces

These two surface forces are observed in thin aqueous films. Their appearance is somehow connected with the unique properties of the water as solvent: small molecular size, large dipole moment, high dielectric constant, and formation of an extensive hydrogen-bonding network.[34,354]

5.4.5.4.1 Repulsive hydration forces

In their experiments with films from aqueous electrolyte solutions confined between two mica surfaces, Israelachvili et al.[355,356] and Pashley[357,358] examined the validity of the DLVO theory at small film thickness. At electrolyte concentrations below 10^{-4} mol/l (KNO_3 or KCl), they observed the typical DLVO maximum (see Figure 13); however, at electrolyte concentrations higher than 10^{-3} mol/l they did not observe the expected DLVO maximum and primary minimum. Instead a strong short-range repulsion was detected. Empirically, this force, called the hydration repulsion, appears to follow an exponential law[34]

$$f_{\text{hydr}}(h) = f_0 e^{-h/\lambda_0} \tag{226}$$

where the decay length $\lambda_0 \approx 0.6$–1.1 nm for 1:1 electrolytes and f_0 depends on the hydration of the surfaces but is usually about 3 to 30 mJ/m^2.

The physical importance of the hydration force is that it stabilizes some dispersions preventing coagulation in the primary minimum. It is believed that the hydration force is connected with the binding of strongly hydrated ions at the interface. This is probably the explanation of the experimental results of Healy et al.,[359] who found that even high electrolyte concentrations cannot cause coagulation of amphoteric latex particles due to binding of strongly hydrated Li^+ ions at the particle surfaces. If the Li^+ ions are replaced by weakly hydrated Cs^+ ions, the hydration repulsion becomes negligible, compared with the van der Waals attraction, and the particles coagulate as predicted by the DLVO theory. Hence, the hydration repulsion can be regulated by ion exchange.

For the time being, there is no generally accepted theory of the repulsive hydration forces. The first quantitative theory by Marčelja and Radič[360] attributes the hydration repulsion to the water structuring in the vicinity of a surface, which leads to the appearance of a decaying polarization profile. This model was further developed by other authors[361,362]. A different approach was proposed by Jönsson and Wennerström,[363] who developed an explicit electrostatic model based on the image charge concept. Leikin and Kornyshev[364] combined the main features of the solvent polarization[360] and image charge[363] models in a

nonlocal electrostatic theory of the repulsion between electroneutral lipid bilayers. On the other hand, Israelachvili and Wennerström[365] demonstrated that the short-range repulsion between lipid membranes may also be a manifestation of undulation, peristaltic and protrusion forces, which are due to thermally excited fluctuations at the interfaces (see the next section).

In the case of charged surfaces, Henderson and Losada-Cassou[366] pointed out that the physical origin of the hydration repulsion can be attributed to the presence of a layer of lower dielectric constant, ε, in the vicinity of the interface. It was demonstrated that the DLVO theory complemented with such a layer correctly predicts the dependence of hydration repulsion on the electrolyte concentration. A further extension of this approach was given by Basu and Sharma,[367] who incorporated the effect of the variation of ε in the theory of electrostatic disjoining pressure. Their model provides quantitative agreement with the experimental data at low electrolyte concentration and pH, and qualitative agreement at higher electrolyte concentration and pH.

A further development of the theory[368] demonstrates that if the theory of Basu and Sharma[367] is further extended by taking into account the finite size of the ions, then quantitative agreement between theory and experiment can be achieved for all electrolyte concentrations and pH. In summary, the hydration repulsion can be attributed to the interplay of the following two effects, which are neglected in the conventional DLVO theory.

The effect of the *dielectric saturation* is due to the presumed preferential alignment of the solvent dipoles near a charged surface. From the viewpoint of the macroscopic continuum theory, this effect is represented by a reduced dielectric permittivity, ε, in the vicinity of the interface.[367,368] One can use the Booth[369] formula to relate ε with the intensity of the electric field, $E = |d\psi/dx|$:

$$\varepsilon(E) = n_r^2 + (\varepsilon_b - n_r^2)\frac{3}{\beta E}\left(\coth \beta E - \frac{1}{\beta E}\right), \qquad \beta \equiv \frac{5\mu(n_r^2 + 2)}{2kT} \tag{227}$$

where $n_r = 1.33$ is the refractive index of water, ε_b is the bulk dielectric constant (for $E = 0$) and $\mu = 1.85 \times 10^{-18}$ CGSE units is the dipole moment of water. Equation 227 is used by Basu and Sharma[367] to calculate the hydration repulsion. However, it turns out that the finite size of the ions also gives a considerable contribution to the hydration repulsion.

The *volume excluded by the ions* becomes important in relatively thin films, insofar as the counterion concentration is markedly higher in the vicinity of a charged surface. This effect was taken into account[368] by means of the Bikerman equation:[370,371]

$$n_i(x) = \frac{1 - \mathrm{v}\sum_k n_k(x)}{1 - \mathrm{v}\sum_k n_{k0}} n_{i0} \exp U_i \tag{228}$$

Here, x is the distance to the charged surface; n_i and U_i are, respectively, the number density and the potential energy (in kT units) of the i-th ion in the double electric layer; n_{i0} is the value of n_i in the bulk solution; the summation is carried out over all ionic species; v is the average excluded volume per counterion and can be theoretically estimated[368] as being equal to 8 times the volume of the hydrated counterion.

The electrostatic boundary problem accounting for the effects of dielectric saturation and ionic excluded volume can be formulated as follows.[368] The electric potential in the film, $\psi(x)$, satisfies the Poisson equation

$$\varepsilon_0 \frac{d}{dx}\left(\varepsilon \frac{d\psi}{dx}\right) = -\rho(x) \tag{229}$$

where ε is given by Equation 227 and the surface charge density, $\rho(x)$, is determined from Equation 228:

$$\rho(x) = \frac{\sum_i Z_i e n_i^* \exp U_i}{1 + \mathrm{v}\sum_i n_i^* \exp U_i}, \qquad n_i^* \equiv \frac{n_{i0}}{1 + \mathrm{v}\sum_k n_{k0}} \tag{230}$$

The potential energy U_i accounts for both the mean-field electrostatic energy and the energy of hydration[367]

$$U_i = -\frac{Z_{ie}\psi + W_i}{kT}, \qquad W_i \equiv \frac{Z_i^2 e^2}{d_i}\left[\frac{1}{\varepsilon(E)} - \frac{1}{\varepsilon_b}\right] \tag{231}$$

where d_i is the diameter of the i-th ion. The boundary condition of the charged surface reads:

$$\left.\frac{d\psi}{dx}\right|_{x=0} = -\frac{\sigma_s}{\varepsilon_0 \varepsilon_s}, \qquad \varepsilon_s \equiv \varepsilon|_{x=0} \tag{232}$$

where σ_s is determined by the Stern isotherm, Equation 183. The boundary problem (Equations 229 to 232) can be solved numerically. Then, the total electrostatic disjoining pressure can be calculated by means of the expression[368]

$$\Pi_{\mathrm{el}}^{\mathrm{tot}} \equiv -\int_0^{\psi_m} \rho_m d\psi = \frac{kT}{\mathrm{v}} \ln\left[\frac{1 + \mathrm{v}\sum_k n_k^* \exp(-Z_i e\psi_m / kT)}{1 + \mathrm{v}\sum_k n_k^*}\right] \tag{233}$$

where the subscript "*m*" denotes values of the respective variables at the midplane of the film. Finally, the non-DLVO hydration force can be determined as an excess over the conventional DLVO electrostatic disjoining pressure:

$$\Pi_{hr} \equiv \Pi_{el}^{tot} - \Pi_{el}^{DLVO} \tag{234}$$

where Π_{el}^{DLVO} is defined by Equation 178, which can be deduced from Equation 233 for $v \to 0$ and $\varepsilon \equiv \varepsilon_b$. Note that both the effect of $v \neq 0$ and $\varepsilon \neq \varepsilon_b$ lead to a larger value of ψ_m, which contributes to a positive (repulsive) Π_{hr}.

The theory[368] based on Equations 227 to 234 gives an excellent numerical agreement with the experimental data of Pashley,[357,358] Claesson et al.[372] and Horn et al.[373] An illustration is given in Figure 29, where v is equal to 8 times the volume of the hydrated Na^+ ion. In all cases, acceptable values of the adjustable parameters, σ_{max} and $\Phi_a = -\Delta\mu_2^{(0)}$ in the Stern isotherm are obtained (see Equations 49 and 183). It is interesting to note that in all investigated cases the effect of $v \neq 0$ gives about 4 times larger contribution in Π_{hr} compared to the effect of $\varepsilon \neq \varepsilon_b$.

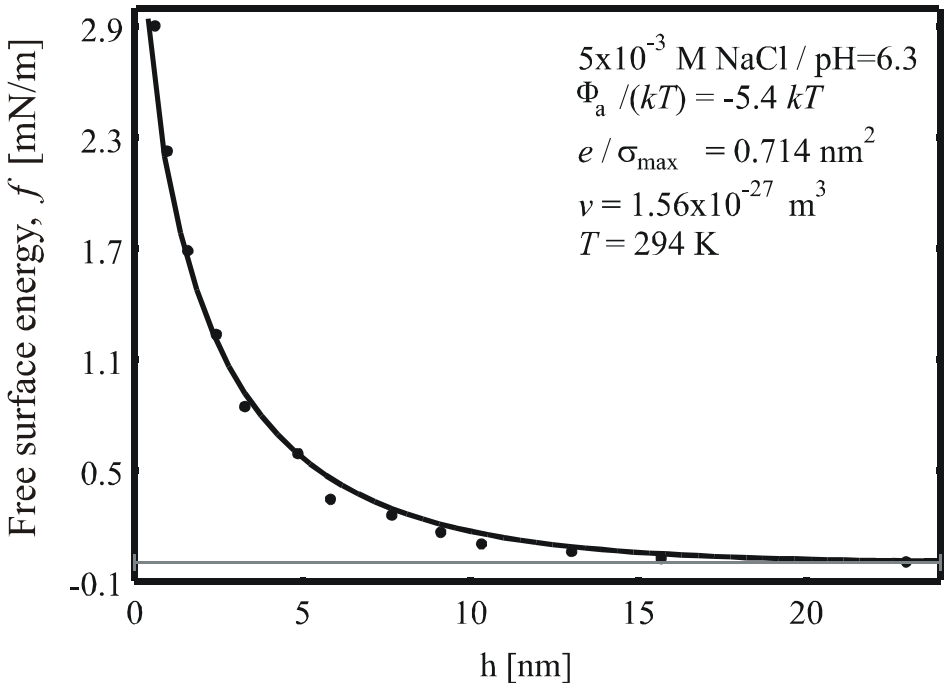

FIGURE 29. Comparison of theory[368] with experimental data[357] measured with solution of 5 mM NaCl at pH = 6.3 between mica surfaces: the total interaction free energy, $f = f_{vw} + f_{el} + f_{hr}$, is plotted against the film thickness h (see Equations 162 and 233). The solid line is the best fit calculated with adsorption energy $\Phi_a = -5.4\ kT$ per Na^+ ion, and area per surface ionizable group 0.714 nm^2.

5.4.5.4.2 Hydrophobic attraction

The water does not spread spontaneously on hydrocarbons and the aqueous films on hydrocarbons are rather unstable.[374] The cause for these effects is a strong attractive *hydrophobi*c force, which is found to appear in aqueous films in contact with hydrophobic surfaces. The experiments showed, that the nature of the hydrophobic surface force is different from the van der Waals and double layer interactions.[375-379] It turns out that the hydrophobic interaction decays exponentially with the increase of the film thickness, h. The hydrophobic free energy per unit area of the film can be described by means of the equation[34]

$$f_{\text{hydrophobic}} = -2\gamma e^{-h/\lambda_0} \tag{235}$$

where typically γ = 10–50 mJ/m^2, and λ_0 = 1–2 nm in the range $0 < h < 10$ nm. Larger decay length, λ_0 = 12–16 nm, was reported by Christenson et al.[379] for the range $20 < h < 90$ nm. This amazingly long-range attraction entirely dominates the van der Waals forces. In particular, it can create rupture of foam films containing small oil droplets or larger hydrophobic surfaces. Ducker et al.[380] measured the force between hydrophobic and hydrophilic silica particles and air bubbles by means of an atomic force microscope.

It was found experimentally that 1:1 and 2:2 electrolytes reduce considerably the long-range part of the hydrophobic attraction.[378,379] The results suggest that this reduction is due to ion adsorption or ion exchange at the surfaces rather than to the presence of electrolyte in the solution itself. Therefore, the physical implication (which might seem trivial) is that the hydrophobic attraction across aqueous films can be suppressed by making the surfaces more hydrophilic. Besides, some special polar solutes are found to suppress the hydrophobic interaction at molecular level in the bulk solution, e.g., urea, $(NH_2)_2CO$, dissolved in water can cause proteins to unfold. The polar solutes are believed to destroy the hydrogen-bond structuring in water; therefore they are sometimes called chaotropic agents.[34]

There is no generally accepted explanation of hydrophobic forces. Nevertheless, many authors agree that hydrogen bonding in water and other associated liquids is the main underlying factor.[34,381] One possible qualitative picture of the hydrophobic interaction is the following. If there were no thermal motion, the water molecules would form an ice-like tetrahedral network with four nearest neighbors per molecule (instead of 12 neighbors at close packing), since this configuration is favored by the hydrogen-bond formation. However, due to the thermal motion a water molecule forms only about 3 to 3.5 transient hydrogen-bonds with its neighbors in the liquid[382] with lifetime of a hydrogen-bond being about 10^{-11} sec. When a water molecule is brought in contact with a non-hydrogen-bonding molecule or surface, the number of its possible favorable configurations is decreased. This effect also reduces the number of advantageous configurations of the neighbors of the subsurface water molecules and some ordering propagates in the depth of the liquid. This ordering might be

initiated by the orientation of the water dipoles at a water-air or water-hydrocarbon interface, with the oxygen atom being oriented toward the hydrophobic phase.[383-386] Such ordering in the vicinity of the hydrophobic wall is entropically unfavorable. When two hydrophobic surfaces approach each other, the entropically unfavored water is ejected into the bulk, thereby reducing the total free energy of the system. The resulting attraction can in principle explain the hydrophobic forces. However, the existing theory[381] is still far from quantitative explanation for the experimental data.

Another hypothesis for the physical origin of the hydrophobic force considers a possible role of formation of gaseous capillary bridges between the two hydrophobic surfaces (see Figure 9(a)).[34,387,388] In this case, the hydrophobic force would be a kind of capillary-bridge force (see Chapter 11 in Reference 35). Such bridges could appear spontaneously, by nucleation (spontaneous dewetting), when the distance between the two surfaces becomes smaller than a certain threshold value, of the order of several hundred nanometers. Gaseous bridges could appear even if there is no dissolved gas in the water phase; the pressure inside a bridge can be as low as the equilibrium vapor pressure of water (23.8 mm Hg at 25°C) owing to the high interfacial curvature of nodoid-shaped bridges (see Section 5.3.1.2.3 and Reference 35). A number of studies[389-397] provide evidence in support of the capillary-bridge origin of the long-range hydrophobic surface force. In particular, the observation of "steps" in the experimental data was interpreted as an indication for separate acts of bridge nucleation.[393]

In summary, it is more likely that two different effects are called hydrophobic interaction: (1) the known molecular hydrophobic effect[34,398] which could bring about a relatively short-range attractive surface force,[381,399] and (2) formation of capillary bridges-cavities between two hydrophobic surfaces.[387-397] For the time being, there are sufficiently evidences showing that both effects exist in reality, often in interplay with each other.

5.4.5.5 Fluctuation Wave Forces

All fluid interfaces, including liquid membranes and surfactant lamellas, are involved in a thermal fluctuation wave motion. The configurational confinement of such thermally exited modes within the narrow space between two approaching interfaces gives rise to short-range repulsive surface forces, which are considered below.

5.4.5.5.1 Undulation forces

The undulation force arises from the configurational confinement related to the *bending mode* of deformation of two fluid bilayers. This mode consists in undulation of the bilayer at constant bilayer area and thickness (Figure 30(a)). Helfrich et al.[400,401] established that two

such bilayers, apart at a mean distance h, experience a repulsive disjoining pressure given by the expression:

$$\Pi_{\text{und}}(h) = \frac{3\pi^2 (kT)^2}{64 k_t h^3} \tag{236}$$

where k_t is the bending elastic modulus of the bilayer as a whole. The experiment[402] and the theory[35,133] show that k_t is of the order of 10^{-19} J for lipid bilayers. The undulation force has been measured, and the dependence $\Pi_{\text{und}} \propto h^{-3}$ confirmed experimentally.[403-405]

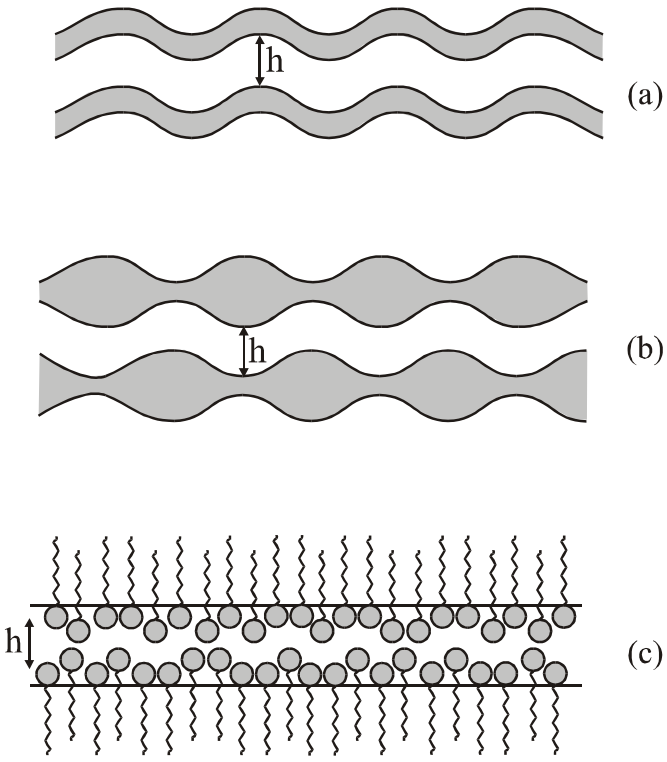

FIGURE 30. Surface forces due to configurational confinement of thermally exited modes into a narrow region of space between two approaching interfaces: (a) bending mode of membrane fluctuations giving rise to the undulation force; (b) squeezing mode of membrane fluctuations producing the peristaltic force; (c) fluctuating protrusion of adsorbed amphiphilic molecules engendering the protrusion surface force.

5.4.5.5.2 Peristaltic force

The peristaltic force[365] originates from the configurational confinement related to the peristaltic (squeezing) mode of deformation of a fluid bilayer (Figure 30(b)). This mode of deformation consists in fluctuation of the bilayer thickness at fixed position of the bilayer midsurface. The peristaltic deformation is accompanied with extension of the bilayer surfaces. Israelachvili and Wennerstöm[365] demonstrated that the peristaltic disjoining pressure is related to the stretching modulus, k_s, of the bilayer:

$$\Pi_{\text{per}}(h) \approx \frac{2(kT)^2}{\pi^2 k_s h^5} \tag{237}$$

The experiment[406] gives values of k_s varying between 135 and 500 mN/m, depending on temperature and composition of the lipid membrane.

5.4.5.6 Protrusion Force

Due to the thermal motion, the protrusion of an amphiphilic molecule in an adsorption monolayer (or micelle) may fluctuate about the equilibrium position of the molecule (Figure 30(c)). In other words, the adsorbed molecules are involved in a discrete wave motion, which differs from the continuous modes of deformation considered above. Anianson et al.[407,408] analyzed the energy of protrusion in relation to the micelle kinetics. These authors assumed the energy of molecular protrusion to be of the form $u(z) = \alpha z$, where z is the distance out of the surface ($z > 0$) and determined $\alpha \approx 3 \times 10^{-11}$ J/m for single-chained surfactants. The average length of the Brownian protrusion of the amphiphilic molecules is on the order of $\lambda \equiv kT/\alpha$.[365]

By using a mean-field approach Israelachvili and Wennerström[365] derived the following expression for the protrusion disjoining pressure which appears when two protrusion zones overlap (Figure 30(c)):

$$\Pi_{\text{protr}}(h) = \frac{\Gamma kT}{\lambda} \frac{(h/\lambda)\exp(-h/\lambda)}{1-(1+h/\lambda)\exp(-h/\lambda)} \tag{238}$$

where λ is the characteristic protrusion length; $\lambda = 0.14$ nm at 25°C for surfactants with paraffin chain; Γ denotes the number of protrusion sites per unit area. Note that Π_{protr} decays exponentially for $h \quad \lambda$, but $\Pi_{\text{protr}} \propto h^{-1}$ for $h < \lambda$, i.e., Π_{protr} is divergent at $h \to 0$. The respective interaction free energy (per unit film area) is

$$f_{\text{protr}} = \int_h^\infty \Pi_{\text{protr}}(\hat{h})\, d\hat{h} = -\Gamma kT \ln\left[1-(1+h/\lambda)\exp(-h/\lambda)\right] \tag{239}$$

Equation 238 was found to fit well experimental data for the disjoining pressure of liquid films stabilized by adsorbed protein molecules: bovine serum albumin (BSA).[409] In that case, Γ was identified with the surface density of the loose secondary protein adsorption layer, while λ turned out to be about the size of the BSA molecule.[409]

REFERENCES

1. Jungermann, E., *Cationic Surfactants,* Marcel Dekker, New York, 1970.
2. Lucassen-Reynders, E.H., *Anionic Surfactants – Physical Chemistry of Surfactant Action*, Marcel Dekker, New York, 1981.
3. Schick, M.J., *Nonionic Surfactants: Physical Chemistry,* Marcel Dekker, New York, 1986.
4. Gibbs, J.W., *The Scientific Papers of J.W. Gibbs*, Vol. 1, Dover, New York, 1961.
5. Ono, S. and Kondo, S., Molecular theory of surface tension in liquids, in *Handbuch der Physik,* Vol. 10, Flügge, S., Ed., Springer, Berlin, 1960.
6. Adamson, A.W. and Gast, A.P. *Physical Chemistry of Surfaces*; Sixth Edition, Wiley, New York, 1997.
7. Freundlich, H., *Colloid and Capillary Chemistry*, Methuen, London, 1926.
8. Langmuir, I., *J. Amer. Chem. Soc.,* 40, 1361, 1918.
9. Volmer, M., *Z. Physikal. Chem.,* 115, 253, 1925.
10. Frumkin, A., *Z. Physikal. Chem.,* 116, 466, 1925.
11. Hill, T.L., *An Introduction to Statistical Thermodynamics*, Addison-Wesley, Reading, MA, 1962.
12. Lucassen-Reynders, E.H., *J. Phys. Chem*., 70, 1777, 1966.
13. Borwankar, R.P. and Wasan, D.T., *Chem. Eng. Sci.,* 43, 1323, 1988.
14. Derjaguin, B.V., *Theory of Stability of Colloids and Thin Liquid Films,* Plenum Press, Consultants Bureau, New York, 1989.
15. Shchukin, E.D., Pertsov, A.V., and Amelina, E.A., *Colloid Chemistry*, Moscow Univ. Press, Moscow, 1982 (Russian); Elsevier, 2001 (English).
16. Zeldowitch, J., *Acta Physicochim. (USSR)*, 1, 961, 1934.
17. Halsey, G. and Taylor, H.S., *J. Chem. Phys.,* 15, 624, 1947.
18. Gurkov, T.G., Kralchevsky, P.A., and Nagayama, K., *Colloid Polym. Sci.,* 274, 227, 1996.
19. Butler, J.A.V., *Proc. Roy. Soc. Ser. A,* 135, 348, 1932.
20. Fainerman, V.B. and Miller, R., *Langmuir*, 12, 6011, 1996.
21. Vaughn, M.W. and Slattery, J. C., *J. Colloid Interface Sci.,* 195, 1, 1997.
22. Makievski, A.V., Fainerman, V.B., Bree, M., Wüstneck, R., Krägel, J., and Miller, R., *J. Phys. Chem. B,* 102, 417, 1998.
23. Landau, L.D. and Lifshitz, E.M., *Statistical Physics,* Part 1, Pergamon, Oxford, 1980.
24. Hachisu, S., *J. Colloid Interface Sci.,* 33, 445, 1970.
25. Kalinin, V.V. and Radke, C.J., *Colloids Surf. A,* 114, 337, 1996.
26. Warszyński, P., Barzyk, W., Lunkenheimer, K., and Fruhner, H., *J. Chys Chem.*, *B,* 102, 10948, 1998.
27. Kralchevsky, P.A., Danov, K.D., Broze, G., and Mehreteab, A., *Langmuir,* 15, 2351, 1999.
28. Prosser, A.J. and Frances, E.I., *Colloids Surf. A,* 178, 1, 2001.

29. Kirkwood, J.G. and Oppenheim, I., *Chemical Thermodynamics*, McGraw-Hill, New York, 1961.
30. Robinson, R.A. and Stokes, R.H., *Electrolyte Solutions,* Butterworths, London, 1959.
31. Gouy, G., *J. Phys. Radium,* 9, 457, 1910.
32. Davies, J. and Rideal, E., *Interfacial Phenomena,* Academic Press, New York, 1963.
33. Grahame, D.C., *Chem. Rev.,* 41, 441, 1947.
34. Israelachvili, J.N., *Intermolecular and Surface Forces*, Academic Press, London, 1992.
35. Kralchevsky, P.A. and Nagayama, K., *Particles at Fluid Interfaces and Membranes*, Elsevier, Amsterdam, 2001.
36. Matijevič, E. and Pethica, B.A., *Trans. Faraday Soc.,* 54, 1382, 1958.
37. van Voorst Vader, F., *Trans. Faraday Soc.*, 56, 1067, 1960.
38. Tajima, K., *Bul. Chem. Soc. Jpn,* 44, 1767, 1971.
39. Stern, O., *Ztschr. Elektrochem.,* 30, 508, 1924.
40. Tajima, K., Muramatsu, M., and Sasaki, T., *Bul. Chem. Soc. Jpn*, 43, 1991, 1970.
41. Tajima, K., *Bul. Chem. Soc. Jpn*, 43, 3063, 1970.
42. Danov, K.D., Kolev, V.L, Kralchevsky, P.A., Broze, G., and Mehreteab, A., manuscript in preparation.
43. Cross, A.W. and Jayson, G.G., *J. Colloid Interface Sci.*, 162, 45, 1994.
44. Johnson, S.B., Drummond, C.J., Scales, P.J., and Nishimura, S., *Langmuir,* 11, 2367, 1995.
45. Alargova, R.G., Danov, K.D., Petkov, J.T., Kralchevsky, P.A., Broze, G., and Mehreteab, A., *Langmuir,* 13, 5544, 1997.
46. Rathman, J.F. and Scamehorn, J.F., *J. Phys. Chem.*, 88, 5807, 1984.
47. Berr, S.S., Coleman, M.J., Marriot, J., and Johnson Jr., J.S., *J. Phys. Chem*., 90, 6492, 1986.
48. Rosen, M.J., *Surfactants and Interfacial Phenomena*, Wiley, New York, 1989.
49. Clint, J., *Surfactant Aggregation*, Chapman & Hall, London, 1992.
50. Alargova, R.G., Danov, K.D., Kralchevsky, P.A., Broze, G., and Mehreteab, A., *Langmuir,* 14, 4036, 1998.
51. Dimov, N.K., Kolev, V.L., Kralchevsky, P.A., Lyutov, L.G., Brose, G., and Mehreteab, A., *J. Colloid Interface Sci*., 256, 23 (2002).
52. Valkovska, D.S., Danov, K.D., and Ivanov, I.B., *Colloids Surf. A,* 175, 179, 2000.
53. Danov, K.D., Kralchevsky, P.A., and Ivanov, I.B., in *Encyclopedic Handbook of Emulsion Technology*, Sjöblom, J., Ed., Marcel Dekker, New York, 2001, chap. 26.
54. Dukhin, S.S., Kretzschmar, G., and Miller, R., *Dynamics of Adsorption at Liquid Interfaces*, Elsevier, Amsterdam, 1995.
55. Eastoe, J. and Dalton, J.S., *Adv. Colloid Interface Sci.,* 85, 103, 2000.
56. Lord Rayleigh, *Proc. Roy. Soc. (Lond.)*, 29, 71, 1879.
57. N. Bohr, *Phil. Trans. Roy. Soc. (Lond.)*, *A*, 209, 281, 1909.
58. Defay, R. and Pétré, G., Dynamic surface tension, in *Surface and Colloid Science,* Vol. 3, Matijevič, E., Ed., Wiley, New York, 1971, p. 27.

59. Miller, R. and Kretzschmar, G., *Adv. Colloid Interface Sci.*, 37, 97, 1991.
60. Wantke, K.-D., Lunkenheimer, K., and Hempt, C., *J. Colloid Interface Sci.*, 159, 28, 1993.
61. Chang, C.-H. and Franses, E.I., *J. Colloid Interface Sci.*, 164, 107, 1994.
62. Johnson, D.O. and Stebe, K.J., *J. Colloid Interface Sci.*, 182, 525, 1996.
63. Horozov, T. and Arnaudov, L., *J. Colloid Interface Sci.*, 219, 99, 1999.
64. Horozov, T. and Arnaudov, L., *J. Colloid Interface Sci.*, 222, 146, 2000.
65. van den Tempel, M. and Lucassen-Reynders, E.H., *Adv. Colloid Interface Sci.*, 18, 281, 1983.
66. Langevin, D., *Colloids Surf.*, 43, 121, 1990.
67. Lemaire, C. and Langevin, D., *Colloids Surf.*, 65, 101, 1992.
68. Grigorev, D.O., Krotov, V.V., and Noskov, B.A., *Colloid J.*, 56, 562, 1994.
69. Mysels, K.J., *Colloids Surf.*, 43, 241, 1990.
70. Kralchevsky, P.A., Radkov, Y.S., and Denkov, N.D., *J. Colloid Interface Sci.*, 161, 361, 1993.
71. Fainerman, V.B., Miller, R., and Joos, P., *Colloid Polym. Sci.*, 272, 731, 1994.
72. Fainerman, V.B. and Miller, R., *J. Colloid Interface Sci.*, 176, 118, 1995.
73. Horozov, T.S., Dushkin, C.D., Danov, K.D., Arnaudov, L.N., Velev, O.D., Mehreteab, A., and Broze, G., *Colloids Surf. A*, 113, 117, 1996.
74. Mishchuk, N.A., Dukhin, S.S., Fainerman, V.B., Kovalchuk, V.I., and Miller, R., *Colloids Surf. A*, 192, 157, 2001.
75. van den Bogaert, R. and Joos, P., *J. Phys. Chem.*, 83, 17, 1979.
76. Möbius, D. and Miller R., Eds., *Drops and Bubbles in Interfacial Research*, Elsevier, Amsterdam, 1998.
77. Jho, C. and Burke, R., *J. Colloid Interface Sci.*, 95, 61, 1983.
78. Joos, P. and van Hunsel, J., *Colloid Polym. Sci.* 267, 1026, 1989.
79. Fainerman, V.B. and Miller, R., *Colloids Surf. A*, 97, 255, 1995.
80. Miller, R., Bree, M., and Fainerman, V.B., *Colloids Surf. A,* 142, 237, 1998.
81. Senkel, O., Miller, R., and Fainerman, V.B., *Colloids Surf. A*, 143, 517, 1998.
82. Bain, C.D., Manning-Benson, S., and Darton, R.C., *J. Colloid Interface Sci.,* 229, 247, 2000.
83. Rotenberg, Y., Boruvka, L., and Neumann, A.W., *J. Colloid Interface Sci.,* 37, 169, 1983.
84. Makievski, A.V., Loglio, G., Krägel, J., Miller, R., Fainerman, V.B., and Neumann, A.W., *J. Phys. Chem.,* 103, 9557, 1999.
85. Joos, P., *Dynamic Surface Phenomena,* VSP BV, AH Zeist, The Netherlands, 1999.
86. Ward, A.F.H. and Tordai, L., *J. Chem. Phys.*, 14, 453, 1946.
87. Miller, R., *Colloid Polym. Sci.*, 259, 375, 1981.
88. McCoy, B.J., *Colloid Polym. Sci.*, 261, 535, 1983.
89. Hansen, R.S., *J. Chem Phys.,* 64, 637, 1960.
90. Filippov, L.K., *J. Colloid Interface Sci.*, 164, 471, 1994.
91. Daniel, R. and Berg, J.C., *J. Colloid Intrface Sci.,* 237, 294, 2001.

92. Sutherland, K.L., *Austr. J. Sci. Res.*, A5, 683, 1952.

93. Abramowitz, M. and Stegun, I.A., *Handbook of Mathematical Functions,* Dover, New York, 1965.

94. Korn, G.A. and Korn, T.M., *Mathematical Handbook*, McGraw-Hill, New York, 1968.

95. Danov, K.D., Kolev, V.L., Kralchevsky, P.A., Broze, G., and Mehreteab, A., *Langmuir,* 16, 2942, 2000.

96. Dukhin, S.S., Miller, R., and Kretzschmar, G., *Colloid Polym. Sci.*, 261, 335, 1983.

97. Dukhin, S.S. and Miller, R., *Colloid Polym. Sci.,* 272, 548, 1994.

98. MacLeod, C. and Radke, C.J., *Langmuir,* 10, 3555, 1994.

99. Vlahovska, P.M., Danov, K.D., Mehreteab, A., and Broze, G., *J. Colloid Interface Sci.*, 192, 194, 1997.

100. Danov, K.D., Vlahovska, P.M., Kralchevsky, P.A., Broze, G., and Mehreteab, A., *Colloids Surf. A*, 156, 389, 1999.

101. Diamant, H. and Andelman, D., *J. Phys. Chem.,* 100, 13732, 1996.

102. Diamant, H., Ariel, G., and Andelman, D., *Colloids Surf. A,* 183-185, 259, 2001.

103. Nayfeh, A.H., *Perturbation Methods*, Wiley, New York, 1973.

104. Danov, K.D., Kolev, V.L., Arnaudov, L.N., Kralchevsky, P.A., Broze, G., and Mehreteab, A., manuscript in preparation.

105. Durbut, P., Surface Activity, in *Handbook of Detergents,* Part A, Broze, G., Ed., Marcel Dekker, New York, 1999, chap. 3.

106. Bond, W.N. and Puls, H.O., *Phil. Mag.*, 24, 864, 1937.

107. Doss, K.S.G., *Koll. Z.*, 84, 138, 1938.

108. Blair, C.M., *J. Chem. Phys.*, 16, 113, 1948.

109. Ward, A.F.H., *Surface Chemistry*, London, 1949.

110. Dervichian, D.G., *Koll. Z.*, 146, 96, 1956.

111. Hansen, R.S. and Wallace, T., *J. Phys. Chem.*, 63, 1085, 1959.

112. Baret, J.F., *J. Phys. Chem.*, 72, 2755, 1968.

113. Baret, J.F., *J. Chem. Phys.*, 65, 895, 1968.

114. Baret, J.F., *J. Colloid Interface Sci.*, 30, 1, 1969.

115. Borwankar, R.P. and Wasan, D.T., *Chem. Eng. Sci.*, 38, 1637, 1983.

116. Dong, C., Hsu, C.-T., Chin, C.-Y., and Lin, S.-Y., *Langmuir,* 16, 4573, 2000.

117. Laplace, P.S., *Traité de mécanique céleste*; Suppléments au Livre X, 1805, 1806.

118. Bakker, G., Kapillatytät und oberflächenspannung, in *Handbuch der Experimentalphysik,* Band 6, Akademische Verlagsgesellschaft, Leipzig, 1928.

119. Princen, H.M., The equilibrium shape of interfaces, drops, and bubbles, in *Surface and Colloid Science*, Vol. 2, Matijevic, E., Ed., Wiley, New York, 1969, p. 1.

120. Finn, R., *Equilibrium Capillary Surfaces*, Springer-Verlag, New York, 1986.

121. Weatherburn, C.E., *Differential Geometry in Three Dimensions*, Cambridge, 1930.

122. McConnell, A.J., *Application of Tensor Analysis,* Dover, New York, 1957.

123. Young, T., *Philos. Trans. Roy. Soc. Lond.*, 95, 55, 1805.

124. Jonson, R.E. and Dettre, Wettability and contact angles, in *Surface and Colloid Science,* Vol. 2, Matijevic, E., Ed., Wiley, New York, 1969, p. 85.

125. Starov, V.M., *Adv. Colloid Interface Sci.*, 39, 147, 1992.

126. Neumann, F., *Vorlesungen über die Theorie der Capillarität,* B.G. Teubner, Leipzig, 1894.

127. Ivanov, I.B., Kralchevsky, P.A., and Nikolov, A.D., *J. Colloid Interface Sci.*, 112, 97, 1986.

128. Hartland, S. and Hartley, R.W., *Axisymmetric Fluid-Liquid Interfaces,* Elsevier, Amsterdam, 1976.

129. Kralchevsky, P.A., Eriksson, J.C., and Ljunggren, S., *Adv. Colloid Interface Sci.*, 48, 19, 1994.

130. Tachev, K.D., Angarska, J.K., Danov, K.D., and Kralchevsky, P.A., *Colloids Surf. B*, 19, 61, 2000.

131. Meunier, J. and Lee, L.T., *Langmuir*, 7, 1855, 1991.

132. Dan, N., Pincus, P., and Safran, S.A., *Langmuir*, 9, 2768, 1993.

133. Kralchevsky, P.A., Paunov, V.N. Denkov, N.D., and Nagayama, K., *J. Chem. Soc. Faraday Trans.*, 91, 3415, 1995.

134. Petsev, D.N., Denkov, N.D., and Kralchevsky, P.A., *J. Colloid Interface Sci.*, 176, 201, 1995.

135. De Gennes, P.G. and Taupin, C., *J. Phys. Chem.*, 86, 2294, 1982.

136. Concus, P., *J. Fluid Mech.*, 34, 481, 1968.

137. Kralchevsky, P.A., Ivanov, I.B., and Nikolov, A.D., *J. Colloid Interface Sci.*, 112, 108, 1986.

138. Abramowitz, M. and Stegun, I.A., *Handbook of Mathematical Functions,* Dover, New York, 1965.

139. Jahnke, E., Emde, F., and Lösch, F., *Tables of Higher Functions,* McGraw-Hill, New York, 1960.

140. Lo, L.L., *J. Fluid Mech.*, 132, 65, 1983.

141. Derjaguin, B.V., *Dokl. Akad. Nauk USSR*, 51, 517, 1946.

142. Scheludko, A., *Proc. Koninkl. Nederl. Akad. Wet.*, B65, 87, 1962.

143. Scheludko, A., *Adv. Colloid Interface Sci.*, 1, 391, 1967.

144. Dimitrov, A.S., Kralchevsky, P.A., Nikolov, A.D., and Wasan, D.T., *Colloids Surf.*, 47, 299, 1990.

145. J. Plateau, Experimental and theoretical researches on the figures of equilibrium of a liquid mass withdrawn from the action of gravity, in *The Annual Report of the Smithsonian Institution*, Washington D.C., 1863; pp. 207-285.

146. J. Plateau, The figures of equilibrium of a liquid mass, in *The Annual Report of the Smithsonian Institution*, Washington D.C., 1864; pp. 338-369.

147. J. Plateau, *Statique Expérimentale et Théoretique des Liquides Soumis aux Seules Forces Moléculaires*, Gauthier-Villars, Paris, 1873.

148. Zettlemoyer, A.C., *Nucleation,* Marcel Dekker, New York, 1969.

149. Abraham, E.F., *Homogeneous Nucleation Theory,* Academic Press, New York, 1974.

150. Thomson, W. (Lord Kelvin), *Proc. Roy. Soc.*, 9, 225, 1858; *Phil.Mag.*, 17, 61, 1859.
151. Lupis, C.H.P. *Chemical Thermodynamics of Matherials,* North-Holland, New York, 1983.
152. Lifshitz, I.M. and Slyozov, V.V., *Zh. Exp. Teor. Fiz.*, 35, 479, 1958 (in Russian).
153. Wagner, C., *Z. Electrochem.*, 35, 581, 1961.
154. Kalhweit, M., *Faraday Discuss. Chem. Soc.*, 61, 48, 1976.
155. Parbhakar, K., Lewandowski, J., and Dao, L.H., *J. Colloid Interface Sci.*, 174, 142, 1995.
156. Kabalnov, A.S., Pertzov, A.V., and Shchukin, E.D., *Colloids Surf.*, 24, 19, 1987.
157. Kabalnov, A.S. and Shchukin, E.D., *Adv. Colloid Interface Sci.*, 38, 69, 1992.
158. McClements, D.J., Dungan, S.R., German, J.B., and Kinsela, J.E., *Food Hydrocolloids*, 6, 415, 1992.
159. Weiss, J., Coupland, J.N., and McClements, D.J., *J. Phys. Chem*., 100, 1066, 1996.
160. Weiss, J., Canceliere, C., and McClements, D.J., *Langmuir*, 16, 6833, 2000.
161. Kabalnov, A.S., *Langmuir,* 10, 680, 1994.
162. Ivanov, I.B. and Kralchevsky, P.A., Mechanics and thermodynamics of curved thin liquid films, in *Thin Liquid Films,* Ivanov, I.B., Ed., Marcel Dekker, New York, 1988, p. 49.
163. Kralchevsky, P.A. and Ivanov, I.B., *J. Colloid Interface Sci.*, 137, 234, 1990.
164. Kralchevsky, P.A., Danov, K.D., and Ivanov, I.B., Thin liquid film physics, in *Foams: Theory, Measurements and Applications*, Prud'homme, R.K., Ed.; Marcel Dekker, New York, 1995, p. 1.
165. Rusanov, A.I., *Phase Equilibria and Surface Phenomena*, Khimia, Leningrad, 1967 (Russian); *Phasengleichgewichte und Grenzflächenerscheinungen,* Akademie Verlag, Berlin, 1978 (German).
166. Derjaguin, B.V. and Kussakov, M.M., *Acta Physicochem. USSR,* 10, 153, 1939.
167. Exerowa, D. and Scheludko, A., *Bull. Inst. Chim. Phys. Bulg. Acad. Sci.*, 4, 175, 1964.
168. Mysels, K.J., *J. Phys. Chem.*, 68, 3441, 1964.
169. Exerowa, D., *Commun. Dept. Chem. Bulg. Acad. Sci.*, 11, 739, 1978.
170. Kruglyakov, P.M., Equilibrium properties of free films and stability of foams and emulsions, in *Thin Liquid Films,* Ivanov, I.B., Ed., Marcel Dekker, New York, 1988, p. 767.
171. Martynov, G.A. and Derjaguin, B.V., *Kolloidn. Zh.*, 24, 480, 1962.
172. Toshev, B.V. and Ivanov, I.B., *Colloid Polym. Sci.*, 253, 558, 1975.
173. Ivanov, I.B. and Toshev, B.V., *Colloid Polym. Sci.*, 253, 593, 1975.
174. Frumkin, A., *Zh. Phys. Khim. USSR*, 12, 337, 1938.
175. de Feijter, J.A., Thermodynamics of thin liquid films, in *Thin Liquid Films,* Ivanov, I.B., Ed., Marcel Dekker, New York, 1988, p. 1.
176. Kralchevsky, P.A. and Ivanov, I.B., *Chem.Phys. Lett.,* 121**,** 111, 1985.
177. Nikolov, A.D., Kralchevsky, P.A., Ivanov, I.B., and Dimitrov, A.S., *AIChE Symposium Ser. 252,* Vol. 82, 82, 1986.
178. de Feijter, J.A. and Vrij, A., *J.Electroanal. Chem.*, 47, 9, 1972.
179. Kralchevsky, P.A. and Ivanov, I.B., *Chem.Phys. Lett.,* 121**,** 116, 1985.
180. Denkov, N.D., Petsev, D.N., and Danov, K.D., *J. Colloid Interface Sci.*, 176, 189, 1995.

181. Derjaguin, B.V., *Acta Physicochim. USSR,* 12, 181, 1940.

182. Princen, H.M. and Mason, S.G., *J. Colloid Sci.*, 20, 156, 1965.

183. Prins, A., *J. Colloid Interface Sci.*, 29, 177, 1969.

184. Clint, J.H., Clunie, J.S., Goodman, J.F., and Tate, J.R., *Nature* (*Lond.*), 223, 291, 1969.

185. Yamanaka, T., *Bull. Chem. Soc. Jap.*, 48, 1755, 1975.

186. Princen, H.M., *J. Phys. Chem.*, 72, 3342, 1968.

187. Princen, H.M. and Frankel, S., *J. Colloid Interface Sci.*, 35, 186, 1971.

188. Scheludko, A., Radoev, B., and Kolarov, T., *Trans. Faraday Soc.*, 64, 2213, 1968.

189. Haydon, D.A. and Taylor, J.L., *Nature (Lond.)*, 217, 739, 1968.

190. Kolarov, T. and Zorin, Z.M., *Kolloidn. Zh.*, 42, 899, 1980.

191. Kruglyakov, P.M. and Rovon, Yu.G., *Physical Chemistry of Black Hydrocarbon Films,* Nauka, Moskow, 1978 (in Russian).

192. Marinova, K.G., Gurkov, T.D., Dimitrova, T.D., Alargova, R.G., and Smith, D., *Langmuir*, 14, 2011, 1998.

193. Françon, M., *Progress in Microscopy,* Pergamon Press, London, 1961.

194. Beyer, H., *Theorie und Praxis der Interferenzmicroscopie,* Academische Verlagessellschaft, Leipzig, 1974.

195. Zorin, Z.M., *Kolloidn. Zh*., 39, 1158, 1977.

196. Zorin, Z., Platikanov, D., Rangelova, N., and Scheludko, A., in *Surface Forces and Liquid Interfaces*, Derjaguin, B.V., Ed., Nauka, Moscow, 1983, p. 200 (in Russian).

197. Nikolov, A.D., Kralchevsky, P.A., and Ivanov, I.B., *J. Colloid Interface Sci.*, 112, 122, 1986.

198. Lobo, L.A., Nikolov, A.D., Dimitrov, A.S., Kralchevsky, P.A., and Wasan, D.T., *Langmuir*, 6, 995, 1990.

199. Dimitrov, A.S., Nikolov, A.D., Kralchevsky, P.A., and Ivanov, I.B., *J. Colloid Interface Sci.*, 151, 462, 1992.

200. Picard, G., Schneider, J.E., and Fendler, J.H., *J. Phys. Chem.*, 94, 510, 1990.

201. Picard, G., Denicourt, N., and Fendler, J.H., *J. Phys. Chem.*, 95, 3705, 1991.

202. Skinner, F.K., Rotenberg, Y., and Neumann, A.W., *J. Colloid Interface Sci.*, 130, 25, 1989.

203. Dimitrov, A.S., Kralchevsky, P.A., Nikolov, A.D., Noshi, H., and Matsumoto, M., *J. Colloid Interface Sci.*, 145, 279, 1991.

204. Hadjiiski, A., Dimova, R., Denkov, N.D., Ivanov, I.B., and Borwankar, R., *Langmuir*, 12, 6665, 1996.

205. Ivanov, I.B., Hadjiiski, A., Denkov, N.D., Gurkov, T.D., Kralchevsky, P.A., and Koyasu, S., *Biophys. J.*, 75, 545, 1998.

206. Nicolson, M.M., *Proc. Camb. Phil. Soc*., 45, 288, 1949.

207. Chan, D.Y.C., Henry, J.D., and White, L.R., *J. Colloid Interface Sci*., 79, 410, 1981.

208. Paunov, V.N., Kralchevsky, P.A., Denkov, N.D., Ivanov, I.B., and Nagayama, K., *J. Colloid Interface Sci*., 157, 100, 1993.

209. Kralchevsky, P.A., Paunov, V.N., Ivanov, I.B., and Nagayama, K., *J. Colloid Interface Sci*., 151, 79, 1992.

210. Kralchevsky, P.A., Paunov, V.N., Denkov, N.D., Ivanov, I.B., and Nagayama, K., *J. Colloid Interface Sci*., 155, 420, 1993.

211. Kralchevsky, P.A. and Nagayama, K., *Langmuir*, 10, 23, 1994.

212. Kralchevsky, P.A. and Nagayama, K., *Adv. Colloid Interface Sci.*, 85, 145, 2000.

213. Denkov, N.D., Velev, O.D., Kralchevsky, P.A., Ivanov, I.B., Nagayama, K., and Yoshimura, H., *Langmuir,* 8, 3183, 1992.

214. Dimitrov, A.S., Dushkin, C.D., Yoshimura, H., and Nagayama, K., *Langmuir,* 10, 432, 1994.

215. Sasaki, M. and Hane, K., *J. Appl. Phys.,* 80, 5427, 1996.

216. Du, H., Chen, P., Liu, F., Meng, F.-D., Li, T.-J., and Tang, X.-Y., *Materials Chem. Phys.*, 51, 277, 1977.

217. Price, W.C., Williams, R.C., and Wyckoff, R.W.G., *Science*, 102, 277, 1945.

218. Cosslett, V.E. and Markham, R., *Nature*, 161, 250, 1948.

219. Horne, R.W. and Pasquali-Ronchetti, I., *J. Ultrastruct. Res.*, 47, 361, 1974.

220. Harris, J.R., *Micron Microscopica Acta*, 22, 341, 1991.

221. Yoshimura, H., Matsumoto, M., Endo, S., and Nagayama, K., *Ultramicroscopy*, 32, 265, 1990.

222. Yamaki, M., Higo, J., and Nagayama, K., *Langmuir*, 11, 2975, 1995.

223. Nagayama, K., *Colloids Surf. A,* 109, 363, 1996.

224. Burmeister, F., Schäfle, C., Keilhofer, B., Bechinger, C., Boneberg, J., and Leiderer, P., *Adv. Mater*., 10, 495, 1998.

225. Xia, Y., Tien, J., Qin, D., and Whitesides, G.M., *Langmuir,* 12, 4033, 1996.

226. Lindström, H., Rensmo, H., Sodergren, S., Solbrand, A., and Lindquist, S.E., *J. Phys. Chem.,* 100, 3084, 1996.

227. Matsushita, S., Miwa, T., and Fujishima, A., *Langmuir,* 13, 2582, 1997.

228. Murray, C.B., Kagan, C.R., and Bawendi, M.G., *Science,* 270, 1335, 1995.

229. Jap, B.K., Zulauf, M., Scheybani, T., Hefti, A., Baumeister, W., Aebi, U., and Engel, A., *Ultramicroscopy*, 46, 45, 1992.

230. De Rossi, D., Ahluwalia, A., and Mulè, M., *IEEE Eng. Med. Biol.*, 13, 103, 1994.

231. Kralchevsky, P.A. and Denkov, N.D., *Current Opinion Colloid Interface Sci*., 6, 383, 2001.

232. Gil, T., Ipsen, J.H., Mouritsen, O.G., Sabra, M.C., Sperotto, M.M., and Zuckermann, M.J., *Biochim. Biophys. Acta*, 1376, 245, 1998.

233. Mansfield, S.L., Gotch, A.J., and Harms, G.S., *J. Phys. Chem.*, *B*, 103, 2262, 1999.

234. Fisher, L.R. and Malloy A.R., *Annu. Rep. Prog. Chem.,* Sect. C, 95, 373, 1999.

235. Kralchevsky, P.A., Paunov, V.N., and Nagayama, K., *J. Fluid Mech.*, 299, 105, 1995.

236. Camoin, C., Roussel, J.F., Faure, R., and Blanc, R., *Europhys. Lett.*, 3, 449, 1987.

237. Velev, O.D., Denkov, N.D., Paunov, V.N., Kralchevsky P.A., and Nagayama, K., *Langmuir*, 9, 3702, 1993.

238. Dushkin, C.D., Kralchevsky, P.A., Yoshimura, H., and Nagayama, K., *Phys. Rev. Lett.*, 75, 3454, 1995.

239. Lucassen, J., *Colloids Surf.*, 65, 131, 1992.

240. Stamou, D., Duschl, C., and Johannsmann, D., *Phys. Rev.*, *E*, 62, 5263, 2000.

241. Kralchevsky, P.A., Denkov, N.D., and Danov, K.D., *Langmuir,* 17, 2001, 7694.

242. Bowden, N., Terfort, A., Carbeck, J., and Whitesides, G.M., *Science*, 276, 233, 1997.

243. Bowden, N., Choi, I.S., Grzybowski, B.A., and Whitesides, G.M., *J. Am. Chem. Soc.*, 121, 5373, 1999.

244. Velikov, K.P., Durst, F., and Velev, O.D. *Langmuir,* 14, 1148, 1998.

245. Sur, J. and Pak, H.K., *J. Korean Phys. Soc.*, 38, 582, 2001.

246. Danov, K.D., Pouligny, B., Angelova, M.I., and Kralchevsky, P.A., in *Studies in Surface Science and Catalysis,* Vol. 132, Iwasawa Y., Oyama N., and Kunieda H., Eds., Elsevier, Amsterdam, 2001; p. 519.

247. Danov, K.D., Pouligny, B., and Kralchevsky, P.A., *Langmuir,* 17, 2001, 6599.

248. Kralchevsky, P.A., Paunov, V.N., Denkov, N.D., and Nagayama, K., *J. Colloid Interface Sci.*, 167, 47, 1994.

249. Velev, O.D., Denkov, N.D., Paunov, V.N., Kralchevsky, P.A., and Nagayama, K., *J. Colloid Interface Sci.*, 167, 66, 1994.

250. Petkov, J.T., Denkov, N.D., Danov, K.D., Velev, O.D., Aust, R., and Durst, F., *J. Colloid Interface Sci.*, 172, 147, 1995.

251. Danov, K.D., Aust, R., Durst, F., and Lange, U., *J. Colloid Interface Sci.,* 175, 36, 1995.

252. Petkov, J.T., Danov, K.D., Denkov, N.D., Aust, R., and Durst, F., *Langmuir,* 12, 2650, 1996.

253. Petkov, J.T., Gurkov, T.D., and Campbell, B.E., *Langmuir,* 17, 4556, 2001.

254. Derjaguin, B.V., Churaev, N.V., and Muller, V.M., *Surface Forces,* Plenum Press: Consultants Bureau, New York, 1987.

255. Derjaguin, B.V., *Kolloid Zeits.*, 69, 155, 1934.

256. Attard, P. and Parker, J.L., *J. Phys. Chem.*, 96, 5086, 1992.

257. Tabor, D. and Winterton, R.H.S., *Nature*, 219, 1120, 1968.

258. Keesom, W.H., *Proc. Amst*., 15, 850, 1913.

259. Debye, P., *Physik*, 2, 178, 1920.

260. London, F., *Z. Physics*, 63, 245, 1930.

261. Hamaker, H.C., *Physics*, 4, 1058, 1937.

262. Usui, S., Sasaki, H., and Hasegawa, F., *Colloids Surf.*, 18, 53, 1986.

263. Lifshitz, E.M., *Soviet Phys. JETP (Engl. Transl.),* 2, 73, 1956.

264. Dzyaloshinskii, I.E., Lifshitz, E.M., and Pitaevskii, L.P., *Adv. Phys.*, 10, 165, 1961.

265. Nir, S. and Vassilieff, C.S., Van der Waals interactions in thin films, in *Thin Liquid Films,* Ivanov, I.B., Ed., Marcel Dekker, New York, 1988, p. 207.

266. Danov, K.D., Petsev, D.N., Denkov, N.D., and Borwankar, R., *J. Chem. Phys.*, 99, 7179, 1993.

267. Casimir, H.R. and Polder, D., *Phys. Rev.*, 73, 360, 1948.

268. Mahanty, J. and Ninham, B.W., *Dispersion Forces,* Academic Press, New York, 1976.

269. Moelwyn-Hughes, E.A., *Physical Chemistry*, Pergamon Press, London, 1961; chap. 21.

270. Langmuir, I., *J. Chem. Phys.*, 6, 873, 1938.

271. Tenchov, B.G. and Brankov, J.G., *J. Colloid Interface Sci.,* 109, 172, 1986.

272. Vassilieff, C.S., Tenchov, B.G., Grigorov, L.S., and Richmond, P., *J. Colloid Interface Sci.*, 93, 8, 1983.

273. Verwey, E.J.W. and Overbeek, J.Th.G., *The Theory of Stability of Liophobic Colloids,* Elsevier, Amsterdam, 1948.

274. Muller, V.M., *Kolloidn. Zh.*, 38, 704, 1976.

275. McCormack, D., Carnie, S.L., and Chan, D.Y.C., *J. Colloid Interface Sci.*, 169, 177, 1995.

276. Hogg, R., Healy, T.W., and Fuerstenau, D.W., *Trans. Faraday Soc.*, 62, 1638, 1966.

277. Usui, S., *J. Colloid Interface Sci.*, 44, 107, 1973.

278. Russel, W.B., Saville, D.A., and Schowalter, W.R., *Colloidal Dispersions,* University Press, Cambridge, 1989.

279. Debye, P. and Hückel, E., *Z. Phys.*, 24, 185, 1923.

280. McCartney, L.N. and Levine, S., *J. Colloid Interface Sci.*, 30, 345, 1969.

281. Derjaguin, B.V. and Landau, L.D., *Acta Physicochim. USSR,* 14, 633, 1941.

282. Efremov, I.F., Periodic colloidal structures, in *Colloid and Surface Science,* Vol. 8, Matijevic, E., Ed., Wiley, New York, 1976, p. 85.

283. Schulze, H., *J. Prakt. Chem.*, 25, 431, 1882.

284. Hardy, W.B., *Proc. Roy. Soc. (Lond.)*, 66, 110, 1900.

285. Guldbrand, L., Jönsson, B., Wennerström, H., and Linse, P., *J. Chem. Phys.,* 80, 2221, 1984.

286. Kjellander, R. and Marčelja, S., *J. Phys. Chem.,* 90, 1230, 1986.

287. Attard, P., Mitchell, D.J., and Ninham, B.W., *J. Chem. Phys.,* 89, 4358, 1988.

288. Kralchevsky, P.A. and Paunov, V.N., *Colloids Surf.,* 64, 245, 1992.

289. Danov, K.D., Kralchevsky, P.A., and Ivanov, I.B., in *Handbook of Detergents, Part A: Properties*, Broze, G., Ed., Marcel Dekker, New York, 1999, p. 303.

290. Marra, J., *J. Phys. Chem.*, 90, 2145, 1986.

291. Marra, J., *Biophys. J.*, 50, 815, 1986.

292. Kjellander, R., Marčelja, S., Pashley, R.M., and Quirk, J.P., *J. Phys. Chem.*, 92, 6489, 1988.

293. Kjellander, R., Marčelja, S., Pashley, R.M., and Quirk, J.P., *J. Chem. Phys.*, 92, 4399, 1990.

294. Khan, A., Jönsson, B., and Wennerström, H., *J. Phys. Chem.,* 89, 5180, 1985.

295. Kohonen, M.M., Karaman, M.E., and Pashley, R.M., *Langmuir*, 16, 5749, 2000.

296. Paunov, V.N. and Kralchevsky, P.A., *Colloids Surf.,* 64, 265, 1992.

297. Tadros, Th.F., Steric interactions in thin liquid films, in *Thin Liquid Films,* Ivanov, I.B., Ed., Marcel Dekker, New York, 1988, p. 331.

298. Patel, S.S. and Tirel, M., *Ann. Rev. Phys. Chem.*, 40, 597, 1989.

299. Ploehn, H.J. and Russel, W.B., *Adv. Chem. Eng.*, 15, 137, 1990.

300. de Gennes, P.G., *Scaling Concepts in Polymer Physics,* Cornell University Press, Ithaca, NY, 1979, chap. 3.

301. Dolan, A.K. and Edwards, S.F., *Proc. Roy. Soc. (Lond.)*, A337, 509, 1974.

302. Dolan, A.K. and Edwards, S.F., *Proc. Roy. Soc. (Lond.)*, A343, 427, 1975.

303. de Gennes, P.G., *C. R. Acad. Sci. (Paris)*, 300, 839, 1985.

304. de Gennes, P.G., *Adv. Colloid Intrface Sci.,* 27, 189, 1987.

305. Alexander, S.J., *Physique*, 38, 983, 1977.

306. Taunton, H.J., Toprakcioglu, C., Fetters, L.J., and Klein, J., *Macromolecules*, 23, 571, 1990.

307. Klein, J. and Luckham, P., *Nature*, 300, 429, 1982; *Macromolecules*, 17, 1041, 1984.

308. Luckham, P.F. and Klein, J., *J. Chem. Soc. Faraday Trans.*, 86, 1363, 1990.

309. Sonntag, H., Ehmka, B., Miller, R., and Knapschinski, L., *Adv. Colloid Interface Sci.*, 16, 381, 1982.

310. Horn, R.G. and Israelachvili, J.N., *Chem. Phys. Lett.*, 71, 192, 1980.

311. Nikolov, A.D., Wasan, D.T., Kralchevsky, P.A., and Ivanov, I.B., Ordered structures in thinning micellar foam and latex films, in *Ordering and Organisation in Ionic Solutions,* Ise N. and Sogami, I., Eds., World Scientific, Singapore, 1988.

312. Nikolov, A.D. and Wasan, D.T., *J. Colloid Interface Sci.*, 133, 1, 1989.

313. Nikolov, A.D., Kralchevsky, P.A., Ivanov, I.B., and Wasan, D.T., *J. Colloid Interface Sci.,* 133, 13, 1989.

314. Nikolov, A.D., Wasan, D.T., Denkov, N.D., Kralchevsky, P.A., and Ivanov, I.B., *Prog. Colloid Polym. Sci.*, 82, 87, 1990.

315. Wasan, D.T., Nikolov, A.D., Kralchevsky, P.A., and Ivanov, I.B., *Colloids Surf.*, 67, 139, 1992.

316. Asakura, S. and Oosawa, F., *J. Chem. Phys.*, 22, 1255, 1954; *J. Polym. Sci.*, 33, 183, 1958.

317. de Hek, H. and Vrij, A., *J. Colloid Interface Sci.*, 84, 409, 1981.

318. Snook, I.K. and van Megen, W., *J. Chem. Phys.*, 72, 2907, 1980.

319. Kjellander, R. and Marčelja, S., *Chem Phys Lett.*, 120, 393, 1985.

320. Tarazona, P. and Vicente, L., *Mol. Phys.*, 56, 557, 1985.

321. Evans, R., and Parry, A.O., *J. Phys. Condens. Matter*, 2, SA15, 1990.

322. Henderson, J.R., *Mol. Phys.*, 59, 89, 1986.

323. Henderson, D., *J. Colloid Interface Sci.*, 121, 486, 1988.

324. Kralchevsky, P.A. and Denkov, N.D. *Chem. Phys. Lett.*, 240, 385, 1995; *Prog. Colloid Polymer Sci.*, 98, 18, 1995.

325. Carnahan, N.F. and Starling, K.E., *J. Chem. Phys.*, 51, 635, 1969.

326. Kjellander, R. and Sarman, S., *Chem. Phys. Lett.*, 149, 102, 1988.

327. Beresford-Smith, B. and Chan, D.Y.C., *Chem. Phys. Lett*., 92, 474, 1982.

328. Richetti, P. and Kékicheff, P., *Phys. Rev. Lett.*, 68, 1951, 1992.

329. Karlström, G., *Chem. Scripta*, 25, 89, 1985.

330. Bondy, C., *Trans. Faraday Soc.*, 35, 1093, 1939.
331. Patel, P.D. and Russel, W.B., *J. Colloid Interface Sci.*, 131, 192, 1989.
332. Aronson, M.P., *Langmuir*, 5, 494, 1989.
333. van Lent, B., Israels, R., Scheutjens, J.M.H.M., and Fleer, G.J., *J. Colloid Interface Sci.*, 137, 380, 1990.
334. Joanny, J.F., Leibler, L., and de Gennes, P.G., *J. Polym. Sci.*, 17, 1073, 1979.
335. Evans, E. and Needham, D., *Macromolecules*, 21, 1822, 1988.
336. Johnnott, E.S., *Phil. Mag.*, 70, 1339, 1906.
337. Perrin, R.E., *Ann. Phys.*, 10, 160, 1918.
338. Bruil, H.G. and Lyklema, J., *Nature*, 233, 19, 1971.
339. Friberg, S., Linden, St.E., and Saito, H., *Nature*, 251, 494, 1974.
340. Keuskamp, J.W. and Lyklema, J., *ACS Symp. Ser.*, 8, 191, 1975.
341. Kruglyakov, P.M., *Kolloidn. Zh.*, 36, 160, 1974.
342. Kruglyakov, P.M. and Rovin, Yu.G., *Physical Chemistry of Black Hydrocarbon Films,* Nauka, Moscow, 1978 [in Russian].
343. Manev, E., Sazdanova, S.V., and Wasan, D.T., *J. Dispersion Sci. Technol.*, 5, 111, 1984.
344. Basheva, E.S., Nikolov, A.D., Kralchevsky, P.A., Ivanov, I.B., and Wasan, D.T., in *Surfactants in Solution,* Vol. 12, Mittal, K.L., and Shah, D.O., Eds., Plenum Press, New York, 1991, p. 467.
345. Bergeron, V. and Radke, C.J., *Langmuir*, 8, 3020, 1992.
346. Kralchevsky, P.A., Nikolov, A.D., Wasan, D.T., and Ivanov, I.B., *Langmuir*, 6, 1180, 1990.
347. Claesson, P.M., Kjellander, R., Stenius, P., and Christenson, H.K., *J. Chem. Soc. Faraday Trans. I,* 82, 2735, 1986.
348. Parker, J.L., Richetti, P., and Kékicheff, P., *Phys. Rev. Lett.*, 68, 1955, 1992.
349. Basheva, E.S., Danov, K.D., and Kralchevsky, P.A., *Langmuir,* 13, 4342, 1997.
350. Dushkin, C.D., Nagayama, K., Miwa, T., and Kralchevsky, P.A., *Langmuir*, 9, 3695, 1993.
351. Pollard, M.L. and Radke, C.J., *J. Chem. Phys.*, 101, 6979, 1994.
352. Chu, X.L., Nikolov, A.D., and Wasan, D.T., *Langmuir*, 10, 4403, 1994.
353. Chu, X.L., Nikolov, A.D., and Wasan, D.T., *J. Chem. Phys.*, 103, 6653, 1995.
354. Stanley, H.E. and Teixeira, J., *J. Chem. Phys.*, 73, 3404, 1980.
355. Israelachvili, J.N. and Adams, G.E., *J. Chem. Soc. Faraday Trans. 1,* 74, 975, 1978.
356. Israelachvili, J.N. and Pashley, R.M., *Nature*, 300, 341, 1982.
357. Pashley, R.M., *J. Colloid Interface Sci.*, 80, 153, 1981.
358. Pashley, R.M., *J. Colloid Interface Sci.*, 83, 531, 1981.
359. Healy, T.W., Homola, A., James, R.O., and Hunter, R.J., *Faraday Discuss. Chem Soc.*, 65, 156, 1978.
360. Marčelja, S. and Radič, N., *Chem. Phys Lett.*, 42, 129, 1976.
361. Schibi, D. and Ruckenstein, E., *Chem. Phys Lett.*, 95, 435, 1983.

362. Attard, P. and Batchelor, M.T., *Chem. Phys. Lett.*, 149, 206, 1988.

363. Jönsson, B. and Wennerström, H., *J. Chem. Soc. Faraday Trans. 2*, 79, 19, 1983.

364. Leikin, S. and Kornyshev, A.A., *J. Chem. Phys.*, 92**,** 6890, 1990.

365. Israelachvili, J.N. and Wennerström, H., *J. Phys. Chem.*, 96, 520, 1992.

366. Henderson, D. and Lozada-Cassou, M., *J. Colloid Interface Sci.*, 114, 180, 1986; *J. Colloid Interface Sci.*, 162, 508, 1994.

367. Basu, S. and Sharma, M.M., *J. Colloid Interface Sci.*, 165, 355, 1994.

368. Paunov, V.N., Dimova, R.I., Kralchevsky, P.A., Broze, G., and Mehreteab, A., *J. Colloid Interface Sci.,* 182, 239, 1996.

369. Booth, F., *J. Chem. Phys.*, 19, 391, 1951.

370. Bikerman, J.J., *Philos. Mag.*, 33, 384, 1942.

371. Rowlinson, J.S., Development of theories of inhomogeneous fluids, in *Fundamentals of Inhomogeneous Fluids,* Henderson, D., Ed., Marcel Dekker, New York, 1992.

372. Claesson, P., Carmona-Ribeiro, A.M., and Kurihara, K., *J. Phys. Chem.*, 93, 917, 1989.

373. Horn, R.G., Smith, D.T., and Haller, W., *Chem. Phys. Lett.,* 162, 404, 1989.

374. Tchaliovska, S., Herder, P., Pugh, R., Stenius, P., and Eriksson, J.C., *Langmuir*, 6, 1533, 1990.

375. Pashley, R.M., McGuiggan, P.M., Ninham, B.W., and Evans, D.F., *Science*, 229, 1088, 1985.

376. Rabinovich, Y.I. and Derjaguin, B.V., *Colloids Surf.*, 30, 243, 1988.

377. Parker, J.L., Cho, D.L., and Claesson, P.M., *J. Phys. Chem.*, 93, 6121, 1989.

378. Christenson, H.K., Claesson, P.M., Berg, J., and Herder, P.C., *J. Phys. Chem.*, 93, 1472, 1989.

379. Christenson, H.K., Fang, J., Ninham, B.W., and Parker, J.L., *J. Phys. Chem.*, 94, 8004, 1990.

380. Ducker, W.A., Xu, Z., and Israelachvili, J.N., *Langmuir*, 10, 3279, 1994.

381. Eriksson J.C., Ljunggren, S., and Claesson, P.M., *J. Chem. Soc. Faraday Trans. 2,* 85, 163, 1989.

382. Joesten, M.D. and Schaad, L.J., *Hydrogen Bonding,* Marcel Dekker, New York, 1974.

383. Stillinger, F.H. and Ben-Naim, A., *J. Chem. Phys.*, 47, 4431, 1967.

384. Conway, B.E., *Adv. Colloid Interface Sci.*, 8, 91, 1977.

385. Kuzmin, V.L. and Rusanov, A.I., *Kolloidn. Z.*, 39, 455, 1977.

386. Dubrovich, N.A., *Kolloidn. Z.*, 57, 275, 1995.

387. Christenson, H.K. and Claesson, P.M., *Science*, 239, 390, 1988.

388. Parker, J.L., Claesson, P.M., and Attard, P., *J. Phys. Chem.*, 98, 8468, 1994.

389. Carambassis, A., Jonker, L.C., Attard, P., and Rutland, M.W., *Phys. Rev. Lett.*, 80, 5357, 1998.

390. Mahnke, J., Stearnes, J., Hayes, R.A., Fornasiero, D., and Ralston, J., *Phys. Chem. Chem. Phys.*, 1, 2793, 1999.

391. Considine, R.F., Hayes, R.A., and Horn, R.G., *Langmuir*, 15, 1657, 1999.

392. Considine, R.F. and Drummond, C., *Langmuir*, 16, 631, 2000.

393. Attard, P., *Langmuir,* 16, 4455, 2000.

394. Yakubov, G.E., Butt, H.-J., and Vinogradova, O., *J. Phys. Chem. B*, 104, 3407, 2000.

395. Ederth, T., *J. Phys Chem. B*, 104, 9704, 2000.

396. Ishida, N., Sakamoto, M., Miyahara, M., and Higashitani, K., *Langmuir,* 16, 5681, 2000.

397. Ishida, N., Inoue, T., Miyahara, M., and Higashitani, K., *Langmuir,* 16, 6377, 2000.

398. Tanford, C., *The Hydrophobic Effect,* Wiley, New York, 1980.

399. Leckband, D.E., Israelachvili, J.N., Schmitt, F.-J., and Knoll, W., *Science,* 255, 1419, 1992.

400. Helfrich, W., *Z. Naturforsch.*, 33a, 305, 1978.

401. Servuss, R.M. and Helfrich, W., *J. Phys. (France),* 50, 809, 1989.

402. Fernandez-Puente, L., Bivas, I., Mitov, M.D., and Méléard, P., *Europhys. Lett.*, 28, 181, 1994.

403. Safinya, C.R., Roux, D., Smith, G.S., Sinha, S.K., Dimon, P., Clark, N.A., and Bellocq, A.M., *Phys. Rev. Lett.*, 57, 2718, 1986.

404. McIntosh, T.J., Magid, A.D., and Simon, S.A., *Biochemistry*, 28, 7904, 1989.

405. Abillon, O. and Perez, E., *J. Phys. (France),* 51, 2543, 1990.

406. Evans, E.A. and Skalak, R., *Mechanics and Thermodynamics of Biomembranes,* CRC Press, Boca Raton, Florida, 1980.

407. Aniansson, G.A.E., Wall, S.N., Almgren, M., Hoffman, H., Kielmann, I., Ulbricht, W., Zana, R., Lang. J., and Tondre, C., *J. Phys. Chem.*, 80, 905, 1976.

408. Aniansson, G.A.E., *J. Phys. Chem.*, 82, 2805, 1978.

409. Dimitrova, T.D., Leal-Calderon, F., Gurkov, T.D., and Campbell, B., *Langmuir*, 17, 8069, 2001.